

91/33

Institute of Geological  
& Nuclear Sciences  
Science Report

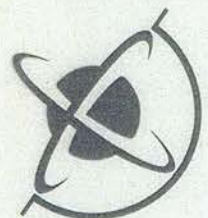
S&G 3649

**3-Dimensional  
Modelling of the  
Effects of Near-  
Surface Ground  
Structure in  
Central  
Christchurch,  
New Zealand, on  
the Passage of  
Seismic Waves**

**A Report Prepared  
for The Earthquake  
Commission**

**A. John Haines,  
Rafael A. Benites  
and Yu Jiashun**

**April 1994**



*Institute of*  
**GEOLOGICAL  
& NUCLEAR  
SCIENCES**  
*Limited*

**3-DIMENSIONAL MODELLING OF THE EFFECTS OF NEAR-SURFACE  
GROUND STRUCTURE IN CENTRAL CHRISTCHURCH, NEW ZEALAND, ON  
THE PASSAGE OF SEISMIC WAVES**

A. John Haines, Rafael A. Benites

Institute of Geological and Nuclear Sciences, P O Box 1320, Wellington

and Yu Jiashun

Institute of Geophysics, Victoria University of Wellington

A Report Prepared for The Earthquake Commission

April 1994

**SYNOPSIS**

To understand how near-surface ground structure affects patterns of 3-dimensional seismic wave amplification in simple sedimentary situations, wavefield modelling has been performed for the top 20 m of soft soil, gravel and sand beneath a 1 km x 1 km area of the central business district of Christchurch. Detailed information from over 100 well logs is available about soil types and layer thicknesses in this area, including results from penetration tests. Weakly consolidated material is restricted to the top 20 m, with the 3 layers present there each varying in thickness by at least 10 m, though in general the rates of spatial variation in thickness are subdued. A model of the distribution of elastic properties in these layers has been developed from published values based on empirical relationships between penetration measurements and elastic moduli, and to demonstrate the sensitivity of the wavefield modelling to the distribution of S wave velocities, which vary from 100 m/s to 350 m/s, a second model of the distribution of elastic properties has been constructed by increasing the S wave velocities by 50 m/s.

In this first such study, the 3-dimensional wavefield modelling has been performed in the frequency domain, using the recently-developed Riccati equation approach. This calculates solutions for a set of incident waves from which solutions for other incident disturbances can

be obtained by weighted superposition of these fundamental solutions. Between 300 and 600 fundamental solutions have been computed for each frequency considered, making a total of 7,506 independent fully-3-dimensional wavefields calculated.

Representative results from a small subset of these solutions are presented in this paper. To illustrate the effects of the individual layers, amplitude values of the total wavefield at the bottom and top of the 20 m thick region, and at the intermediate layer boundaries, are shown normalised relative to the incident wavefield, and phase contours are shown for the top and bottom levels, primarily to demonstrate the seemingly-random standing-wave-like patterns of the scattered waves that are generated. For low frequencies up to 1.5 Hz it is found that the 3 surface layers in central Christchurch have virtually no effect on the amplitudes at the ground surface. For higher frequencies less than 3 Hz significant amplification of the ground motion is restricted to where the top layer of soft sediment is thickest. In all instances where marked amplification occurs there are large, random-like differences in amplitude between the ground motion at closely spaced points, and these spatial fluctuations in amplitude appear to be increasingly arbitrary as the frequency increases. Similarly, at any given site in a region where marked amplification occurs, there are large differences, of as much as a factor of 5 times, in the amplification for waves from slightly different incidence directions.

The predictions from this study are compared with measurements of spectral ratios for earthquakes recorded in a study undertaken subsequently, which included the same region of central Christchurch. There is agreement about how big the range of amplification at any one site can be for different events, and about the occurrence between 1.75 Hz and 4 Hz of large amplification, peaking at 2.5 Hz, at sites where the top layer of soft soil is thickest. On the other hand, amplification predicted to occur between 3 Hz and 4 Hz at sites where the top layer is thin was not observed. The explanation for this discrepancy is that some details are in error in the model of the distribution of S wave velocities in the gravel and sand layers, which has been inferred from penetration measurements. As well, there is evidence that the anelastic-attenuation factor  $Q_s=10$  assumed in this study for the soft-soil layer is inappropriate for the very weak level of ground motion for the earthquakes observed, as some of the observed ground motion is significantly less damped than predicted by the wavefield modelling. From this the conclusion is that, obviously, before wavefield modelling is likely to

provide predictions that are accurate in every detail, it is necessary to have better-determined values of the elastic properties, which ideally should be obtained by direct measurement.

Two firm conclusions about seismic hazard in central Christchurch, and similarly-simple environments, relate to seismic microzonation and the predictability of seismic-wave amplifications. First, a subdivision of the small 1 km x 1 km area into regions likely to respond differently during major earthquakes can be made according to the relative thicknesses of the layers in the top 20 m. In particular, the regions where the surface layer of soft sediment is thickest stand out because of the marked amplification between 1.75 Hz and 4 Hz, which for frequencies less than 3 Hz the wavefield modelling predicts to be confined to the surface layer. Second, in practice the question is not well-posed as to whether it is possible to predict exactly how a particular site will be shaken in a given earthquake, since in regions where there is marked amplification the precise amplification at any one site depends critically on the source details of the earthquake which are extremely unlikely to be predicted accurately enough. On the hand, 3-dimensional wavefield modelling can predict for each frequency the likely range of amplifications at a given site for earthquakes from particular azimuths, provided enough is known about the distribution of elastic properties in the near-surface layers.

## INTRODUCTION

The full character of truly-3-dimensional seismic wave amplification has been little explored even for simple sedimentary environments. There is, of course, semi-anecdotal evidence that ground motion can be quite different at closely spaced sites: for example, how often does one hear of very similar buildings being subjected to different shaking in a region of fairly uniform ground conditions. To examine such phenomena in detail it is necessary either to deploy very dense arrays of instruments or to perform intricate 3-dimensional numerical modelling. So far only the density of the SMART arrays in Taiwan approaches the 300-400 seismometers or accelerometers per sq.km that would match the coverage of the modelling in this paper. On the other hand, before the development of the Riccati equation approach used here modellers lacked accurate tools to handle shallow soil layers. Exact methods based on analytic results are limited in their applicability to uniform soil properties in either perfectly flat layers or

idealised geometries such as hemispheroidal basins, whereas the main numerical methods finite-differences and finite-elements tend to require either equally spaced grids or nearly equally sized elements in all directions, with the result that the metre-scale resolution needed in the vertical direction to treat minor fluctuations in layer thicknesses cannot be achieved on present-day computers using these techniques.

An interesting test case is the central business area of Christchurch (Figure 1), the main city in the South Island, New Zealand (Haines and Benites, 1992; Haines, 1993). Christchurch is underlain by 500 m of flat-lying interbedded gravels and compacted sands, with weakly-consolidated material restricted to the top 20 m. The purpose of this study is to examine how the distribution of soil properties at shallow depths in such regions influences the pattern of seismic wave amplitudes at the surface. An important question that is addressed is whether it is possible to predict exactly how a particular site will be shaken in a given earthquake. It will be demonstrated that even in environments like Christchurch, where there are mild variations in layer thicknesses of soft sediments, there are large, very much more rapid lateral variations in the amplitudes of individual-frequency components of the seismic wavefield. At low frequencies, less than 2 Hz in the case of Christchurch, the top soil layers have little affect on the wave amplitudes. Otherwise at each point the precise level of shaking at any given frequency is strongly dependent on both the directions of arrival of the seismic waves and the elastic properties of the soils.

#### CHRISTCHURCH SOIL LAYERS IN THE TOP 20 M

Detailed information is available about soil types and layer thicknesses in central Christchurch. Elder et al. (1991) have collated over 100 well logs from the 1 km x 1 km area shown as the "large region" in Figure 1, from which the distribution of soil types in Figure 2 has been derived. In the top 20 m there are 3 main layers which are continuous across the region, with minor lenses of other material in the bottom 2 layers and a variety of material comprising the top layer. The lenses in the bottom 2 layers are generally no more than 1-2 m thick and are difficult to correlate from one well log to the next. The soil models in Figure 2 used in the wavefield calculations, have been simplified slightly by overlooking the existence of the lenses,

with the effect that the results of the calculations are almost certainly a little smoother spatially than would be the case in reality. A similar simplification discussed below is made in the case of the top layer. This also contributes to the smoothness of the results, as does some smoothing inherent in the wavefield modelling which is explained later.

As well as the 1 km x 1 km "large region" in Figure 1, a 650 m x 650 m "small region" is also shown. The wavefield modelling involves both areas, with the "large region" being used for low frequencies and the "small region" being used for high frequencies.

In Figure 2 and subsequent figures showing calculated wavefields, the region is being viewed from an elevated point to the south-south-east. In these figures the southern and northern boundaries of the region being considered are shown horizontal, and the eastern and western boundaries are slanted. The ground surface, shown as Level 0, is flat in central Christchurch, with the only noticeable topography being a shallow depression along the course of the Avon River, just outside the northern and western boundaries of the "small region" in Figure 1. This depression is not taken into account in the wavefield modelling, since it is too shallow to have a marked effect. The topography of the other levels in Figure 2 is exaggerated 8 times. Even with this exaggeration, Levels 1 and 2 which are the boundaries between the 3 main layers, appear to be nearly flat interfaces.

The top layer is composed of recently deposited soft soils, which are predominantly silts and peats. The greatest thickness is 12 m in the northwest corner of the "large region" in Figure 1, and there is an almost flat depression in much of the eastern quadrant of the "small region", where the soft material is up to 10 m thick. In contrast, in the western quadrant of the "small region" there is little or no soft material. This region where the top layer is thinnest covers the centre of the "large region" and extends into that region's southern quadrant. By way of orientation, the Cathedral Square, where the top layer is almost non-existent, is in the middle of the western quadrant of the "small region" and slightly south of centre in the "large region".

Below the softest material is a layer of poorly-consolidated gravel. The top layer tends to be thickest where this layer is thinnest, and vice-versa. The gravel layer is non-existent below the depression in the eastern quadrant of the "small region" filled with the soft material. Crossing

the northern boundary of the "small" region, in the vicinity of the Avon River, there is a ridge in the top surface of the gravel above which the top layer is very thin. The greatest thickness of gravel, 16 m, is at the point where this ridge reaches the present course of the river. North of this there is another area where there is no gravel. Elsewhere, in the north-north-west, west, centre and south of the "large" region, the gravel layer is typically 5-10 m thick.

The third layer is firm sand, which completes the top 20 m. Beneath this there is a further 500 m of alluvium, in which the rigidity increases gradually with depth to reach basement-rock-like values at the bottom of the sequence. Here we are concerned with only wave propagation in the top 20 m, to examine how the properties and distribution of the least consolidated alluvial material, which is in this depth range, influence the character of the wavefields at the surface. In the next section it is explained how the Riccati equation approach is particularly suitable for problems like this. What it does is enable the calculation of the seismic response of the top 20 m for any incident wavefield arriving at the base of this region. In this paper the responses are normalised to the amplitudes of the incident wavefields at the bottom of the sand layer, irrespective of how these wavefields may have been affected in propagating through the underlying 500 m of alluvium.

As well as propagation through the underlying alluvium being only indirectly relevant to the questions we are addressing, there are practical reasons for not considering it here. It can be separated into two problems of equal complexity to the problem of propagation in the top 20 m. For low-frequency waves from 1/3 Hz to 2 Hz the underlying alluvium, in conjunction with the top 20 m, can act as a waveguide trapping seismic energy entering from below, much as the top 20 m alone does for higher frequency waves. Also, enough is known from well logs (Elder et al., 1991) to infer that, on the other hand, for higher frequencies the underlying alluvium is an effectively-random phase and amplitude filter with very many minor fluctuations in elastic properties acting as lenses, each of which bends and either focuses or defuses the waves that pass through it. For neither case is there sufficient known about the distribution of the deep alluvial material for the appropriate type of 3-dimensional wave propagation modelling to be undertaken. For 1-dimensional analyses of wave propagation through the full alluvial sequence, readers are referred to Elder et al. (1991) and Berrill et al. (1993).

Two models of the distribution of seismic wave velocities are shown in Figure 2. Many of the well logs in the central city area include results from a range of penetration tests, in which probes pushed into the ground measure how much the soil at each depth resists this intrusion. From this information Elder et al. (1991) have inferred S wave velocities using empirical relationships based on Californian data. Model A in Figure 2 is derived from the distribution of S wave velocity with depth that Elder et al. take to be representative.

Some minor modifications are made to keep the soil model as simple as possible while retaining gross features of the properties at Christchurch. Instead of having the S wave velocity in the top layer of very soft material increase with depth as Elder et al. have inferred, an average value of 100 m/s is used throughout this layer. The reason for doing this is as follows. Though it is commonly observed elsewhere that the S velocity increases with depth, it can be inferred from the considerable scatter in the data for the empirical relationships used by Elder et al. that the range of S velocities is likely to be highly variable in the top layer at Christchurch because of the variety of the soil types present in the well logs. Even when the type of material is the same, it is unlikely that the S velocity at, say, 2 m depth will be the same where the layer is very thick as where the layer is very thin, given that the ages of the material at 2 m may be different at two such sites. Furthermore, at most sites the departure from a smooth velocity-depth relationship, based on the increase in velocity with compaction of a uniform material, is almost certainly as big as the lateral variation in velocity, particularly as the full range of soil types in the top layer is seen in very many of the well logs. Thus, for the 3-dimensional wavefield modelling performed here, a velocity model for the top layer incorporating, for instance, a simple increase in velocity with depth would not have been significantly closer to reality than using a uniform velocity as is done here.

For the other two layers there is a stronger case for including the increase in S velocity with depth, primarily because it is likely to be the dominant variation in velocity. For each of these layers the S velocity is assigned a uniform value at the top of the layer and a uniform value at the bottom of the layer. At points within the layers the values are obtained by assuming linear variation of the S velocity with depth at each horizontal position. So, for example, where the gravel layer starts at 2 m depth and goes down to 10 m the S velocity for model A at 8 m is

225 m/s, whereas where the gravel layer starts at 5 m and goes down to 11 m the S velocity at 8 m is 200 m/s.

In the second model, model B, the S velocities are all increased by 50 m/s. This is an indicative amount by which the S velocity at each point might differ from the value given by model A. All the same, accepting that model A approximates the actual distribution of elastic properties in Christchurch, the amounts by which the true S velocities differ from the values given by model A are probably randomly distributed with roughly equal proportions of positive and negative values. The precise statistical properties of this random distribution are, however, unknown. The reason for performing wavefield calculations for model B as well as model A is to see what effects systematic changes in velocity have on the results. Not surprisingly, these effects are close to those expected. The frequencies at which particular phenomena occur within each layer tend to be governed by the S velocities there, and, to a good approximation, a change in S velocity results in a directly proportional change in frequency. So, for example, strong resonances that occur in the greatest thicknesses of the top layer and which are largest at frequencies around 2.5 Hz for model A, are largest for model B around 3.75 Hz, being equal to 2.5 Hz multiplied by the ratio of the velocities 150 m/s and 100 m/s for the top layer in the two models. Similarly, the lowest frequency at which there is amplification in the other two layers that is clearly discernible on the same scale as these resonances, is about 3 Hz for model A and again 3.75 Hz for model B, since in this case the relevant ratio of velocities is closer to 1.0.

In both model A and model B the P wave velocity is taken to be 1500 m/s throughout, corresponding to water saturation of the soils, and the density, which like the P velocity is generally much less variable than the S velocity, is taken to be uniformly  $2 \text{ Mg/m}^3$ .

## THE RICCATI EQUATION APPROACH

The Riccati equation approach (Haines, 1989; Benites and Haines, 1991) is an efficient frequency-domain method for numerically solving the elastodynamic equation for linear motion in 2 and 3 dimensional dimensions to obtain complete ranges of possible seismic

wavefields inside heterogeneous bodies. For problems like Christchurch central business district, where the top 20 m of soft soil, gravel and sand is the heterogeneous body being considered, the starting point is the construction of a curvilinear coordinate system in which one coordinate is chosen so that it has a constant value at each layer boundary. This coordinate is called the range variable and other coordinates in the curvilinear system are called cross-range variables. The wavefield is expanded as a Fourier series in terms of the cross-range variables in which the Fourier coefficient associated with each wavenumber in the series is a function of the range variable. The elastodynamic equation, which is a second-order linear partial differential equation, is, thereby, reduced to a system of coupled second-order linear ordinary differential equations in terms of the range variable, which is to be solved for the Fourier coefficients, or wavenumber components. Next this set of second-order equations is factorized to give a first-order Riccati differential equation and a set of coupled first-order linear differential equations. The Riccati equation is satisfied by matrix functions of the range variable whose elements, which relate pairs of the wavenumber components, are themselves coupled to one another in the Riccati equation. Once the Riccati equation has been solved, the set of coupled first-order linear equations, which requires the matrix solutions to the Riccati equation, can be solved for the wavenumber components.

In practice what is done is that two complementary solutions to the Riccati equation are computed numerically. Then a property of complementary solutions to the Riccati equation is applied based on the following concept. Any type of initial wavefield at the boundary of the heterogeneous body can be expanded as a Fourier series in terms of the cross-range variables, in the same way that the wavefield inside the body is, except that at the boundary the Fourier coefficients for the initial field are constants rather than functions of the range variable. The resulting wavefield inside the body is the corresponding sum of a set of fundamental solutions to the elastodynamic equation weighted by these constant coefficients. Each of the fundamental solutions in the sum is the solution inside the body for a particular Fourier component of the initial wavefield. Using this concept in conjunction with the two solutions to the Riccati equation and appropriate initial conditions for the coupled first-order linear equations, it is straight-forward to compute a complete set of fundamental solutions to the elastodynamic equation that can be used in this fashion to obtain any other solution to the elastodynamic equation (Haines and de Hoop, in prep.). This procedure of solving the Riccati

equation and generating a complete set of fundamental solutions to the elastodynamic equation is repeated for each frequency.

With the Riccati equation approach, as with other methods involving separating the spatial coordinates into a range variable and cross-range variables, it is normal to employ different spatial resolutions in the range and cross-range directions. In the range direction one typically solves the Riccati equation, the coupled first-order linear equations, and analogous differential equations for other such methods, at closely spaced points separated by a small fraction of the smallest wavelength in the problem. This fraction is never more than  $1/12$  for the Riccati equation and  $1/6$  for the coupled first-order equations, and often is very much smaller, for example, where layers are very thin. On the other hand, the Fourier decomposition with respect to cross-range variables generally gives accurate representations of the seismic wavefield provided enough terms are taken in the Fourier series to correspond to sampling the wavefield at least every  $1/2$  wavelength. Truncating the Fourier series with respect to the cross-range variables amounts to doing spatial averaging along the coordinate surfaces on which the range variable is constant. The distances over which this spatial averaging is performed are given by the effective sampling intervals for the cross-range variables which are determined by the number of terms in the Fourier series.

For the Christchurch example, the number of terms in the Fourier decomposition with respect to the cross-range variable was controlled by the size and speed of the computer used. For example, doubling the number of terms in the Fourier series requires 4 times as much "central processing unit" memory and typically 8 times as much computer time for the same wave frequency, while, if the number of terms in the Fourier series is held constant, the amount of computer time required is roughly proportional to the wave frequency, since the sampling interval in the range-variable direction is generally proportional to wavelength. The principal computations were performed on a Sky Warrior II array processor inside a SUN 4/330 workstation. 16 Mbytes of fast memory is shared by the array processor and the workstation and the operating speed of the array processor for large problems is about 20 million floating point operations per second (Mflops). For 3-dimensional seismic wave problems this limits the number of 2-component wavenumbers in the Fourier decomposition with respect to the

cross-range variables to just under 200. With the maximum number of wavenumbers, the computations take, for instance, over 2 days for frequency 2.5 Hz for model A in Figure 2.

What is actually limited in the Fourier series is the total number of independent components in the wavefield which cannot be more than just under 600 when there are 16 Mbytes of fast memory available - for 3-dimensional problems there are 3 independent components of motion for each wavenumber. In the computations for each frequency the output generated is a complete set of fundamental wavefield solutions for the truncated Fourier decomposition with respect to the cross-range variables. Each fundamental solution is for a different initial wavefield at the boundary of the region where the wavefield is being solved, and, as explained above, the solution inside this region for any initial wavefield at the boundary can be obtained by combining the fundamental solutions: the only limitation is that the initial wavefield has to be expandable in terms of the truncated Fourier decomposition. In the Christchurch example, the free-surface boundary condition at the Earth's surface means that the only initial wavefields that need to be considered are those that are incident from below (in contrast to what happens for problems when the heterogeneous body of interest is below the Earth's surface, where one has to consider waves incident from above as well). This results in there being one fundamental solution computed for each independent wavefield component allowed for in the Fourier series (rather than 2 fundamental solutions for each independent component when considering subterranean bodies). When the total computation time is just over 2 days for just under 600 independent 3-dimensional wavefield solutions for a single frequency, as for 2.5 Hz, the effective computation time per fundamental solution is 5-6 minutes.

#### FREQUENCIES CONSIDERED AND THE WAVENUMBER SET FOR EACH CASE

18 sets of solutions have been obtained for different combinations of frequency, either the large or small region in Figure 1 and either model A or model B from Figure 2. The combinations considered are listed in Table 1. Also given in Table 1 is the total number of 2-component wavenumbers used in each case and the average effective spacing of points in the horizontal directions that this number of wavenumbers corresponds to. In total 7,506

independent 3-dimensional single-frequency fundamental solutions to the elastodynamic equation have been computed.

TABLE 1: Frequencies, numbers of wavenumbers and corresponding horizontal spacings

	Frequency (Hz)	Wavenumbers	Spacing (m)
Large region, model A			
	0.5	109	95
	1.0	109	95
	1.5	109	95
	1.75	145	81
	2.0	145	81
	2.25	193	71
	2.5	193	71
Small region, model A			
	2.5	109	62
	3.0	145	53
	3.5	145	53
	4.0	145	53
Large region, model B			
	0.75	109	95
	1.5	109	95
	2.25	145	81
	3.0	193	71
Small region, model B			
	3.0	109	62
	3.75	145	53
	4.5	145	53

The 3 sets of wavenumbers used are shown in Figure 3. The largest set contains all 193 wavenumbers shown, the second largest contains 145 wavenumbers, and smallest set contains the innermost 109 wavenumbers. To understand what the values in Figure 3 mean it is necessary to know that in performing the wavefield calculations the region considered is enlarged a little by adding a narrow surrounding area where the heterogeneous body is taken to be of zero thickness. This is done to compensate for truncating the Fourier series so that the wavefield at each side of the region of interest is not artificially required to be the same as the wavefield at the opposite side of the region: the width of the area that is added has to be

roughly proportional to the smallest wavelength considered in each of the horizontal directions.

Each of the wavenumbers in Figure 3 has 2 integer components. The first component is the number of cycles the wave has across the enlarged region in the east-west direction, and a positive sign indicates that the wave is moving from west to east, whereas a negative sign indicates that the wave is moving from east to west. If the first component is zero the wavelength of the wave is infinite in the east-west direction. Similarly, the second component is the number of cycles the wave has in the north-south direction. A positive sign indicates that the wave is moving from north to south, whereas a negative sign indicates that the wave is moving from south to north, and if the second component is zero the wavelength of the wave is infinite in the north-south direction.

The effective spacing over which spatial averaging is performed in each horizontal direction as a result of truncating the Fourier series, is approximately half the smallest wavelength considered in that direction. Because of the nearly circular shape of the sets of wavenumbers used (see Figure 3) this effective spacing is almost the same for all horizontal directions and differs little from the average value given in Table 1. The number of wavenumbers listed there for each case has been chosen so that the effective horizontal spacing decreases with increasing frequency to allow for more rapid variations in the wavefields. Because of the restrictions on how many wavenumbers can be handled by the array processor used, it was necessary to have effective horizontal spacings no smaller than 50 m, and the upper limit was chosen to be about 100 m.

In comparison the spacing of the points where there are well-logs from which the layer thicknesses in Figure 2 are derived, is typically about 70-100 m, and at places in Figure 1 outside the "small region" but inside the "large region" this spacing is much bigger. Consequently, it cannot be argued that more accurate reproduction of what actually happens in Christchurch would have been obtained if the wavefields had been computed with less-coarse horizontal resolutions. On the contrary, there is a reasonable match between what was feasible with the Riccati equation method and the spatial resolution from the well-logs. All the same, with effective horizontal spacings between 50 m and 100 m in the wavefield modelling it

is impossible to synthesise any lateral variations that occur over shorter distances, and, from the practical point of view, what has been done amounts to smoothing that removes such variations.

## SAMPLE RESULTS

Typical results from 3 of the 7,506 fundamental solutions are presented in Figures 4 to 6. Figures 4 and 5 show the normalised amplitude of the ground motion at the following 4 levels:

- Level 3 = the base of the sand layer at 20 m depth,
- Level 2 = the interface between the sand layer and the gravel layer,
- Level 1 = the interface between the gravel layer and the layer of soft sediment, and
- Level 0 = the ground surface.

In all diagrams the total wavefield is presented, consisting of the incident wave, surface reflection and response of the heterogeneity.

Because the fundamental solutions are single frequency waveforms, it is immaterial whether the ground motions are viewed as being displacements, velocities or accelerations, since to convert between velocity and acceleration, for example, one simply scales by the frequency. The 3 components of motion are

- $U_x$  = motion in the horizontal east-west direction,
- $U_y$  = motion in the horizontal north-south direction, and
- $U_z$  = motion in the vertical direction.

The amplitudes have been normalised by setting the combined amplitude of the 3 components of motion in the incident wave at the base of the sand layer (Level 3) to be 1. If the top 20 m considered were of uniform composition with the same elastic properties as at the base of the sand layer, in most cases the combined amplitude of the 3 components of motion at the ground surface (Level 0) would have been about 2, since the incident wave would not have been

altered in amplitude in propagating up to the surface and would combine constructively with the reflected wavefield that is generated there. When the maximum amplitude of each component is greater than 2 at any of the 3 levels, this can be seen in a change in the amplitude scale at the left of the figure for that component: the largest amplitude on the scale is equal to the result of adding 7 to the maximum amplitude anywhere in the figure, except where this maximum amplitude is less than 2. Another point to note is that at the edge of the region considered in the wavefield modelling the thickness is required to go to zero, which ties in with having an area of zero thickness surrounding the region. The tapering of the thicknesses of the layers to zero has been done smoothly over the 50 m closest to the edge. The effect of this is as though the region were surrounded there by uniform material with the same properties as at the base of the sand layer. Consequently, the wave amplitudes at the edge tend to be larger than where the base of the sand layer is at 20 m depth, because at the edge the wavefield reflected by the ground surface is of similar amplitude to the incident wave and combines constructively with it.

Mainly because of this tapering to zero thickness of the region considered, the incident wavefield for each of the fundamental solutions is not exactly the same as a plane wave. Even so, it is a very close approximation. Each of the fundamental solutions is characterised by the type of plane wave corresponding to the incident wavefield, the two horizontal wavenumbers  $k_x$  and  $k_y$  and the frequency in Hz.  $k_x$  and  $k_y$  are integers giving the direction of arrival of the incident wavefield (see the description above of Figure 3). The largest wavenumbers are generally associated with evanescent incident waves which travel along the base of the sand layer and decay exponentially with depth below that. Medium-sized wavenumbers are generally associated with waves arriving at the base of the sand layer at shallow or medium angles of incidence between 15 and 90 degrees to vertical, whereas the smallest wavenumbers are associated with waves arriving vertically or nearly vertically. When account is taken of propagation through the underlying 500 m of alluvium in which the rigidity increases with depth to basement-like values, Snell's Law requires that under most circumstances almost all seismic energy arriving at the base of the sand layer arrives almost vertically. Consequently, earthquakes are likely to excite the fundamental solutions with the smallest wavenumbers more than the other fundamental solutions.

For the fundamental solutions in Figures 4 and 5  $k_x$  and  $k_y$  are zero, which corresponds to vertical incidence. In the case of vertical incidence, the two independent incident S waves are taken to be those involving ground motion in the east-west X direction (X-input in Figure 4) and north-south Y direction (Y-input in Figure 5), whereas incident P waves involve ground motion in the vertical Z direction. Both the solutions in Figures 4 and 5 are for relatively high frequencies: 3.5 Hz and 3.75 Hz for model A and model B respectively. They have features in common with most of the fundamental solutions for frequencies 3.5 Hz or greater. At Level 3 (base of the sand layer) each solution is similar in amplitude to the incident wave, except at the edge of the region considered where the tapering to zero of the layer thicknesses has the effect described above. At Level 2 there is evidence of some amplification of the waves in the sand layer, whereas much more amplification occurs in the gravel and soft soil layers, as can be seen at Levels 1 and 0 respectively. The net result at the ground surface (level 0) is a seemingly random pattern of amplification, with peaks and troughs in the magnitude of the ground motion at points separated by little more than the effective horizontal sampling in the wavefield modelling. As well as the amplification in the same component of motion as the incident wave in each case, there is some scattering of energy into other components, particularly the horizontal components.

A relatively minor feature in Figure 4 is that the amplification of the major component  $U_x$  at the ground surface (Level 0) is smaller and flatter over the area of thick soft sediment in the eastern quadrant of the "small region" than elsewhere in the figure where the soft sediment is thinner and the gravel layer is present. What is controlling this is the anelastic attenuation factor  $Q_s$  for S waves in the soft sediment which has been assigned the value 10 (Figure 2). The lower the value of  $Q$ , the greater the rate of attenuation: the total anelastic attenuation in travelling a distance  $x$  is given by the factor

$$\exp(-[\omega]x/2cQ)$$

where  $[\omega]$  is the angular frequency and  $c$  is the velocity for the type of wave being attenuated. This value of 10 for  $Q_s$  in the soft sediment means that the amplitude of an S wave decays by about 30% in propagating one wavelength, which for S wave velocity 100 m/s and frequency 3.5 Hz is between 25 m and 30 m. If  $Q_s$  was instead, say, 5 for the soft sediment, the distance

over which the amplitude decays by 30% would be half a wavelength, with the result that the amplification over the area of the thick soft sediment at relatively high frequencies such as 3.5 Hz would be much more subdued. Conversely, if  $Q_s$  for the soft sediment was somewhat larger, say, 20 which is the value assumed for the gravel layer, there would not be as obvious diminishment in amplification over the soft sediment as in Figure 4.  $Q_s = 10$  is possibly a conservatively high value for the soft sediment, though observations discussed below indicate that a higher value of  $Q_s$  is appropriate for weak levels of ground motion associated with small earthquakes. For strong ground motion in very large earthquakes there is a marked tendency for soft soils with low plasticity indices to behave nonlinearly, in a fashion that involves considerably more rapid anelastic absorption of the seismic energy than for weak ground motion. Marsh et al. (in press) demonstrate for simple 2-dimensional problems that the amplitudes of such nonlinear motion in the frequency domain can be modelled as though the motion were linear with very low values of  $Q_s$ , even though the waveforms for the linear and nonlinear motion are quite different in the time domain. The implications for Christchurch are that the level of amplification for 3.5 Hz in Figure 4, for linear motion with  $Q_s = 10$ , may be significantly larger than what might occur in this area of soft sediment in a large earthquake.

The fundamental solution in Figure 6 is for the lower frequency 2.5 Hz, at which the amplification at the ground surface is much more strongly influenced by the soft soil layer than by the gravel and the sand. The particular solution for 2.5 Hz shown is for an SV wave incident from the north-east with horizontal wavenumber  $(k_x, k_y) = (-2, 2)$ . For cases of non-vertical incidence such as this, the fundamental solutions have been split into those for the standard decomposition of incident wavefields into the SH, SV and P wave types: SH is the horizontally polarised S wave involving ground motion in the horizontal direction perpendicular to the horizontal component of the direction of propagation of the wave, whereas SV is the perpendicular S wave involving a vertical component of motion.  $(k_x, k_y) = (-2, 2)$  implies a medium angle of incidence for the SV wave of 20 degrees at the base of the sand layer for model A. Taking the model of Elder et al. (1991) for the underlying alluvium, assuming only slight lateral variations in the S wave velocity there and applying Snell's Law, such an incident wave would have been propagating horizontally at the depth of 200 m where the S velocity in the alluvium is 1000 m/s; that is, the source of this incident wave would be extremely shallow.

The horizontal direction of propagation of the waves can be seen in the phase diagrams in Figure 6b. In Figure 6 results are shown for Level 3 at the base of the sand layer and Level 0 at the ground surface. Between the pairs of heavy lines in phase diagrams like Figure 6b the phase of the waves changes by 360 degrees, equivalent to one full cycle. This gives the effective wavelength in the horizontal plane. The contour interval of the lines of constant phase is 40 degrees. Negative phases are shown by dashed lines, while positive phases are shown by solid lines. The progression from negative phases to positive phases between the heavy lines indicates the direction of propagation. For the fundamental solution in Figure 6 the waves are propagating from the north-east in the top right-hand corner of the diagrams to the south-west in the bottom left-hand corner. There are clear departures from a regular change in phase with position, particularly for the vertical component  $U_z$  and also for the horizontal components  $U_x$  and  $U_y$  at the ground surface. These departures are due to the presence of scattered waves which are not travelling in the same direction as the incident wave. Here the incident wave involves motion in all 3 components  $U_x$ ,  $U_y$  and  $U_z$ . After the next section examples are shown in which the incident wave involves motion in only 1 or 2 of these components. In such cases it is seen from the phases of the other components that the scattered waves have random-looking standing-wave-like patterns involving propagation in no particular horizontal direction.

At frequencies around 2.5 Hz for model A the areas of the thickest soft sediment resonate in their fundamental S-wave mode of resonance. The largest amplitudes at the ground surface in Figure 6a are over the thickest deposits of soft sediment along the northern edge and in the north-west corner of the "large region" and in the flat depression in the eastern quadrant (see Figure 2). In contrast to what happens at the ground surface where the influence of the soft sediment is clearly evident, the amplitudes at the base of the sand layer are very little altered from the values they would have had if there was sand of uniform velocity throughout the top 20 m.

For model B these resonances occur around 3.75 Hz because, as explained earlier, the S wave velocities are 50 m/s higher in model B than in model A. In Figure 5 the amplitudes at Level 0 are generally larger where the soft- sediment layer is thick than where it is thin or non-existent.

This contrasts with the results for model A at 3.5 Hz in Figure 4. The reason that anelastic attenuation in the soft sediment has less effect in Figure 5 than in Figure 4 is that the S wavelength is longer for the case in Figure 5, since the S velocity in the soft sediment is higher in model B. For anelastic attenuation to have as much effect in model B as in Figure 4 for model A, the frequency would have to be about 5.25 Hz (which is equal to 3.5 Hz multiplied by the ratio of the velocities): in this case the S wavelength in the soft sediment would be the same as in Figure 4.

### COMPARISON WITH WEAK-MOTION OBSERVATIONS

Taber and Cowan (1993) have recently measured ground shaking at 6 sites in Christchurch, 3 of which are inside the present study area. These 3 sites were chosen to be representative of the sites considered here. One site was over the thick soft sediment in the eastern quadrant. Two earthquakes were recorded at this site and at a rock site deep in an artificial cavern 5 km south of the central city. The Fourier spectral ratio of the soft-soil site relative to the rock site shows strong amplification at the soft-soil site between 2.5 Hz and 4 Hz with the largest peaks with ratios over 10 being at these frequencies. The other 2 sites in the present study area were in Cathedral Square in the middle of the eastern quadrant of the "small region" (Figure 1), where there is practically no soft sediment, and 200 m south of there where there is an intermediate thickness of soft sediment. The Fourier spectral ratio for the site in Cathedral Square relative to the rock site from 2 earthquakes shows a flat amplification of about 3 for all frequencies up to 8 Hz. Only one earthquake was recorded at the other site. For this event the spectral ratio relative to the rock site is very similar to the spectral ratio at the site in Cathedral Square, except that there is a narrow peak at 4 Hz at which the ratio is 6. The site at which Taber and Cowan observed the largest amplifications was at Christchurch Womens Hospital 1 km north of our study area. There the site conditions are very similar to those at the soft-soil site in our area, though the soft sediments at the hospital are marginally thicker, at 8.5 m compared with 7.5 m, and slightly different in composition. The Fourier spectral ratios at this site relative to the rock site for individual events have broad peaks between 1.75 Hz and 2 Hz, with an average peak value of about 20 at 2.5 Hz.

At the site at Christchurch Womens Hospital 12 earthquakes were recorded from which spectral ratios relative to the rock site could be calculated. For any one frequency there is wide variation - as much as a factor of 5 - in the spectral ratios from the individual events. This variation is very similar in size to the spatial variations in amplitude at Level 0 in Figures 4, 5 and 6. Furthermore, examples are presented in the next section which illustrate that the amplification can vary equally as much at any one site among different fundamental solutions for the same frequency with different directions of incidence, as between different sites for each of the solutions.

How do the results of the wavefield modelling compare otherwise with the measurements made by Taber and Cowan? First, it is necessary to convert from having the synthetic results normalised relative to the magnitude of the incident wave at the base of the sand layer, to having them normalised relative to the corresponding motion at the deep rock site. From energy considerations a crude correction can be deduced, which takes no account of possible lateral variations in seismic energy arriving across the Christchurch region. Assuming that the S waves incident at the base of the sand layer and at the rock site transport the same amount of energy per unit time in their directions of propagation, the ratios of the amplitudes will be inversely proportional to the square root of the ratio of the S-wave seismic impedances. The seismic impedance is the product of density and seismic wave velocity. The volcanic material at the rock site can be expected to have a slightly higher density than at the base of the sand layer, where the S wave velocity is no more than 1/4 the S wave velocity of the volcanic material of about 1700 m/s assumed by Elder et al. (1991). Thus, the factor that amplitudes relative to the incident wave at the base of the sand layer have to be multiplied by to convert them into amplitudes relative to the deep rock site is likely to be between 2 and 2.5. This makes no allowance for how the amplitudes of the waves at the rock site are affected by either the presence of the artificial cavern or reflections from the ground surface above it, though it may be reasonable to assume that neglecting these influences is unlikely to introduce a systematic bias.

Thus, when multiplied by this factor of between 2 and 2.5, the amplitudes of between 4 and 5 in Figure 6, for example, at the soft-soil sites where the fundamental resonances are predicted to occur about 2.5 Hz for model A, are in broad agreement with the peak about 2.5 Hz in the

spectral ratio observed at the soft-soil site in our study area by Taber and Cowan. This confirms that the S wave velocity of 100 m/s in model A is a better estimate for the soft sediment layer than the velocity of 150 m/s in model B. On the other hand, the presence of the equally strong peak observed at 4 Hz indicates that the  $Q_s = 10$  value we have used is too small for small earthquakes, since our wavefield modelling predicts that over the soft sediment the wave amplitudes at such frequencies should be slightly damped. Other evidence for  $Q_s = 10$  being too small are the large spectral ratios between 1.75 Hz and 4 Hz at Christchurch Womens Hospital. Even though this site is not in our study area, what happens there is very likely to be much the same as at the very similar soft-soil sites we have considered. Consequently, the site at Christchurch Womens Hospital and the soft-soil site inside our area indicate the range of spectral ratios that our modelling should predict for sites where the soft-soil layer is thick. Our amplitudes are, perhaps, between 1.5 and 2 times too small, which could be corrected by at least doubling the value of  $Q_s$  in the soft-soil layer so that anelastic attenuation would have much less influence.

As well, there is evidence that our S velocities taken from Elder et al. (1991) for the gravel layer are too low and that these velocities should be at least as high as the velocities in the sand layer. This evidence comes from the other 2 sites in our study area where observations were made by Taber and Cowan. There, with the correction factor between 2 and 2.5, at high frequencies our modelling predicts spectral ratios between 10 and 20, such as in Figure 4 for 3.5 Hz, whereas Taber and Cowan found ratio values close to 3. The cause of the large amplitudes predicted by our modelling are fundamental resonances occurring in the gravel layer, and these resonances would be diminished if the S velocity in the gravel were the same or higher than the velocities in the sand. Also, it is likely that the agreement between the modelling and the observations would be further improved if the S velocities in both these layers varied much less with depth than we have assumed, as this would prevent the occurrence of any resonance-like phenomena confined to these layers. Another way to stop the formation of resonances would be to have very small  $Q_s$  values, since this would damp out multiple reflections which combine to make up the resonances. However, for anelastic attenuation to be strong enough to have this effect between 3 Hz and 4 Hz, it would tend to damp out all the signal at higher frequencies, which conflicts with the observation that the spectral ratios are flat up to 8 Hz at the 2 stations in question.

## FURTHER EXAMPLES

The main purpose of this study is not to predict exactly what is likely happen in Christchurch. It is instead to illustrate the sorts of phenomena that can occur in such environments. Further examples are presented below to illustrate some important features.

Figure 7 shows a sequence of results at different frequencies for vertically incident S waves with north-south components of motion (Y input). These results are for model A, and the normalised amplitudes are shown at the base of the soft sediment (Level 1) and at the ground surface (Level 0). At low frequencies up to 1.5 Hz the amplitudes at both levels are virtually indistinguishable from the amplitudes at the base of the sand layer. At 1.75 Hz and 2 Hz there is some amplification at the ground surface where the layer of soft sediment is thickest, while there is no evidence of the amplification at the bottom of the layer. This amplification at the top of the soft sediment is increasing with increasing frequency. By 2.25 Hz and 2.5 Hz the amplification is very pronounced and is wide spread where the layer of soft sediment is thick. Also, at these frequencies the east-west component  $U_x$  of the scattered wavefield is growing in the same areas.

Two sets of results are shown for 2.5 Hz in Figures 7f and 7g, for the large and small regions in Figure 1 respectively. These results were computed using slightly different effective horizontal spacings (see Table 1). There is good agreement where the two regions coincide, which indicates that the spatial smoothing, introduced in the wavefield modelling by truncating the Fourier series, is not strongly influencing the results.

At the higher frequencies 3 Hz, 3.5 Hz and 4 Hz the amplification in the gravel layer mentioned previously is important. This can be seen in Figures 7h, 7i and 7j where at the top of this layer (Level 1), and also at the ground surface (Level 0), the amplitudes are increasing with increasing frequency in the western half of the "small region" where the layer is thick. While this is happening the amplification associated with thick soft sediment is diminishing slightly at the ground surface in the east of the region.

Figure 8 shows corresponding results for 3 Hz and 4.5 Hz for model B, which are to be viewed in conjunction with the results for 3.75 Hz in Figure 5. Again the incident disturbances are vertically propagating S waves with motion in the north-south direction. At 3 Hz there is only slight amplification at the top of the gravel layer (Level 1) where the maximum amplitude is about 3, which is 1.5 times what it would have been if there had been uniform material in the top 20 m with the same S velocity as at the base of the sand layer. Also, the amplitudes at the ground surface (Level 0) over the thick soft sediment in the east of the "small region" are only half as big at 3 Hz as they are at 3.75 Hz. This is very similar to the ratio of the amplitudes at 2 Hz and 2.5 Hz for model A, in line with the comment made previously about the way frequencies scale in proportion to the S wave velocities for the two models. As for 3.75 Hz in Figure 5, the amplitudes at all 4 levels are shown for 4.5 Hz. There is not much difference between the patterns for these two frequencies, except that the amplification associated with the gravel layer is slightly stronger at 4.5 Hz.

In Figure 8d phase diagrams are presented for 4.5 Hz at Level 3 and 0. The main component of motion is  $U_y$  in the north-south direction. Since the incident wave is propagating vertically, the phase of  $U_y$  is almost constant at both levels. At the base of the sand layer (Level 3) the phase of  $U_y$  is negative, whereas at the ground surface (Level 0) it is positive, indicating that the total wavefield at the top of our 20 m region is delayed in phase relative to the total wavefield at the bottom. The other components  $U_x$  and  $U_z$  are made up entirely of scattered waves, and the phase diagrams for these components show the seemingly random patterns typical of the scattered wavefields from the modelling.

Another set of phase diagrams is shown in Figure 9. These are for 3 Hz waves incident from the north for model A with  $(k_x, k_y) = (0, 2)$ . Results are shown at Levels 3 and 0 for SH, SV and P incidence. For SH and SV the angle of incidence at the base of the sand layer is 18 degrees, whereas the incident P wave is an evanescent (horizontally propagating) wave. The incident motion is in the east-west direction ( $U_x$ ) for SH and the north-south and vertical directions ( $U_y$  and  $U_z$ ) for SV and P. The other components in each case show similar scattered-wave patterns to  $U_x$  and  $U_z$  in Figure 8d, with there being no clear, consistent direction in which the scattered waves are propagating. In slight contrast to the results for 2.5

Hz at Level 3 in Figure 6b, the random-like scattered wavefields have as much influence on the phases of the main components,  $U_x$  for SH and  $U_y$  and  $U_z$  for SV and P, at Level 3 as they do at Level 0, though this is less pronounced for SV and P than it is for SH. This is a feature of the scattered waves as the frequency is increased. At low frequency they are mainly confined to the top layer of soft sediment, whereas at high frequency they have similar amplitudes to the incident waves throughout the whole region we are considering.

The amplitude patterns at the ground surface (Level 0) are shown in Figure 10 for 3 Hz waves incident both from the north, as in Figure 9, and from the west. Again the results are for model A, and 3 sizes of incident wavenumber are included. For  $(k_x, k_y) = (0, 1)$  and  $(1, 0)$ , with incidence directions from the north and west respectively (see Figure 3), the angles of incidence at the base of the sand layer are 9 degrees for SH and SV and 42 degrees for P. For  $(k_x, k_y) = (0, 2)$  and  $(2, 0)$  the incidence conditions are the same as in Figure 9, with the S waves being incident at 18 degrees and the incident P wave being evanescent, and for  $(k_x, k_y) = (0, 4)$  and  $(4, 0)$  the S waves are incident at 39 degrees and the P wave is again evanescent. In the cases where the incident P wave is evanescent the amplitude patterns at the ground surface are very similar to the corresponding amplitude patterns for incident SV waves with the same wavenumber  $(k_x, k_y)$ . In general, the amplitudes resulting from incident SV waves are less than those resulting from SH waves, except in the case of vertical incidence when the distinction between SH and SV is meaningless. For wide angles of incidence, such as 39 degrees in Figures 10g and 10h, the difference is very marked, with there being strong amplification for SH and virtually no amplification for SV.

A relevant feature of P waves inside the heterogeneity, here and in Figure 6, is that, since the P wave velocity is the same everywhere (Figure 2), when an incident P wave is evanescent the P waves with the same horizontal wavenumber are evanescent throughout the whole heterogeneity. In this case, these P waves are unable to transport seismic energy vertically, though they do transport it horizontally. This obviously impedes the occurrence of resonance-like phenomena which rely on constructive interference of multiply-reflected waves with vertical components to their directions of propagation. The reason for SV incidence giving rise to less amplification than SH incidence, is that SV waves couple strongly inside the heterogeneity to P waves with the same horizontal wavenumber. Also, this is the likely reason

for the amplitude patterns for the cases of incident evanescent P waves being very similar to the amplitude patterns for the corresponding incident SV waves, as for both P and SV incidence only the one wave-type, SV, can contribute significantly to amplification within the heterogeneity.

The last point to note is the large variations in amplitude at the same sites between the different solutions in Figure 10, which are all for the same frequency 3 Hz. As already remarked, these variations are very similar in magnitude to the variations in spectral ratios for different earthquakes that were observed in Christchurch by Taber and Cowan (1993). To perform a fair comparison with these observations, it is necessary to exclude the results for  $(k_x, k_y) = (0,2), (2,0), (0,4)$  and  $(4,0)$ , since, as explained in connection with Figure 6, these are all for incident waves that would have to be generated inside the 500 m thick alluvial deposits, rather than by earthquakes deep below the alluvium. Also, one should limit attention to incident S waves, which give rise to the largest amplitudes in earthquakes. This leaves only the 4 solutions in Figures 10a and 10b for  $(k_x, k_y) = (0,1)$  and  $(1,0)$  which can be compared with the solution in Figure 7h for  $(k_x, k_y) = (0,0)$ . Even so, the largest variations in amplitude at the same sites are still equally large between these 5 solutions.

Of particular interest in this regard are the comparisons of the solution in Figure 7h for  $(k_x, k_y) = (0,0)$  with the solutions for  $(k_x, k_y) = (1,0)$  in Figure 10a and for  $(k_x, k_y) = (0,1)$  in Figure 10b respectively. Nearly vertically incident SH waves from earthquakes due west of Christchurch will result in wavefields dominated by the solution for  $(k_x, k_y) = (0,0)$  in Figure 7h and the solution for  $(k_x, k_y) = (1,0)$  in Figure 10a, with the weights assigned to each of the fundamental solutions in the expansions of the wavefields being dependent on the angles of incidence: for angles of incidence very close to vertical the solution for  $(k_x, k_y) = (0,0)$  will make the largest contributions, whereas for angles close to 90 degrees the contributions from this fundamental solution will be less important than the contributions from the solution for  $(k_x, k_y) = (1,0)$ . Similarly, nearly vertically incident SV waves from earthquakes due north of Christchurch will result in wavefields dominated by the same solution for  $(k_x, k_y) = (0,0)$  and the solution for  $(k_x, k_y) = (0,1)$  in Figure 10b. The differences in amplitude between each of these two pairs of solutions is indicative of the likely variation in amplification at any given site for earthquakes from the same azimuth.

In summary, the examples in this section illustrate the following characteristics of the solutions. First, how much the surface layers influence the ground motion depends on the frequency of the waves. At low frequencies up to 1.5 Hz for model A and 2.25 Hz for model B the surface layers have almost no influence, whereas at higher frequencies the influence of the surface layers is strong, especially where the layer of soft sediment is thickest. Elsewhere, where the gravel layer is thick, the wavefield modelling predicts strong amplification at frequencies 3 Hz and higher for model A and 3.75 Hz and higher for model B, though such amplification was not observed by Taber and Cowan (1993). In all cases, the secondary wavefields scattered within the surface layers have seemingly random, standing-wave-like patterns. Further points from the examples in Figure 10 are included in the conclusions below.

## CONCLUSIONS

From this first wavefield-modelling study of 3-dimensional seismic wave amplification in shallow soil layers in a simple alluvial setting, there are both positive and negative conclusions. On the positive side, it has been demonstrated that the 3-dimensional wavefields in such environments do indeed have a highly spatially-variable, random-like character, and that the seemingly-random nature of the spatial variability becomes increasingly marked with increasing frequency. Furthermore, there is considerable variation at individual points between the wavefield amplitudes resulting from different incident disturbances at the same frequency. Among the features illustrated are (i) that the frequencies at which phenomena like resonances occur depend critically on the wave velocities, (ii) that evanescent P waves result in very similar wavefields to those generated by incident SV waves with the same horizontal wavenumbers, (iii) that SV waves with wide angles of incidence give rise to very little amplification, whereas (iv) the amplification resulting from SH incidence is much less dependent on the angle of incidence, and (v) that the amplitudes resulting from incident SH waves are generally larger than the amplitudes resulting from SV incidence.

The negative result is that even with a high density of geotechnical data from well-logs, including results of penetration tests, this is not adequate to define the S wave velocities and

attenuation properties sufficiently well for the wavefield modelling to make accurate predictions of wave amplitudes. In fact, in some features of the distribution of S wave velocities the inferences from the well-logs made using empirical relationships have been in error, since they lead to predictions of strong wavefield amplification in instances where this is not observed. What is needed are direct measurements of the elastic properties, such as those obtained in Wellington by Stephenson and Barker (1992). In addition, more observations of earthquakes like those made by Taber and Cowan (1993) would help to refine the model of the S wave velocities and  $Q_s$  attenuation factors. Ideally these observations should be made at many more sites, and for a much longer time to ensure that an adequate number of earthquakes are recorded. Even so, the uncertainty remains over how to correct for the difference between incident waves in central Christchurch and wavefields at the distant deep rock site which Taber and Cowan use as their reference site.

What has been learnt about seismic hazard in central Christchurch is that a subdivision, or microzonation, of the small 1 km x 1 km area into regions likely to respond differently during major earthquakes can be made according to the relative thicknesses of the soil layers in the top 20 m. In particular, where the surface layer of soft sediment occupies over 30% of the top 20 m the motion of the ground surface at frequencies around 2.5 Hz is likely to be of the order of 5 times larger than elsewhere. There are a number of moderately high buildings (see Figure 1) for which amplification of ground motion in this frequency range is a seismic risk. Deep piles, for example, in the soft sediment are likely to have to cope with horizontal ground motion at the surface that is several times larger than the ground motion at the bottom of each pile. Precise predictions of the likely levels of amplification elsewhere in central Christchurch cannot be made using wavefield modelling until better information becomes available about the distribution of S wave velocities and  $Q_s$  values. All the same, it has been demonstrated that any marked amplification that does occur in the top 20 m, other than where the soft sediment layer is thick, is likely to be for frequencies 3 Hz or higher.

In all instances where marked amplification occurs in one of the regions into which central Christchurch can be microzoned, the amplitude of the ground motion at each frequency is very likely to be highly variable in that region, with amplitudes differing by up to a factor of 5 between points as close as 50-100 m apart; that is, it is highly likely that there will be points,

for instance, where very little amplification occurs even though the amplification at neighbouring points in the same region is large. Much the same applies at each site for earthquakes in slightly different positions or with different source mechanisms and rupture processes: it is likely that there will be much less amplification for some earthquakes than for others. Consequently, for zones where marked amplification is likely, the answer to the question of whether it is possible to predict exactly how a particular site will be shaken in a given earthquake, is that this is not possible in practice. That is the case even if the S wave velocities and  $Q_s$  values are known precisely both in the vicinity of the site and everywhere between there and the earthquake's source, since it is extremely unlikely that the location, source mechanism and rupture pattern of the earthquake can be predicted accurately enough. A better-posed question is whether for a region like central Christchurch it is possible to predict for each frequency the likely range of amplifications at a given site for earthquakes from particular azimuths. This can be predicted provided enough is known about how all the elastic properties and, especially, the near-surface S wave velocities and  $Q_s$  values are distributed in that region.

#### ACKNOWLEDGMENTS

Helpful comments on this manuscript were provided by Euan Smith, and Soils and Foundations Ltd supplied the well-logs from which the layer thicknesses were obtained. As well, the authors are especially grateful to The Earthquake Commission for the financial support it has provided, including the support for Yu Jiashun's Ph.D. studies.

#### REFERENCES

Benites, R.A. and A.J. Haines (1991) "The Riccati matrix equation - boundary integral method to compute seismic wavefields in heterogeneous media", EOS, Transactions, American Geophysical Union, Vol. 72, No. 44, 332 (abstract).

- Berrill, J.B., R.O. Davis and I.F. McCahon (1993) "Christchurch seismic hazard pilot study", Bull. NZ Nat. Soc. Earthquake Engineering, 26, 14-27.
- Elder, D.McG., I.F. McCahon and M.D. Yetton (1991) "The earthquake hazard in Christchurch: a detailed evaluation", Research report to EQC, Soils and Foundations Ltd, 131pp.
- Haines, A.J. (1989) "On the structure of one-way elastic-wave propagation and exact solutions to the elastodynamic equations: theory for 2-dimensional SH waves", 259pp monograph.
- Haines, A.J. (1993) "Developments in computer modelling of microzonation effects", Proc. Tech. Conf. NZ Nat. Soc. Earthquake Engineering.
- Haines, A.J. and R.A. Benites (1992) "Three dimensional seismic response of irregular sedimentary deposits", EOS, Transactions, American Geophysical Union, Vol. 73, No. 43, 339 (abstract).
- Haines, A.J. and M.V. de Hoop (in prep) "Generalised Riccati equation for multi-dimensionally heterogeneous anisotropic, poro-elastic inclusions", Geophysical Journal International.
- Marsh, J., T.J. Larkin, A.J. Haines and R.A. Benites (in press) "Comparison of linear and non-linear seismic responses of 2-dimensional alluvial basins", Bull. Seism. Soc. Am.
- Stephenson, W.R. and P.R. Barker (1992) "Evaluation of sediment properties in the Lower Hutt and Porirua areas by means of cone and seismic cone penetration tests", Bull. NZ Nat. Soc. Earthquake Engineering, 25, 265-285.
- Taber, J.J. and H.A. Cowan (1993) "Measurements of earthquake ground shaking at characteristic sites in Christchurch", Research report to EQC, 38pp.

## FIGURE CAPTIONS

Figure 1: Central Christchurch, showing the 1 km x 1 km "large region" and 650m x 650m "small region" for which wavefield modelling was performed

Figure 2: The models of the distribution of elastic properties in the top 20 m beneath central Christchurch used in the wavefield modelling. The layer thicknesses are from well-logs, and in model A the distribution of S wave velocities is derived from inferences made by Elder et al. (1991) from penetration results. In model B all the S velocities are increased by 50 m/s to demonstrate the sensitivity of the wavefield modelling to such changes.

Figure 3: The horizontal wavenumbers ( $k_x, k_y$ ) in the Fourier expansions of the wavefields with respect to the cross-range variables. Three sets of wavenumbers were used in the wavefield modelling: the innermost set contains 109 wavenumbers, the next set including the darkly-shaded area contains 145 wavenumbers, and the largest set contains 193 wavenumbers. For each of the components  $k_x$  and  $k_y$  the magnitude of the value is the number of cycles across the area being considered, and for  $k_x$  positive and negative signs indicate propagation from the west and east respectively, while for  $k_y$  these signs indicate propagation from the north and south.

Figure 4: Wavefield amplitudes for the case of vertically incident 3 Hz S waves with ground motion in the east-west X direction. Total-wavefield amplitudes for the 3 components  $U_x$ ,  $U_y$  and  $U_z$  are shown (a) at the bottom of the 20 m thick zone (Level 3) and the boundary between the sand and gravel layers (Level 2), and (b) at the boundary between the gravel and soft-sediment layers (Level 1) and the ground surface (Level 0). In this and subsequent figures, the amplitudes are normalised by setting the combined amplitude of the 3 components of motion in the incident wave to be 1. Here the results are for the "small region" and model A.

Figure 5: Amplitudes for the case of vertically incident 3.75 Hz S waves with ground motion in the north-south Y direction for the "small region" and model B. Everything else is as in Figure 4.

Figure 6: Amplitudes (a) and phases (b) at Levels 3 and 0 for the case of 2.5 Hz SV waves incident from the northeast with horizontal wavenumber  $(k_x, k_y) = (-2, 2)$  for the "large region" and model A. The contour interval in the phase diagrams is 40 degrees. Dashed and solid lines indicate negative and positive phases respectively, and between each pair of thick lines the phase changes by one full cycle, or 360 degrees.

Figure 7: Amplitudes at Levels 1 and 0 for cases of vertically incident S waves with ground motion in the north-south Y direction for model A. Results are shown for the "large region" for (a) 1 Hz, (b) 1.5 Hz, (c) 1.75 Hz, (d) 2 Hz, (e) 2.25 Hz and (f) 2.5 Hz, and for the "small region" for (g) 2.5 Hz, (h) 3 Hz, (i) 3.5 Hz and (j) 4 Hz.

Figure 8: Corresponding results for model B for the "small region" to those in Figure 7 for model A. Amplitudes are shown (a) for 3 Hz at Levels 1 and 0 and for 4.5 Hz at (b) Levels 3 and 2 and (c) Levels 1 and 0, and (d) phases are shown for 4.5 Hz at Levels 3 and 0. These results complement those in Figure 5 for 3.75 Hz.

Figure 9: Phases at Levels 3 and 0 for the "small region" and model A for the cases of 3 Hz (a) SH, (b) SV and (c) P waves incident from the north with horizontal wavenumber  $(k_x, k_y) = (0, 2)$ .

Figure 10: Amplitudes at the ground surface (Level 0) for the "small region" and model A for cases of 3 Hz waves incident from the north and incident from the west: (a) SH, (b) SV and (c) P for  $(k_x, k_y) = (0, 1)$  and  $(1, 0)$ , (d) SH, (e) SV and (f) P for  $(k_x, k_y) = (0, 2)$  and  $(2, 0)$ , and (g) SH, (h) SV and (i) P for  $(k_x, k_y) = (0, 4)$  and  $(4, 0)$ .



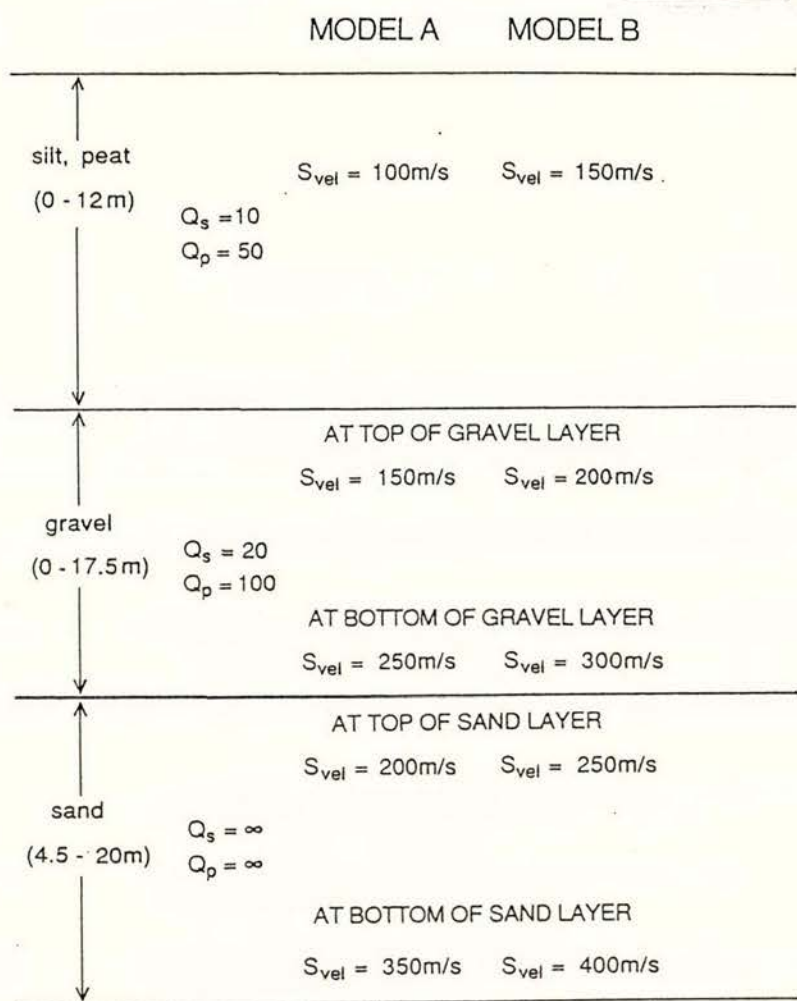
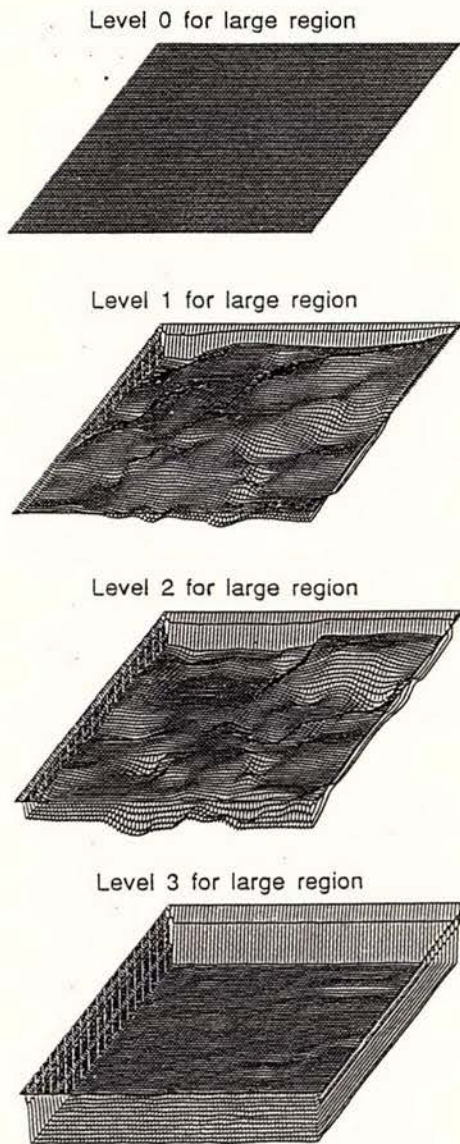
Figure 1

City of Christchurch: Central Area

Height of Buildings in Central Commercial Zones (Note: not RSA etc.)

■ 5 - 9 stores      ■ 10+ stores

**Figure 2**



THROUGHOUT Density =  $2\text{Mg/m}^3$ ,  $P_{vel} = 1500\text{ m/s}$

Figure 3

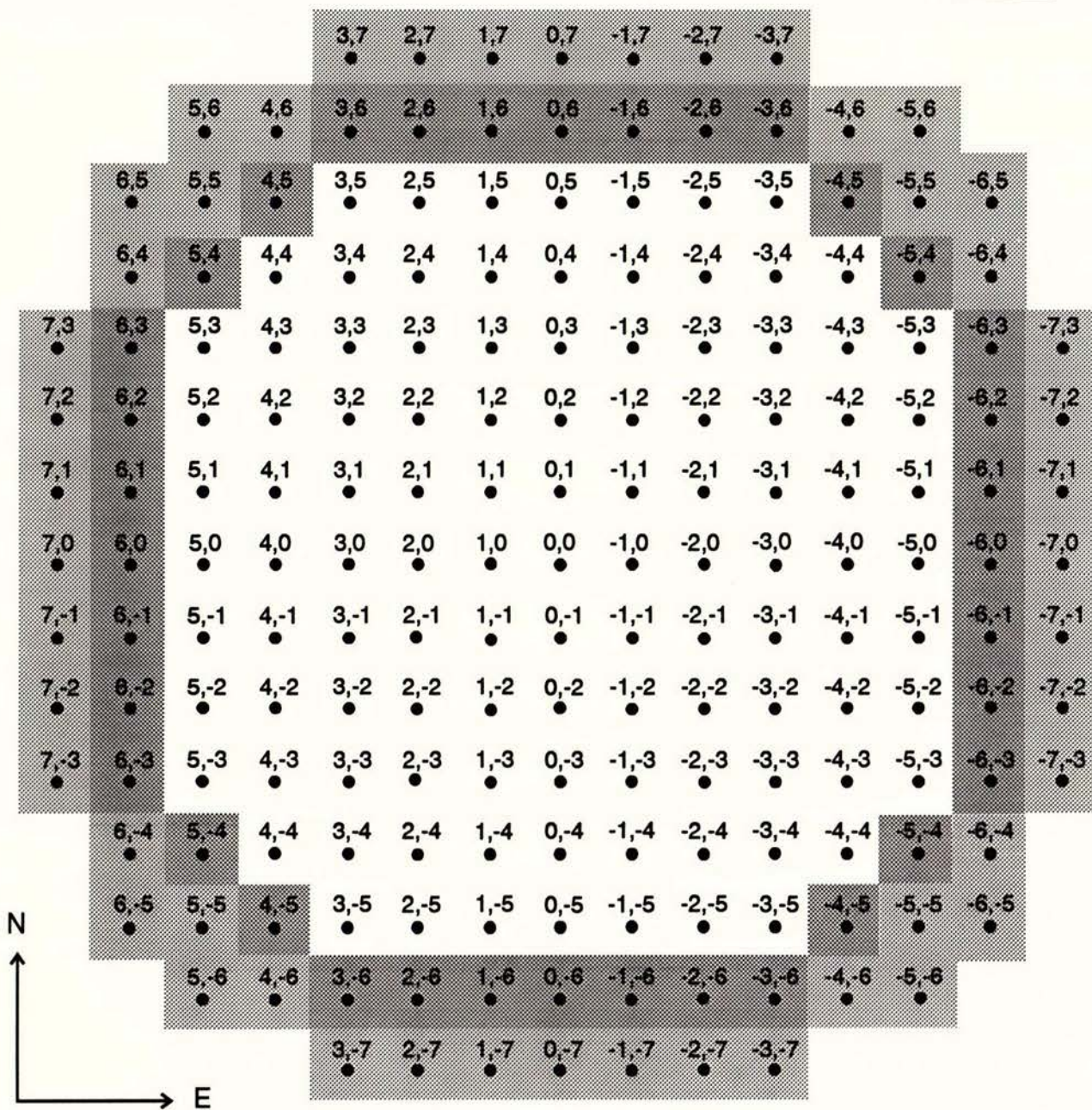
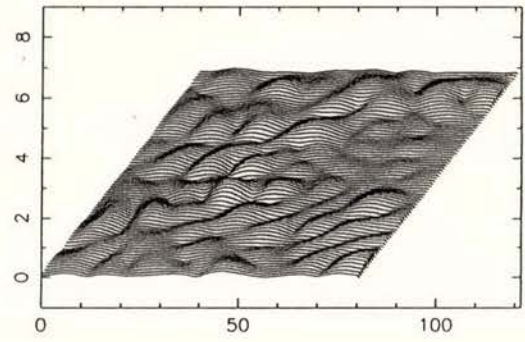
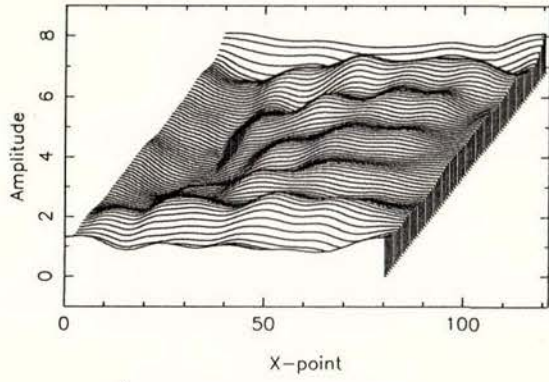


Figure 4a

Ux

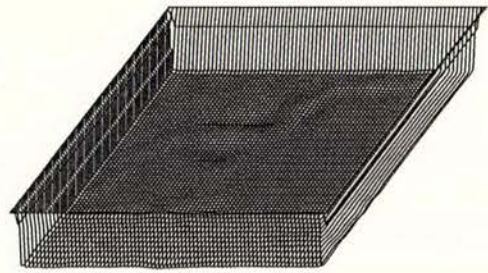
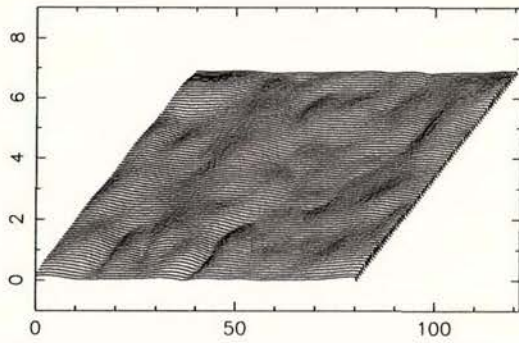
X input with  $(k_x, k_y) = (0, 0)$ , freq = 3.50

Uy



Uz

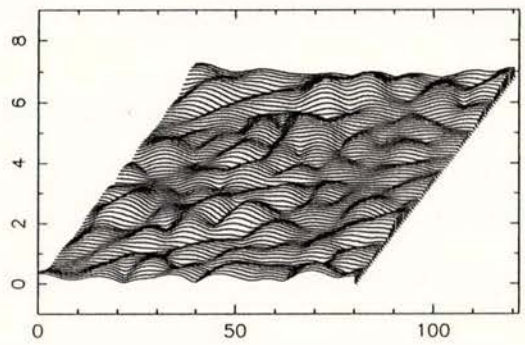
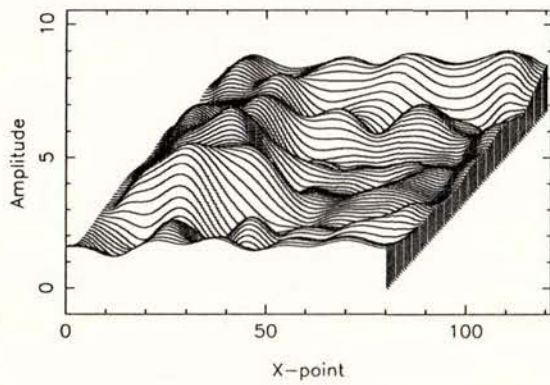
Level 3 for small region, model A



Ux

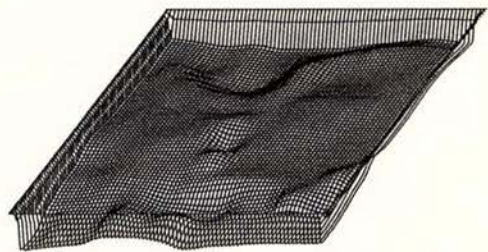
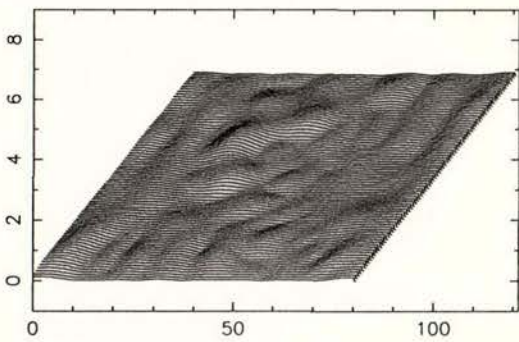
X input with  $(k_x, k_y) = (0, 0)$ , freq = 3.50

Uy



Uz

Level 2 for small region, model A

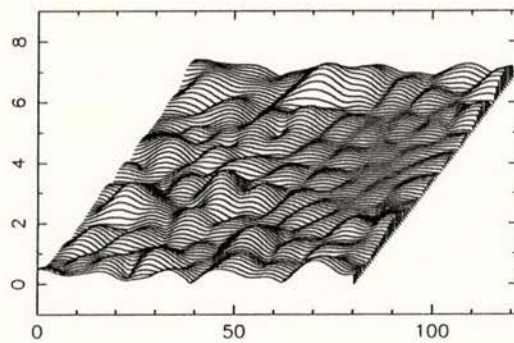
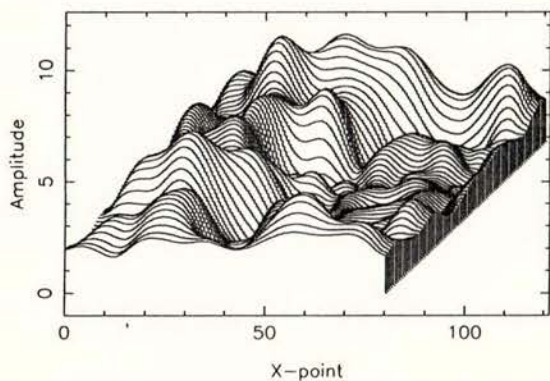


Ux

X input with  $(k_x, k_y) = (0, 0)$ , freq = 3.50

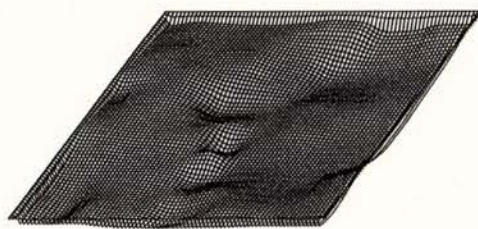
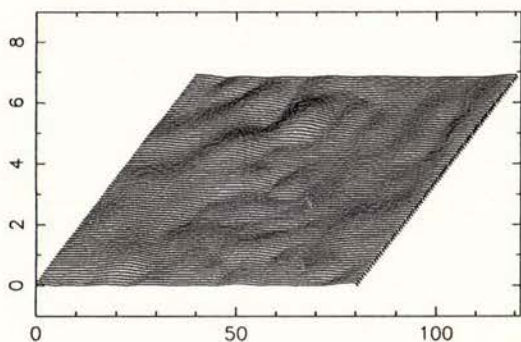
Uy

Figure 4b



Uz

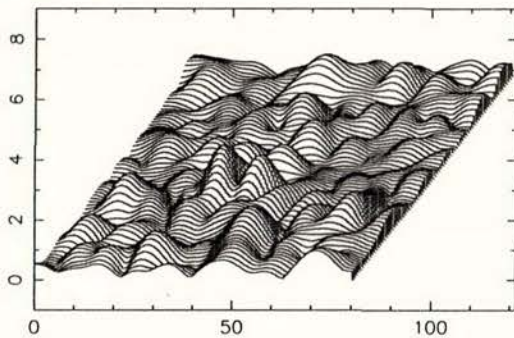
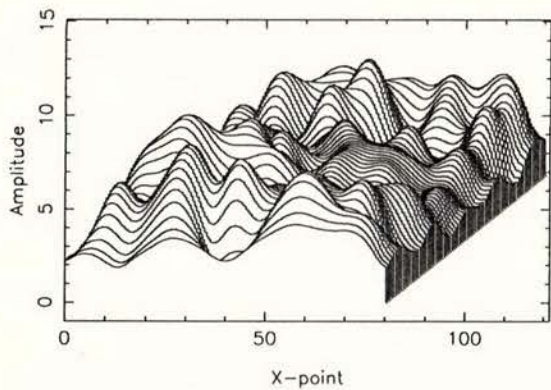
Level 1 for small region, model A



Ux

X input with  $(k_x, k_y) = (0, 0)$ , freq = 3.50

Uy



Uz

Level 0 for small region, model A

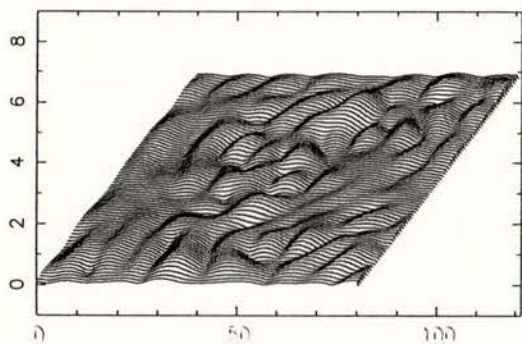
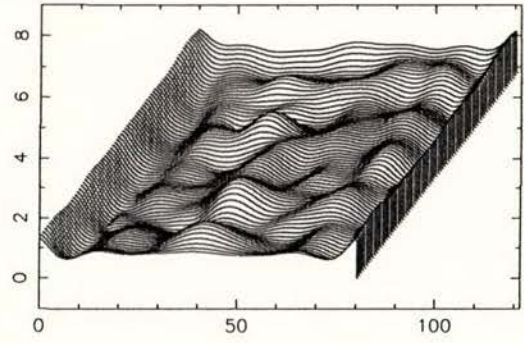
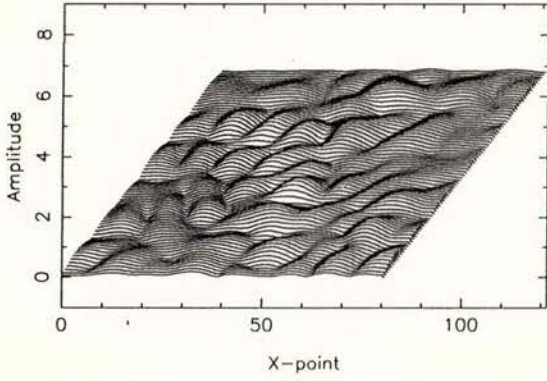


Figure 5a

$U_x$

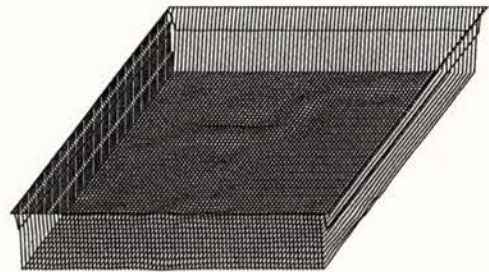
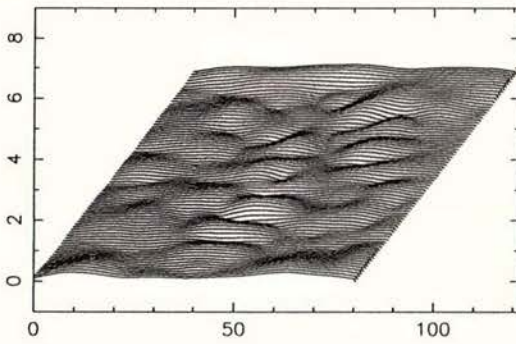
Y input with  $(k_x, k_y) = (0, 0)$ , freq = 3.75

$U_y$



$U_z$

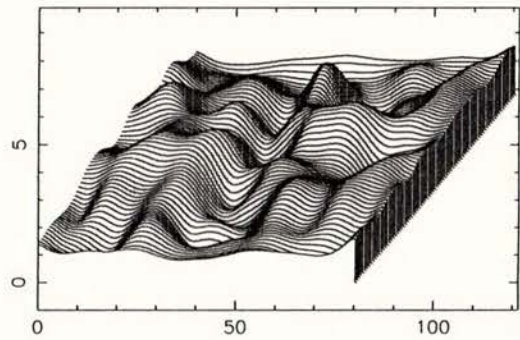
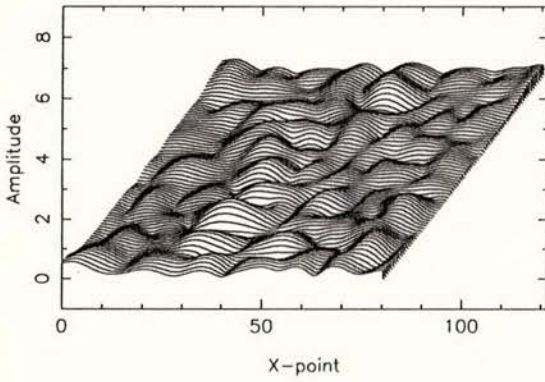
Level 3 for small region, model B



$U_x$

Y input with  $(k_x, k_y) = (0, 0)$ , freq = 3.75

$U_y$



$U_z$

Level 2 for small region, model B

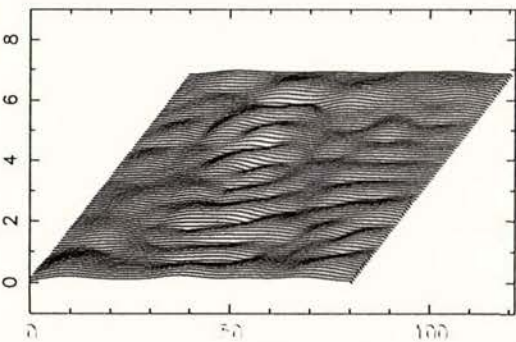
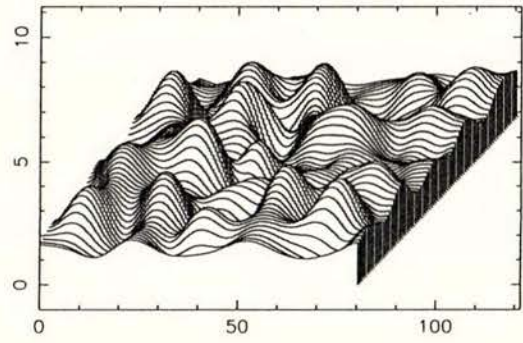
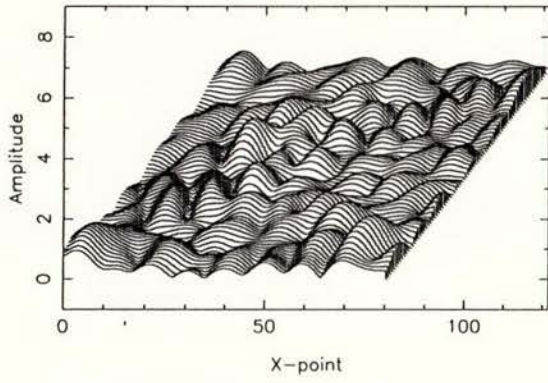


Figure 5b

$U_x$

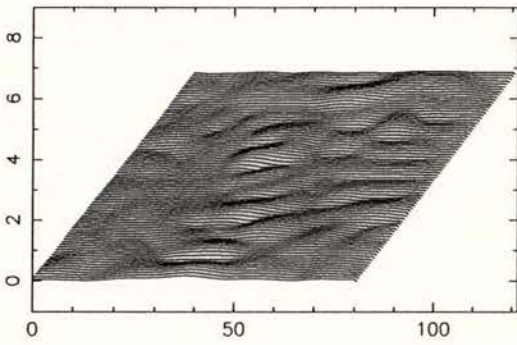
Y input with  $(k_x, k_y) = (0, 0)$ , freq = 3.75

$U_y$



$U_z$

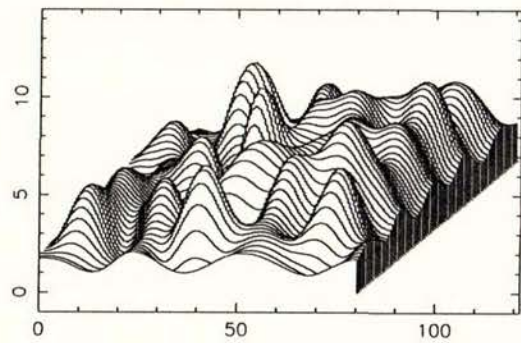
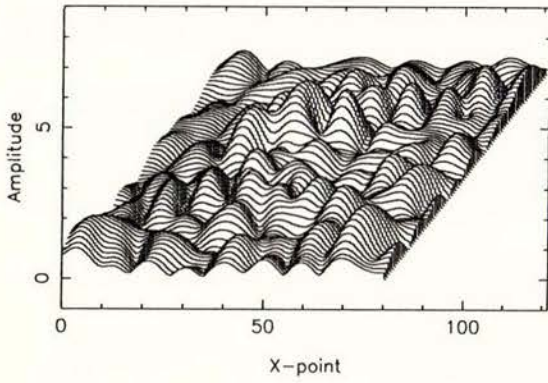
Level 1 for small region, model B



$U_x$

Y input with  $(k_x, k_y) = (0, 0)$ , freq = 3.75

$U_y$



$U_z$

Level 0 for small region, model B

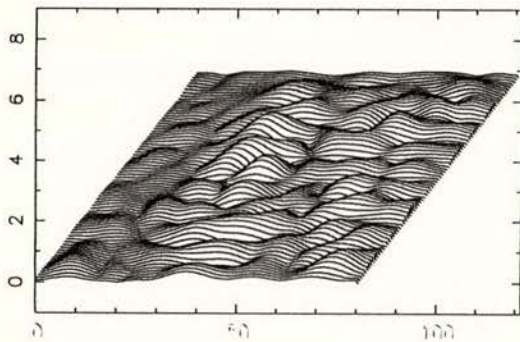


Figure 6a

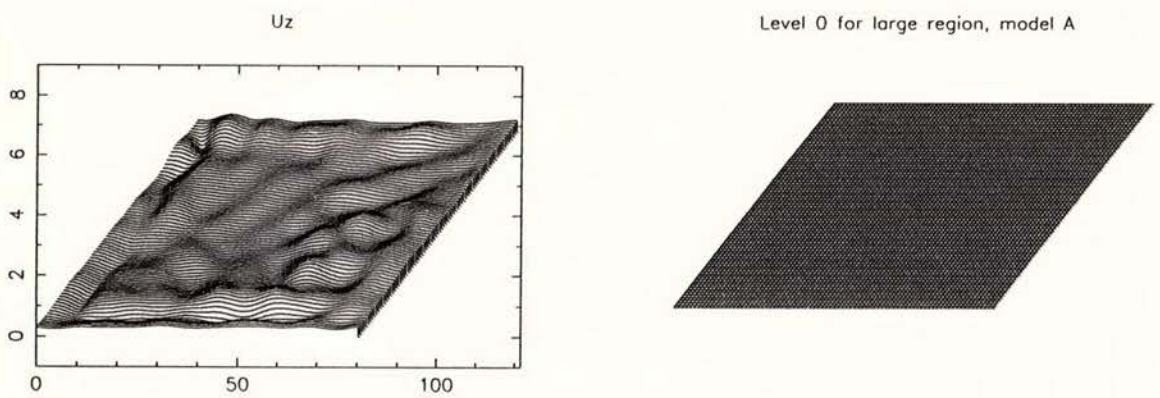
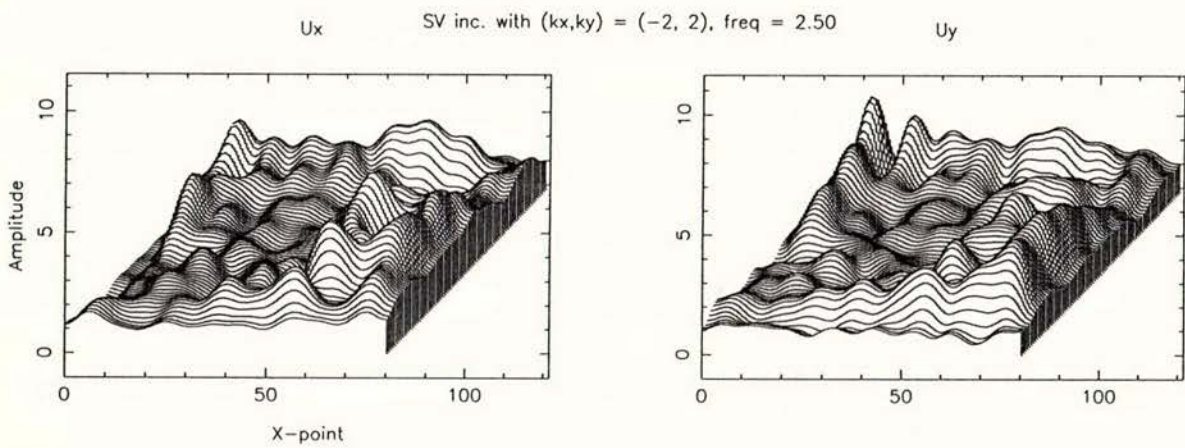
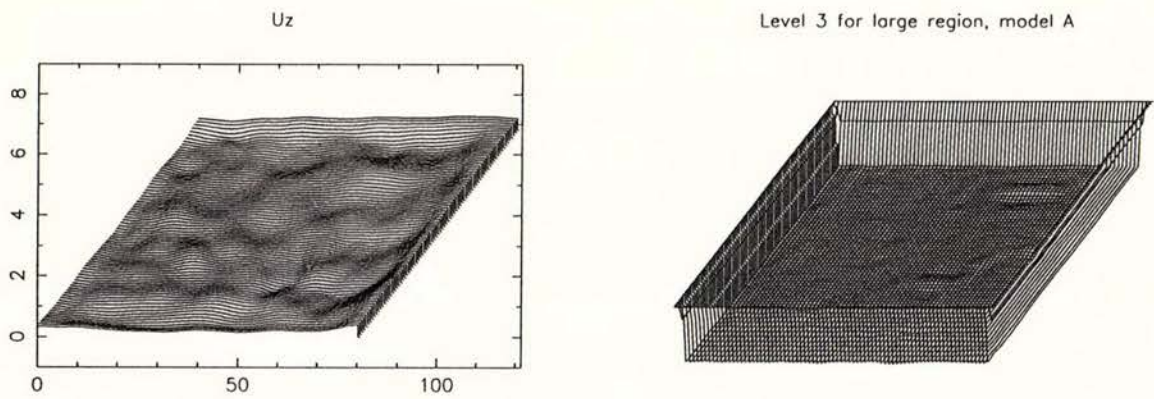
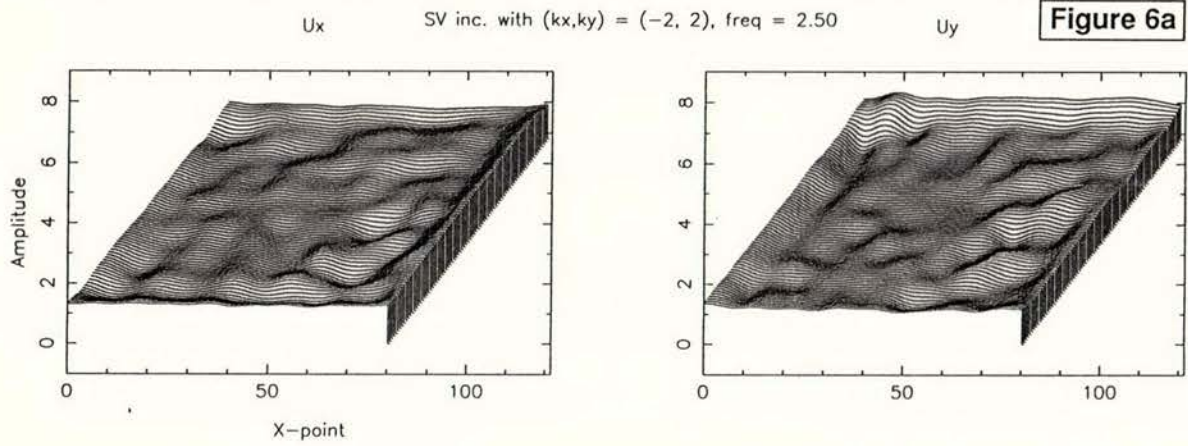
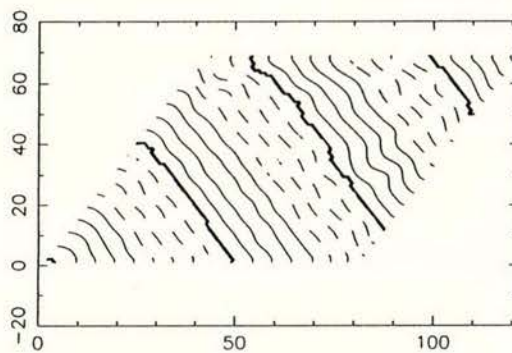
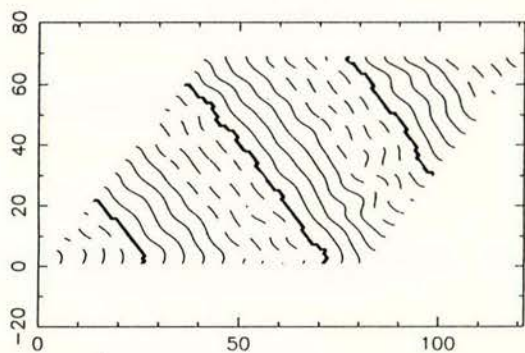


Figure 6b

phase  $U_x$

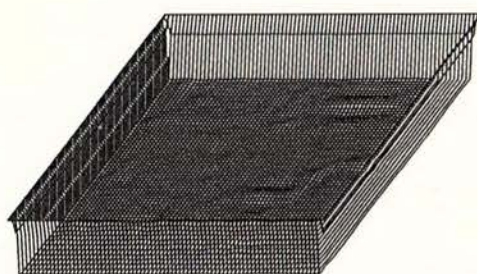
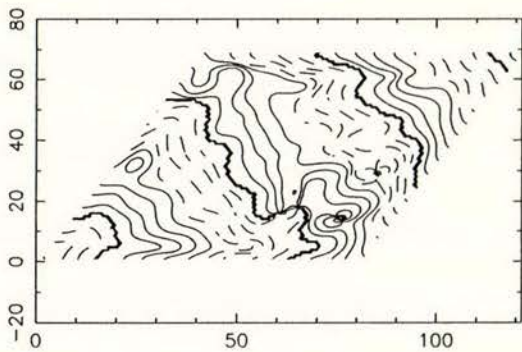
SV inc. with  $(k_x, k_y) = (-2, 2)$ , freq = 2.50

phase  $U_y$



phase  $U_z$

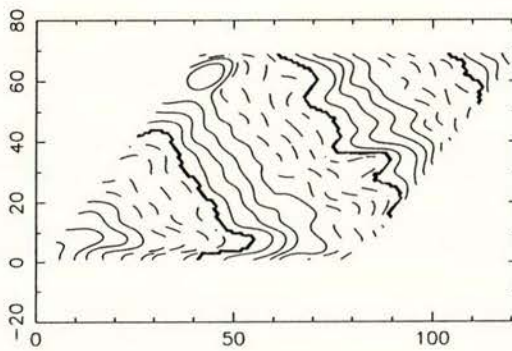
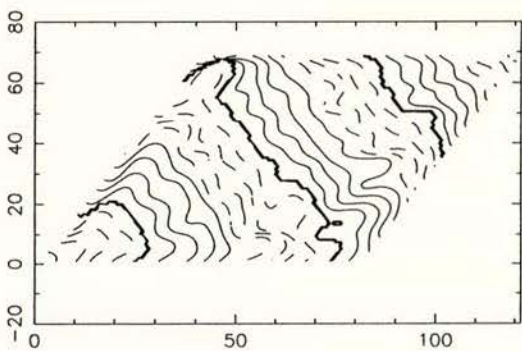
Level 3 for large region, model A



phase  $U_x$

SV inc. with  $(k_x, k_y) = (-2, 2)$ , freq = 2.50

phase  $U_y$



phase  $U_z$

Level 0 for large region, model A

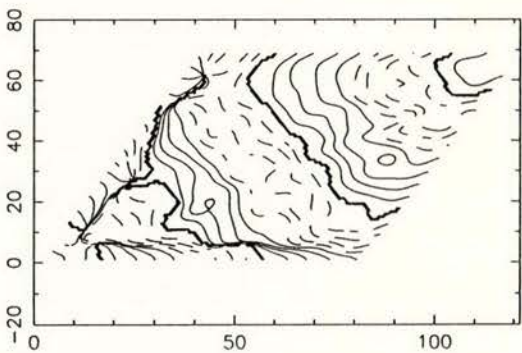
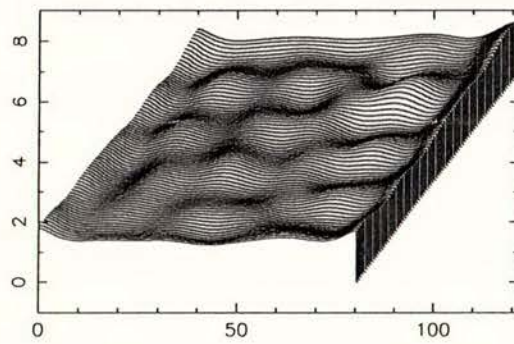
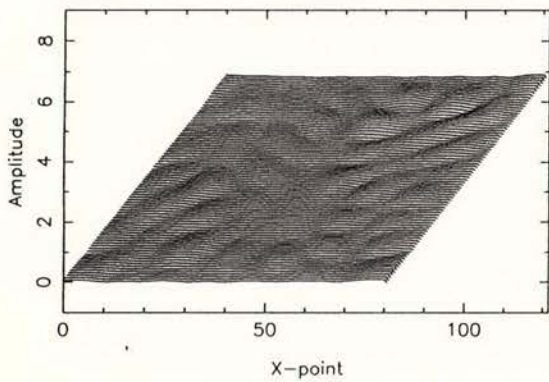


Figure 7a

$U_x$

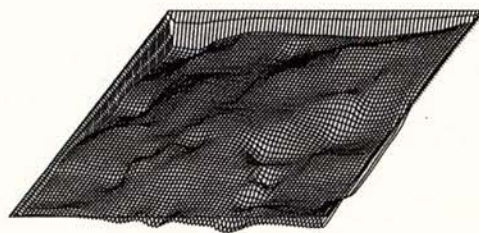
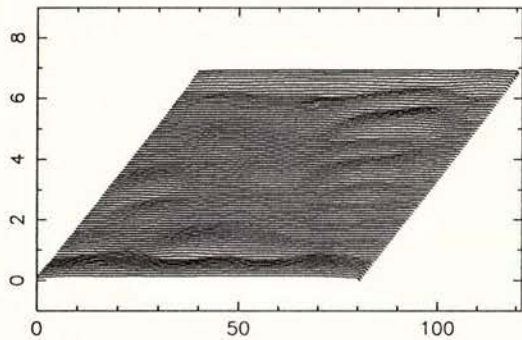
Y input with  $(k_x, k_y) = (0, 0)$ , freq = 1.00

$U_y$



$U_z$

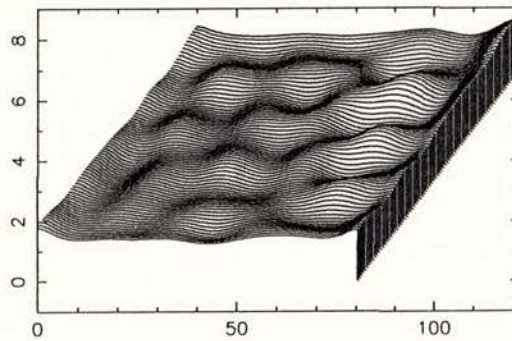
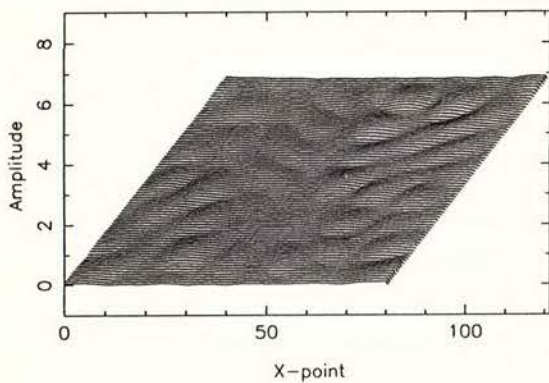
Level 1 for large region, model A



$U_x$

Y input with  $(k_x, k_y) = (0, 0)$ , freq = 1.00

$U_y$



$U_z$

Level 0 for large region, model A

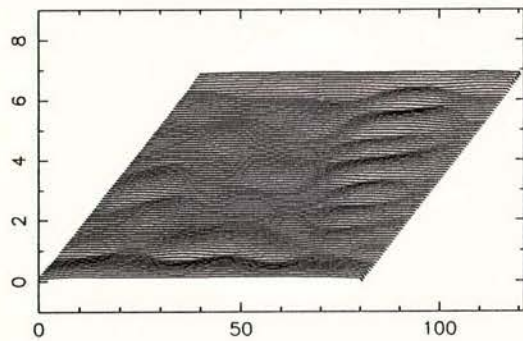
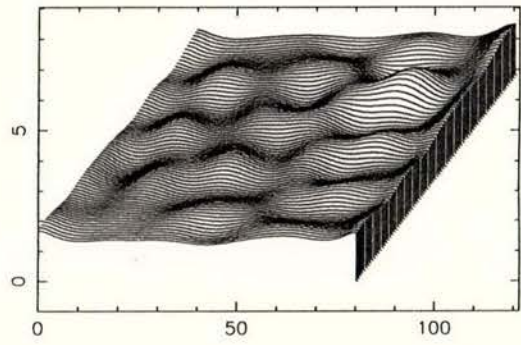
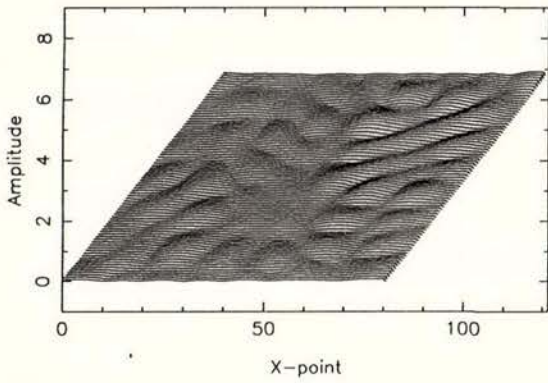


Figure 7b

Ux

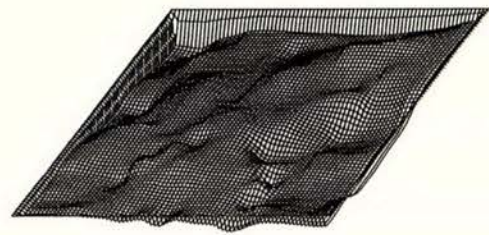
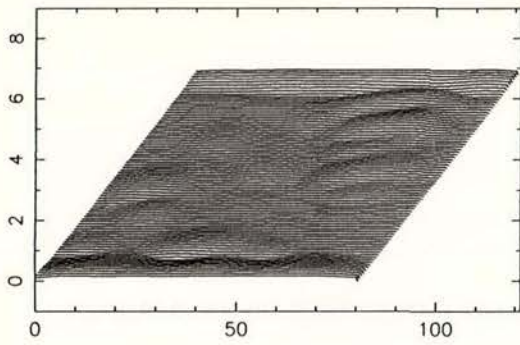
Y input with  $(k_x, k_y) = (0, 0)$ , freq = 1.50

Uy



Uz

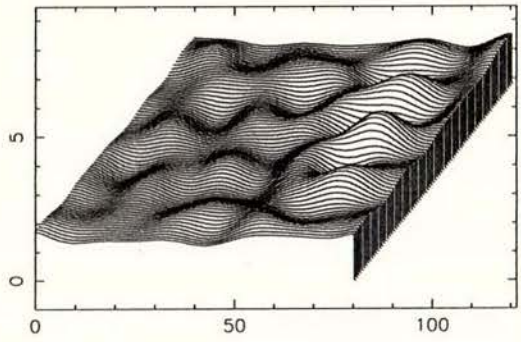
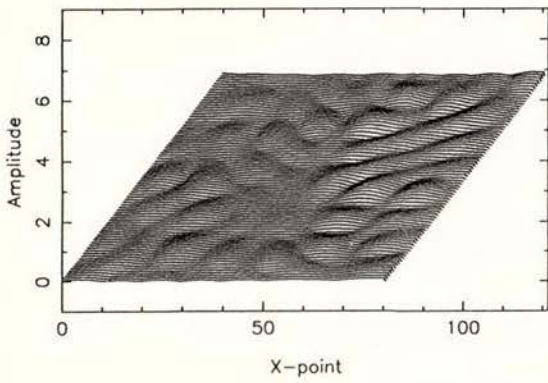
Level 1 for large region, model A



Ux

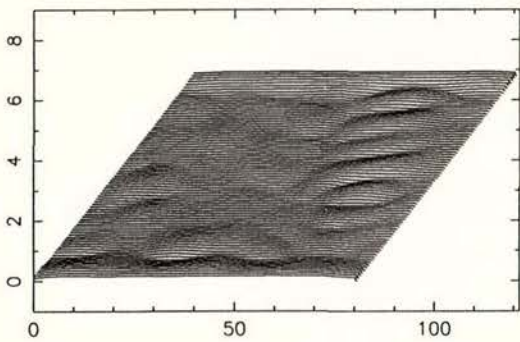
Y input with  $(k_x, k_y) = (0, 0)$ , freq = 1.50

Uy



Uz

Level 0 for large region, model A

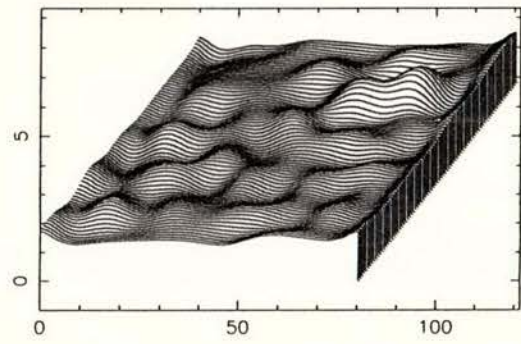
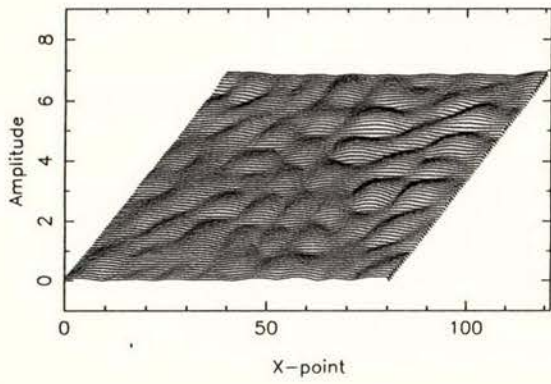


$U_x$

Y input with  $(k_x, k_y) = (0, 0)$ , freq = 1.75

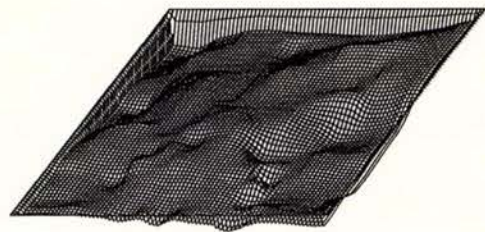
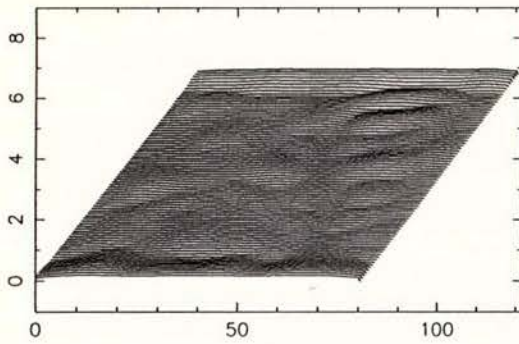
$U_y$

Figure 7c



$U_z$

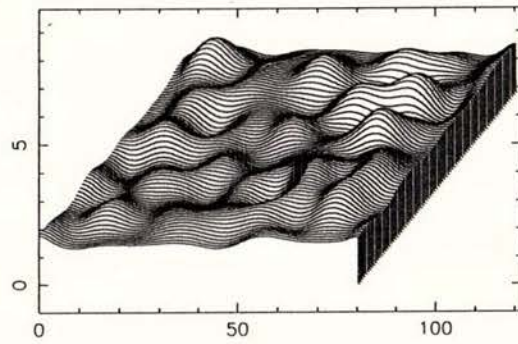
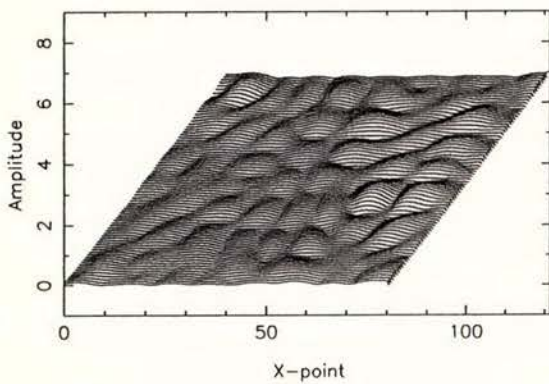
Level 1 for large region, model A



$U_x$

Y input with  $(k_x, k_y) = (0, 0)$ , freq = 1.75

$U_y$



$U_z$

Level 0 for large region, model A

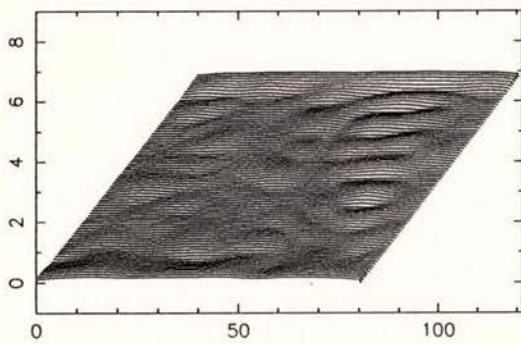
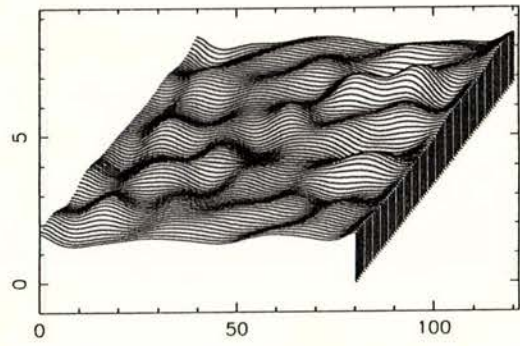
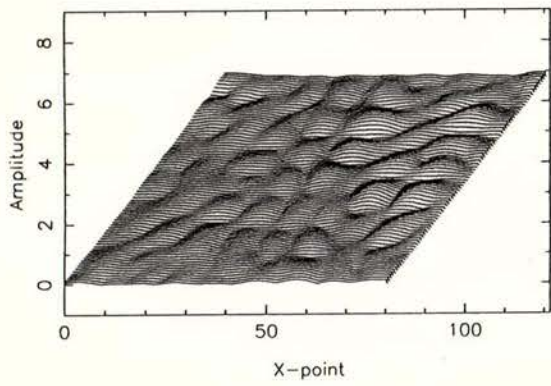


Figure 7d

$U_x$

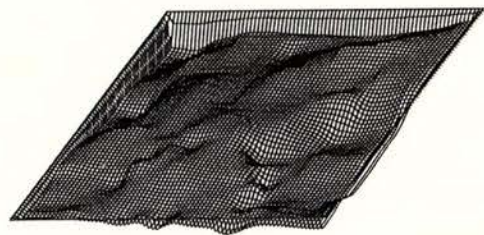
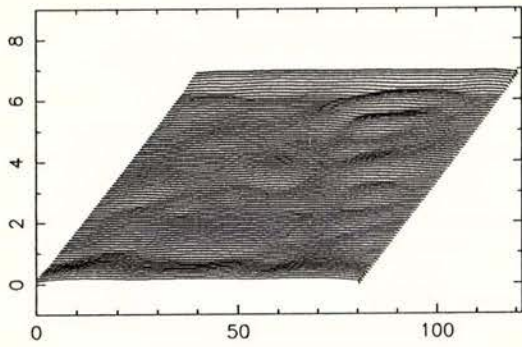
Y input with  $(k_x, k_y) = (0, 0)$ , freq = 2.00

$U_y$



$U_z$

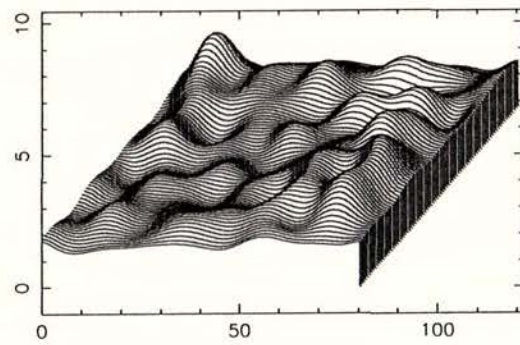
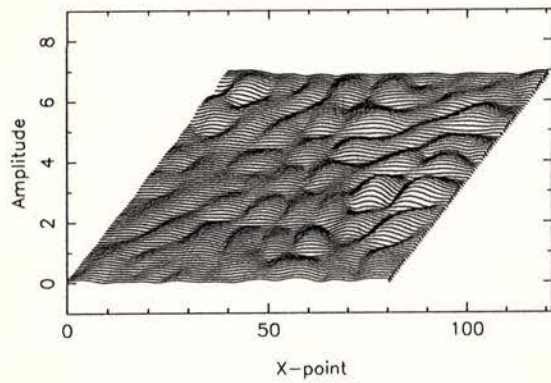
Level 1 for large region, model A



$U_x$

Y input with  $(k_x, k_y) = (0, 0)$ , freq = 2.00

$U_y$



$U_z$

Level 0 for large region, model A

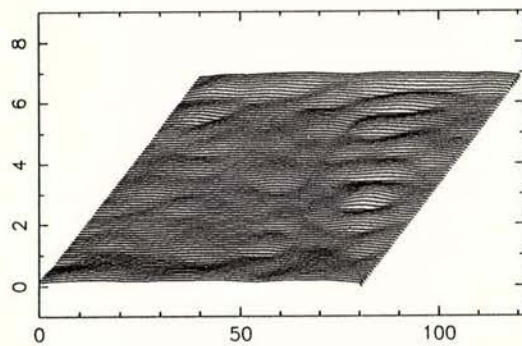
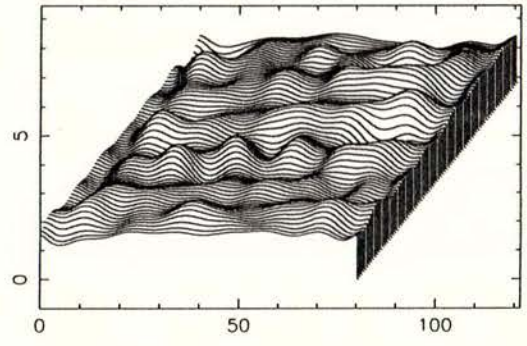
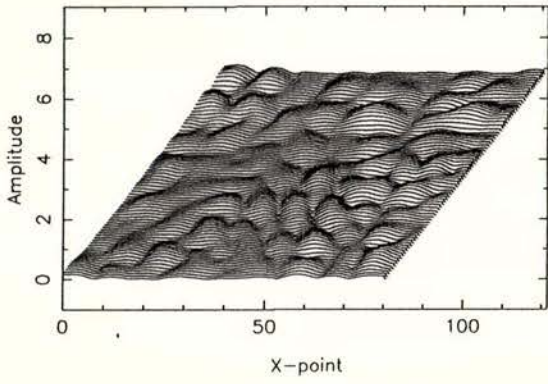


Figure 7e

$U_x$

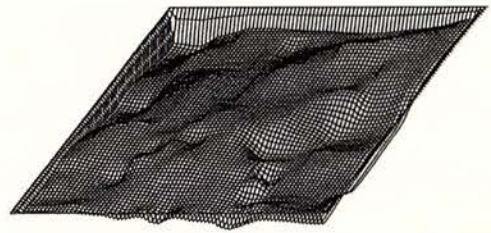
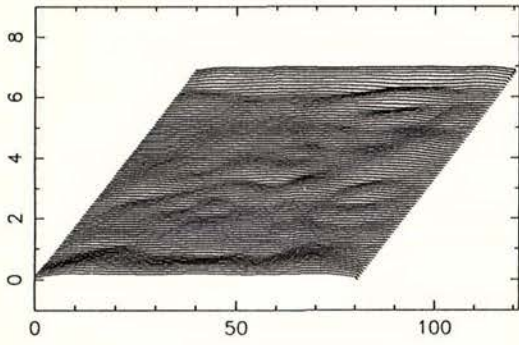
Y input with  $(k_x, k_y) = (0, 0)$ , freq = 2.25

$U_y$



$U_z$

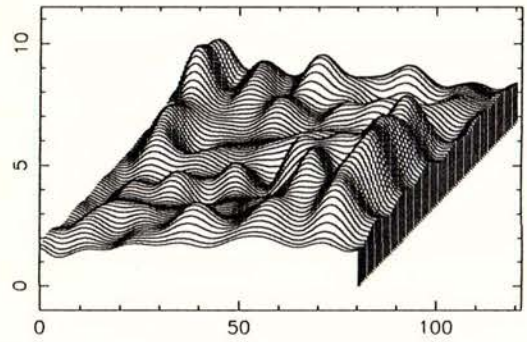
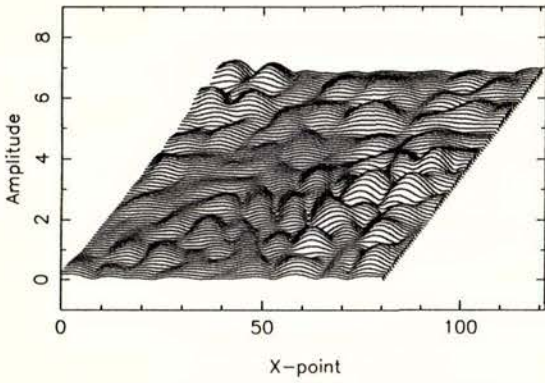
Level 1 for large region, model A



$U_x$

Y input with  $(k_x, k_y) = (0, 0)$ , freq = 2.25

$U_y$



$U_z$

Level 0 for large region, model A

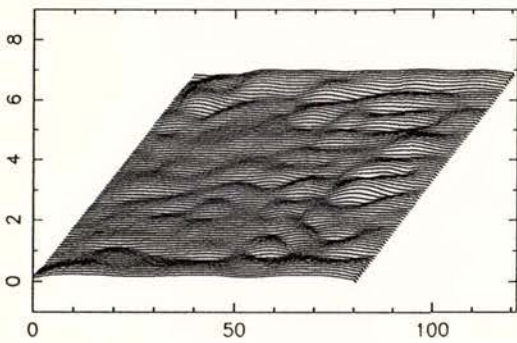
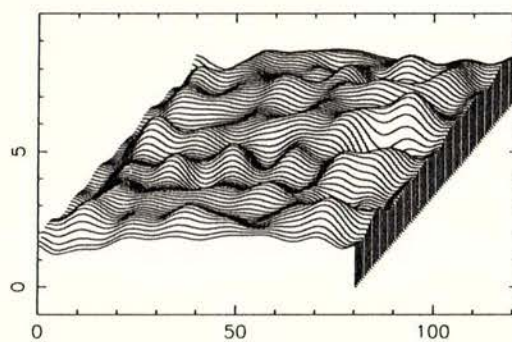
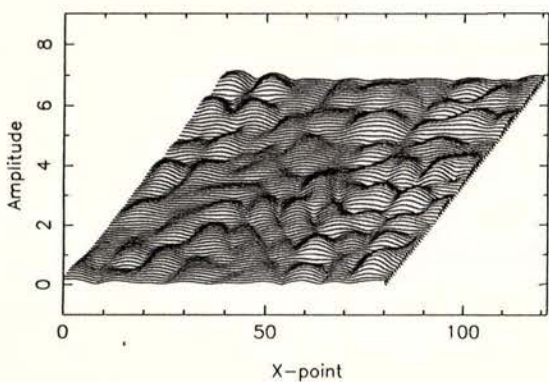


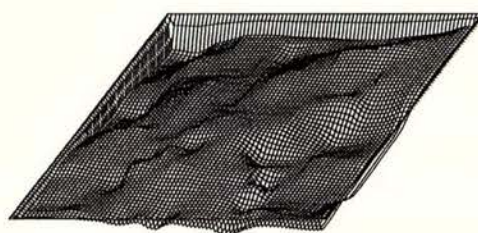
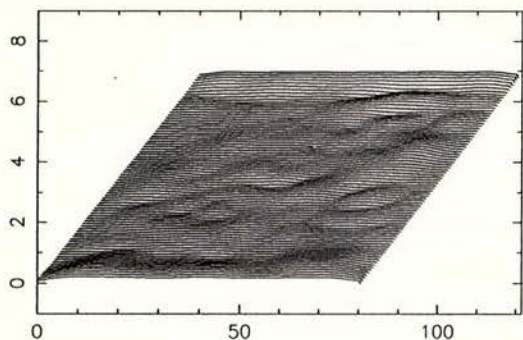
Figure 7f

$U_x$  Y input with  $(k_x, k_y) = (0, 0)$ , freq = 2.50  $U_y$

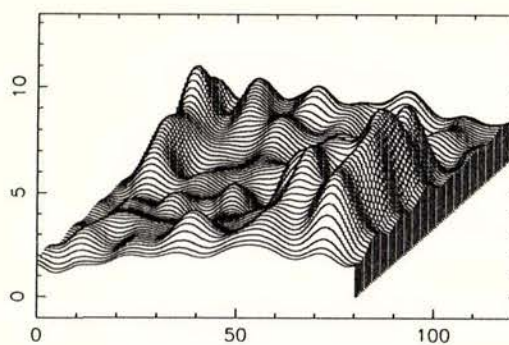
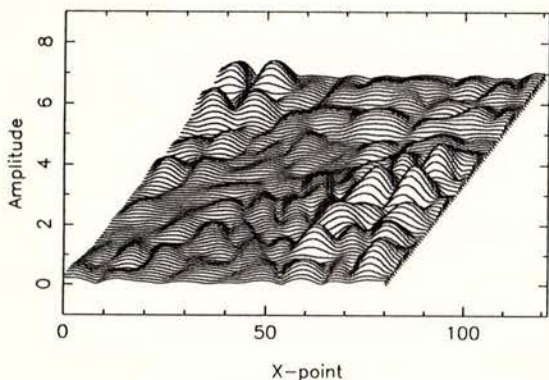


$U_z$

Level 1 for large region, model A



$U_x$  Y input with  $(k_x, k_y) = (0, 0)$ , freq = 2.50  $U_y$



$U_z$

Level 0 for large region, model A

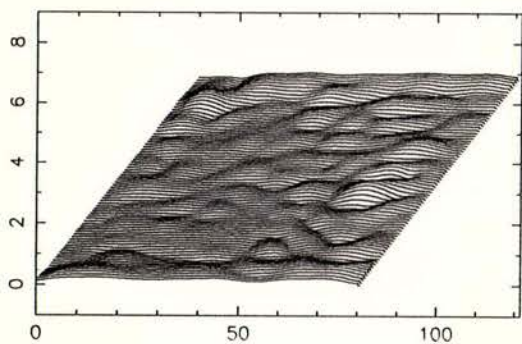
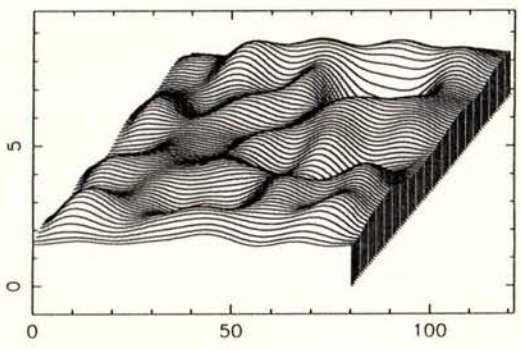
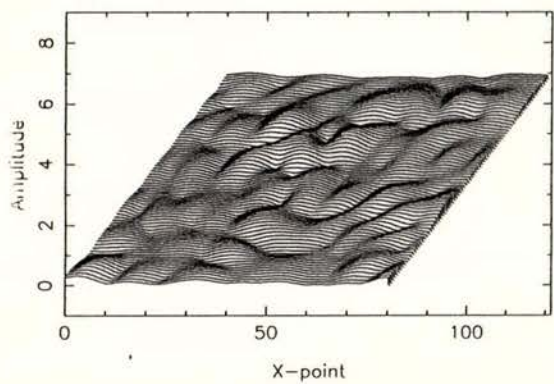


Figure 7g

Ux

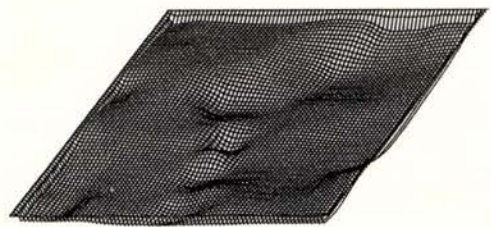
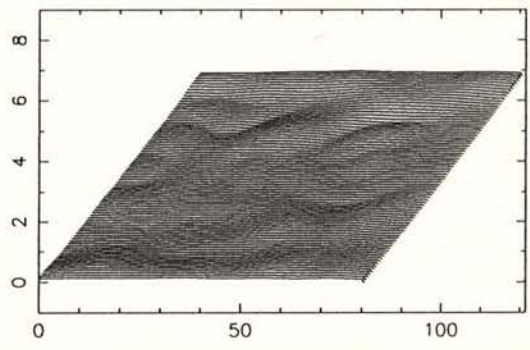
Y input with  $(k_x, k_y) = (0, 0)$ , freq = 2.50

Uy



Uz

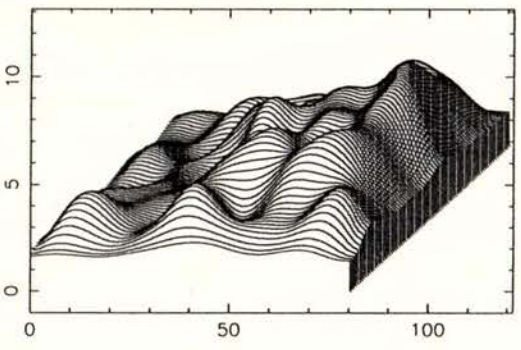
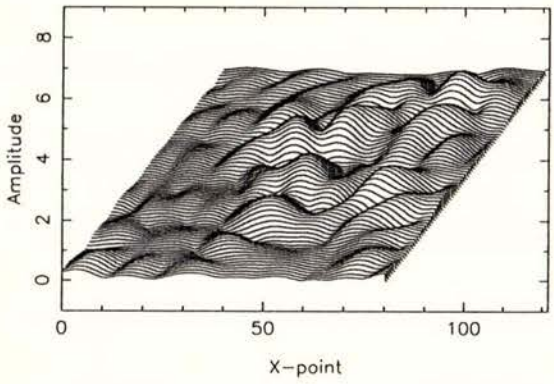
Level 1 for small region, model A



Ux

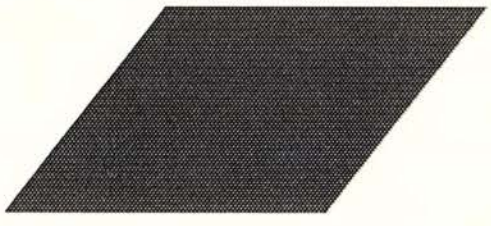
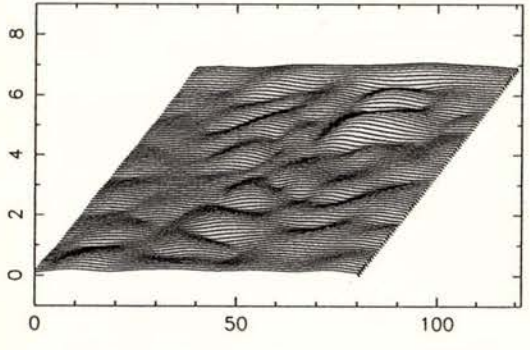
Y input with  $(k_x, k_y) = (0, 0)$ , freq = 2.50

Uy



Uz

Level 0 for small region, model A

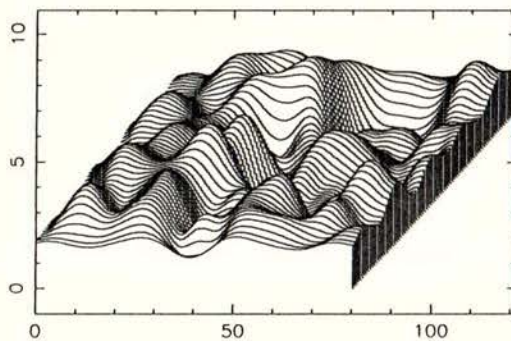
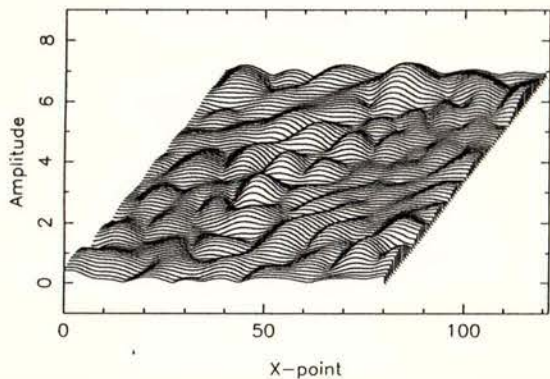


Ux

Y input with  $(k_x, k_y) = (0, 0)$ , freq = 3.00

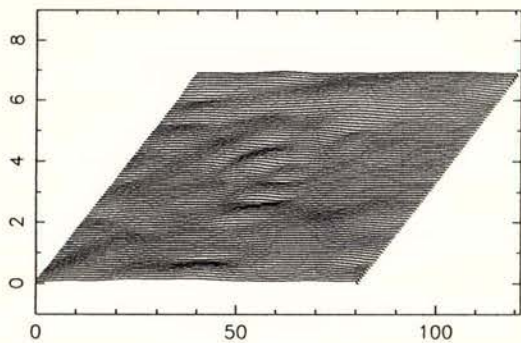
Uy

Figure 7h



Uz

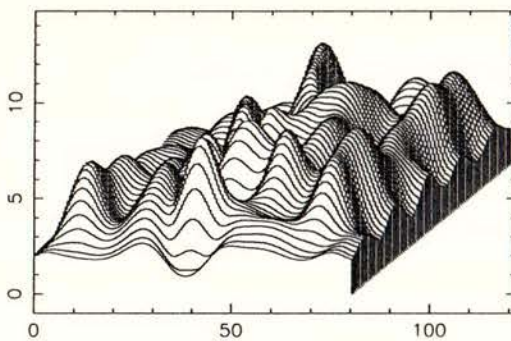
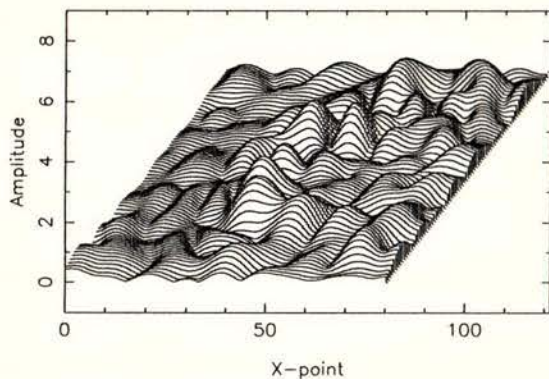
Level 1 for small region, model A



Ux

Y input with  $(k_x, k_y) = (0, 0)$ , freq = 3.00

Uy



Uz

Level 0 for small region, model A

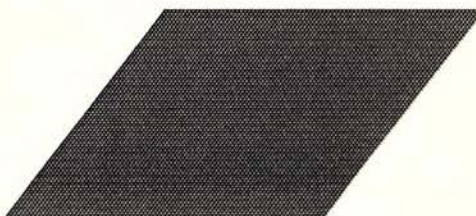
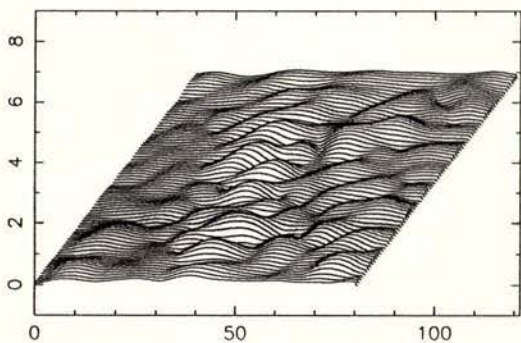
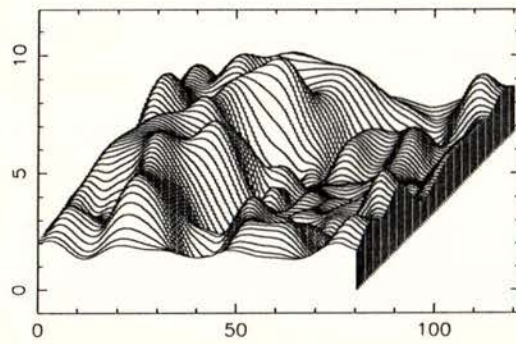
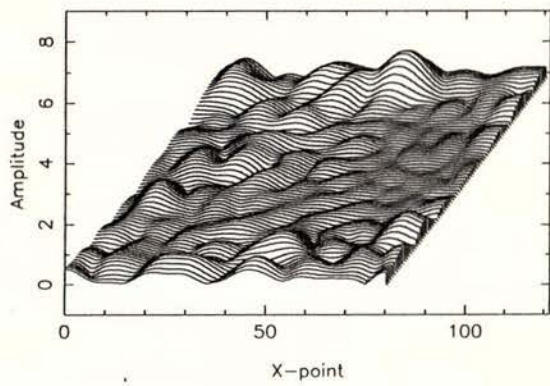


Figure 7i

$U_x$

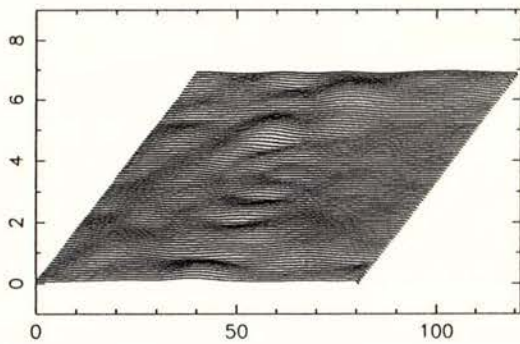
Y input with  $(k_x, k_y) = (0, 0)$ , freq = 3.50

$U_y$



$U_z$

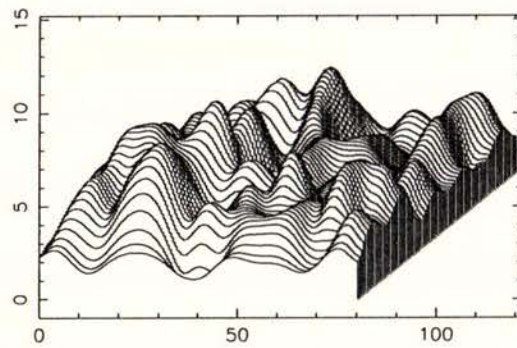
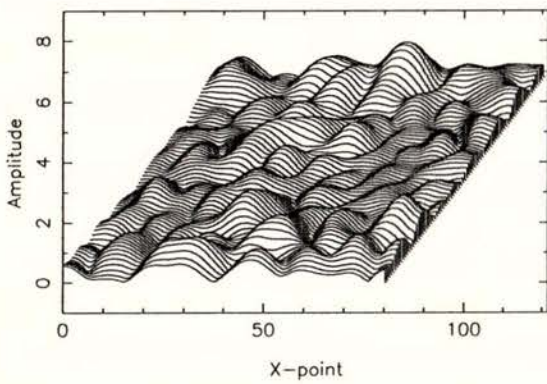
Level 1 for small region, model A



$U_x$

Y input with  $(k_x, k_y) = (0, 0)$ , freq = 3.50

$U_y$



$U_z$

Level 0 for small region, model A

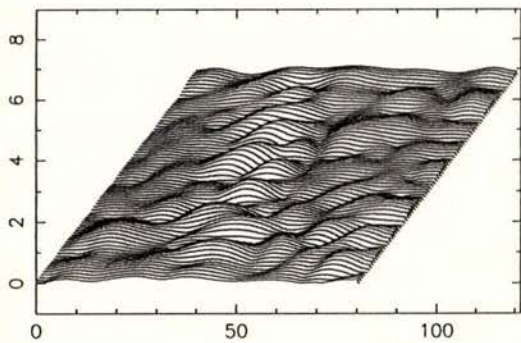
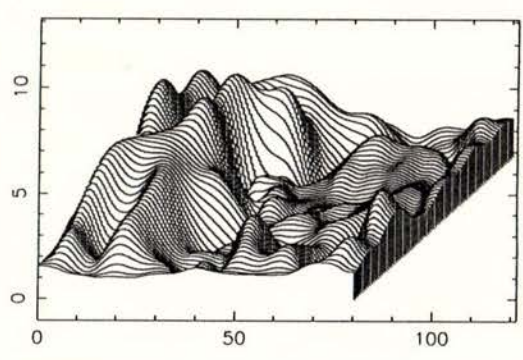
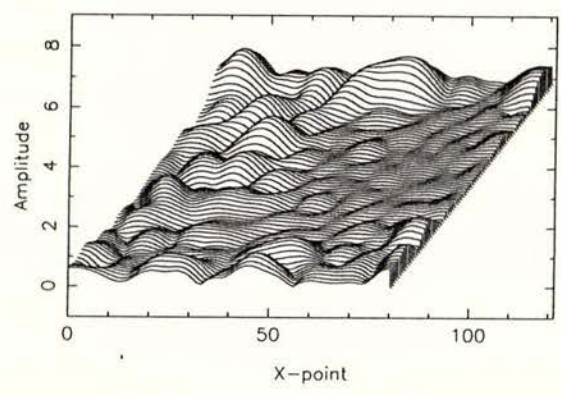
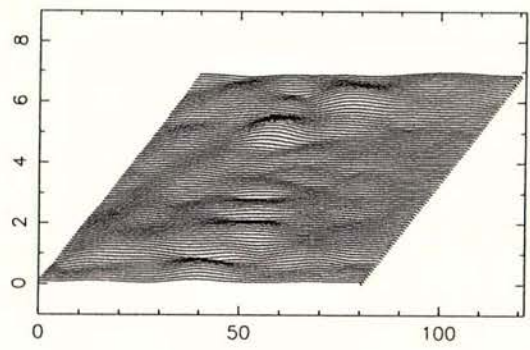


Figure 7j

Y input with  $(k_x, k_y) = (0, 0)$ , freq = 4.00



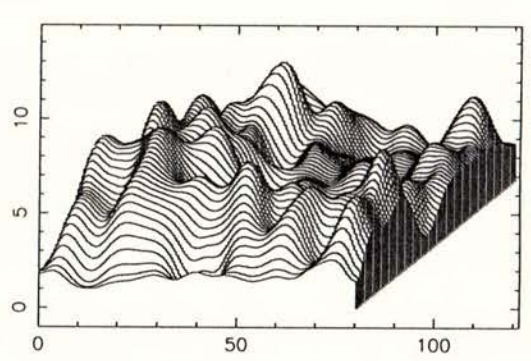
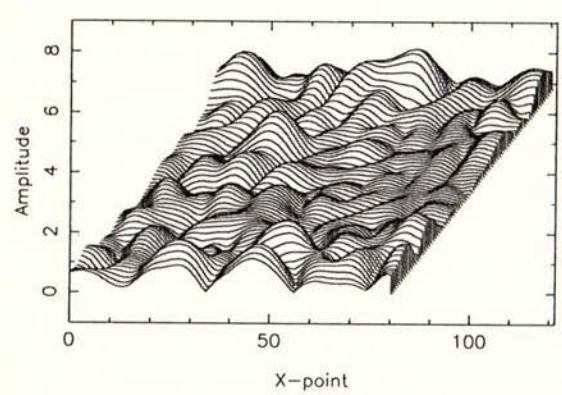
Uz



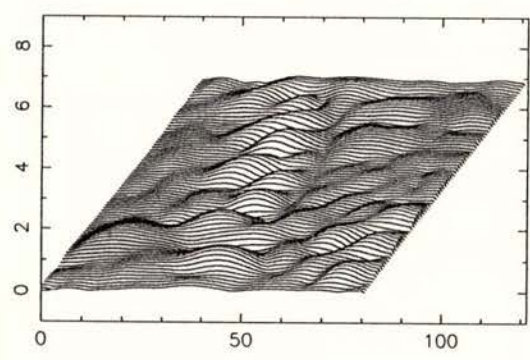
Level 1 for small region, model A



Y input with  $(k_x, k_y) = (0, 0)$ , freq = 4.00



Uz



Level 0 for small region, model A

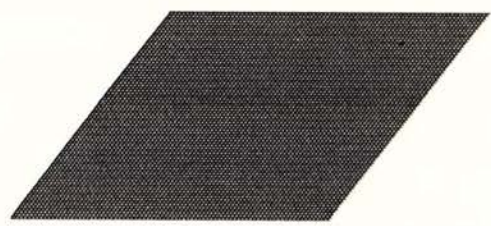
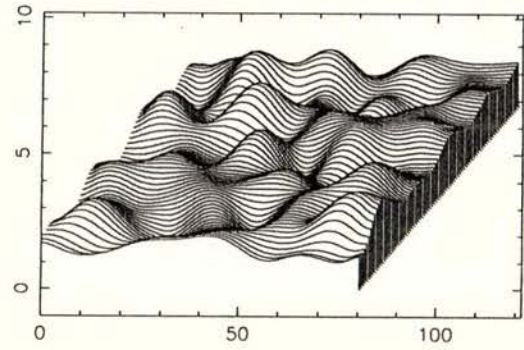
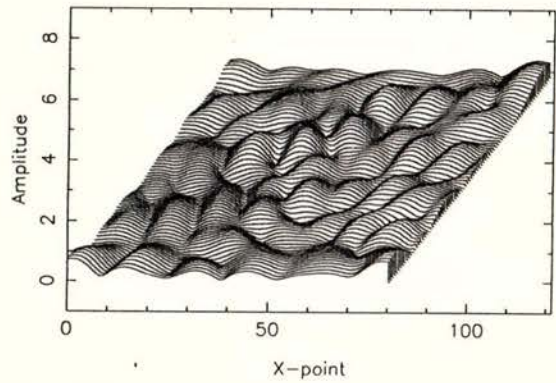
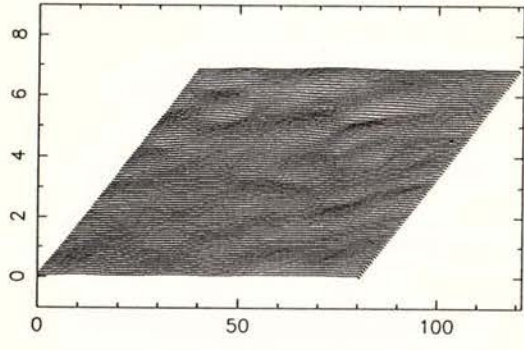


Figure 8a

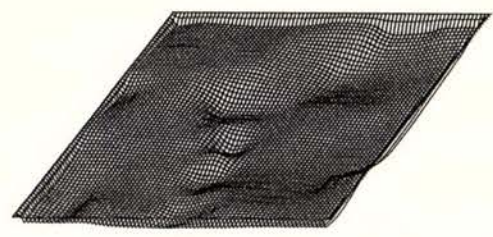
Y input with  $(k_x, k_y) = (0, 0)$ , freq = 3.00



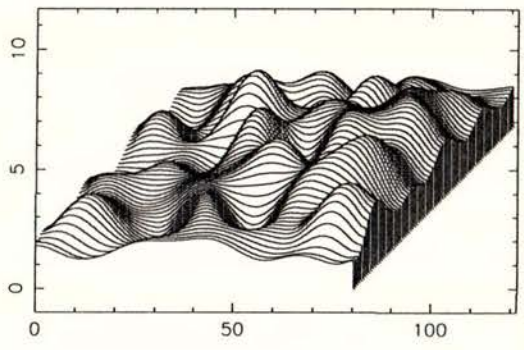
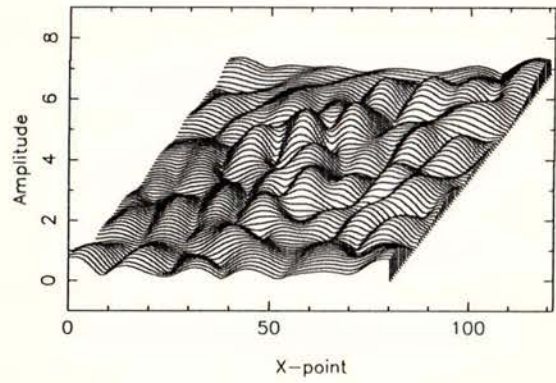
Uz



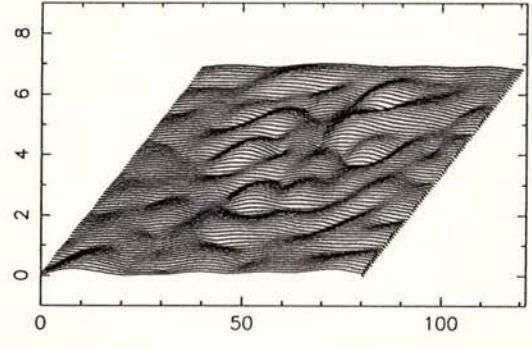
Level 1 for small region, model B



Y input with  $(k_x, k_y) = (0, 0)$ , freq = 3.00



Uz

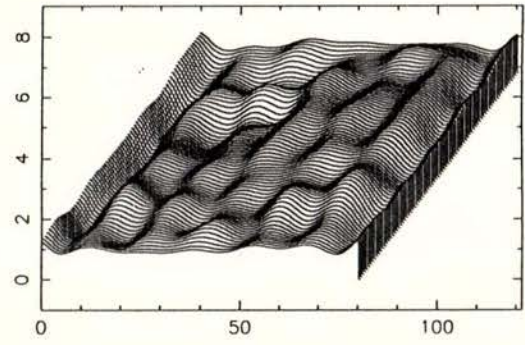
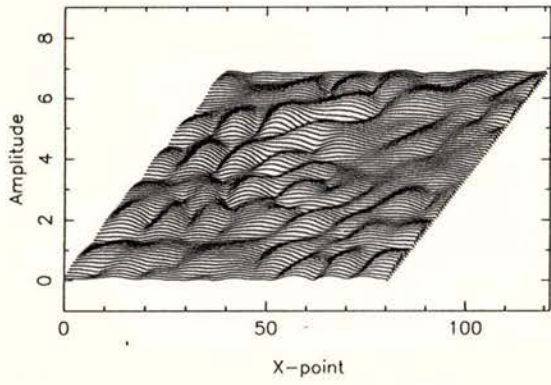


Level 0 for small region, model B

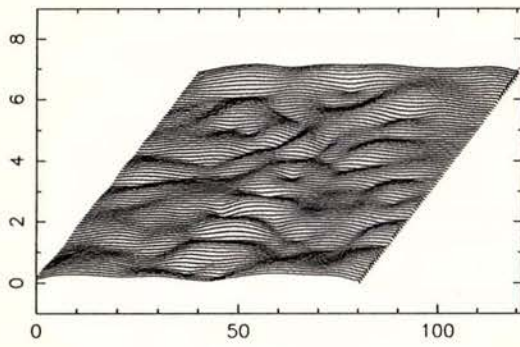


Figure 8b

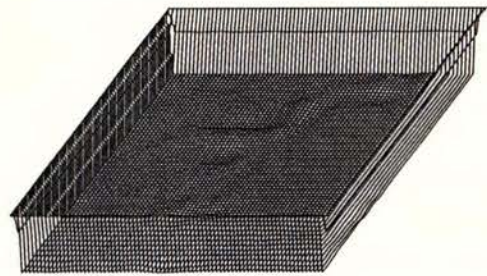
Y input with  $(k_x, k_y) = (0, 0)$ , freq = 4.50



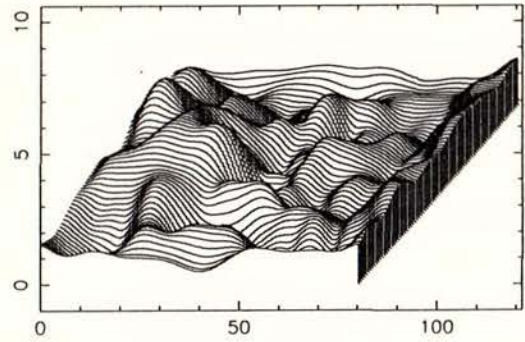
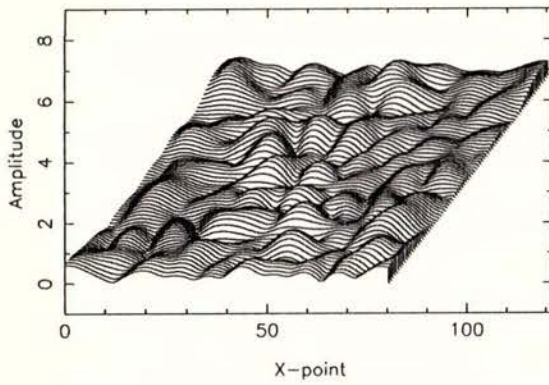
U<sub>z</sub>



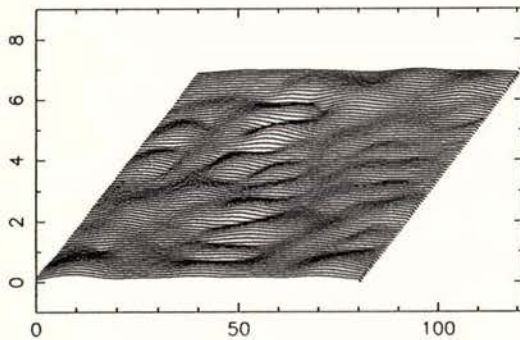
Level 3 for small region, model B



Y input with  $(k_x, k_y) = (0, 0)$ , freq = 4.50



U<sub>z</sub>



Level 2 for small region, model B

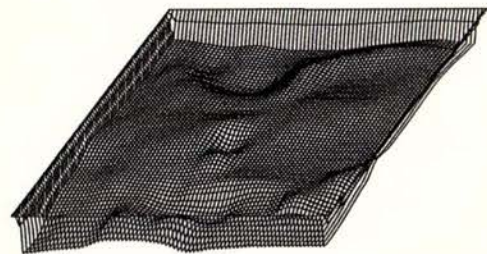
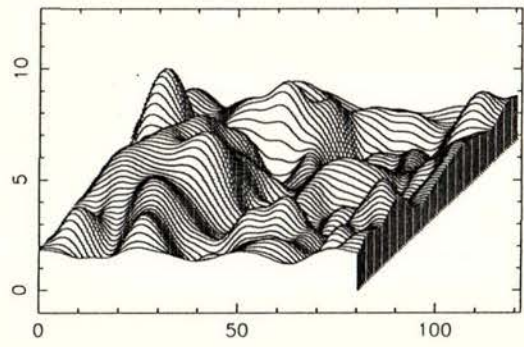
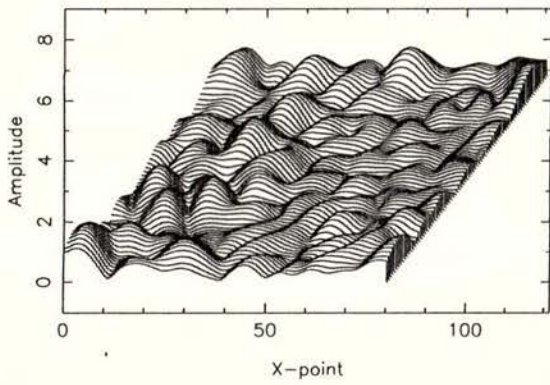


Figure 8c

Ux

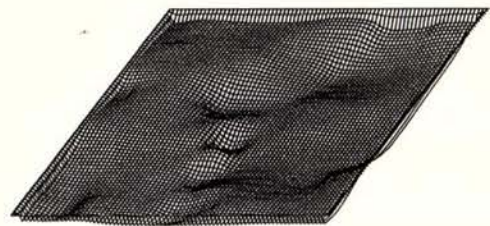
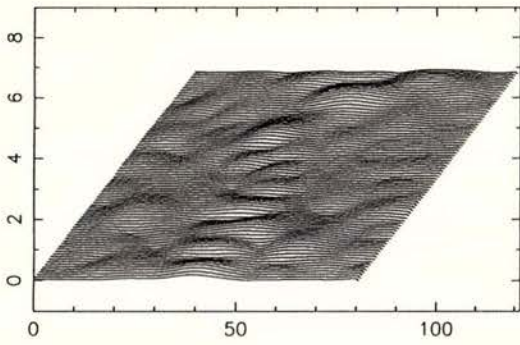
Y input with  $(k_x, k_y) = (0, 0)$ , freq = 4.50

Uy



Uz

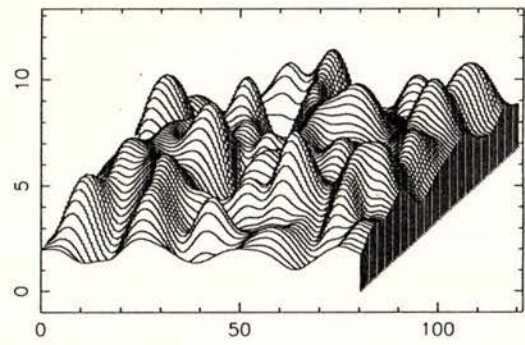
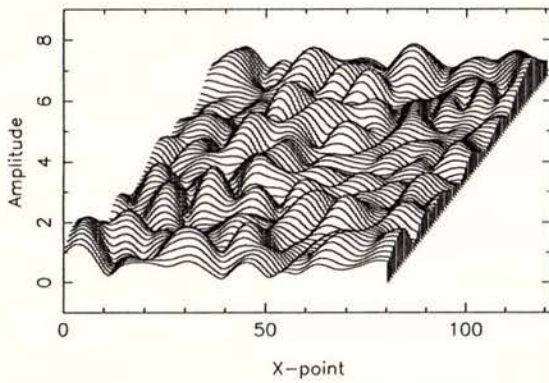
Level 1 for small region, model B



Ux

Y input with  $(k_x, k_y) = (0, 0)$ , freq = 4.50

Uy



Uz

Level 0 for small region, model B

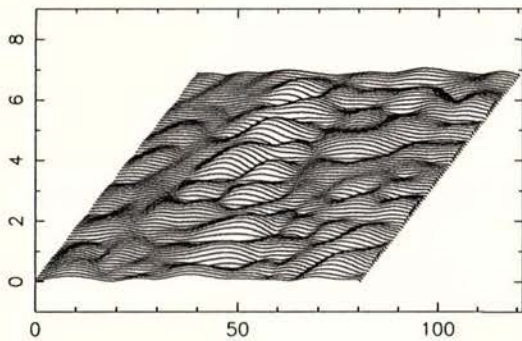
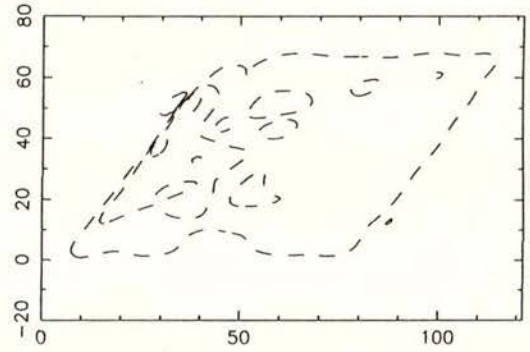
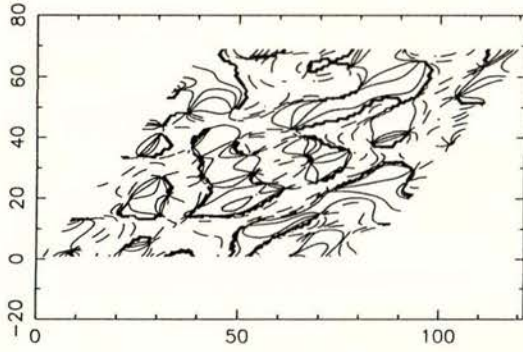


Figure 8d

phase Ux

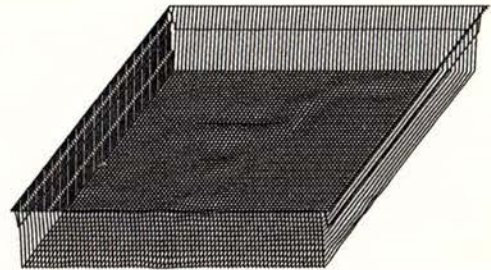
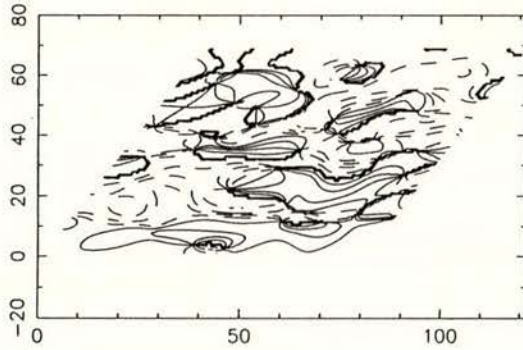
Y input with  $(k_x, k_y) = (0, 0)$ , freq = 4.50

phase Uy



phase Uz

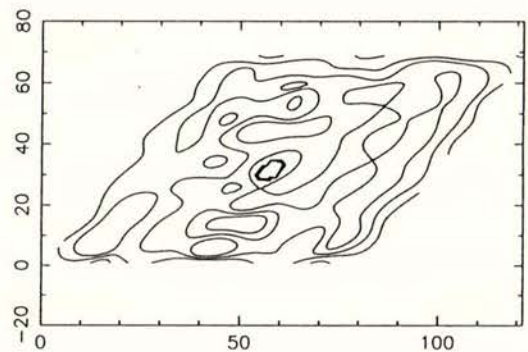
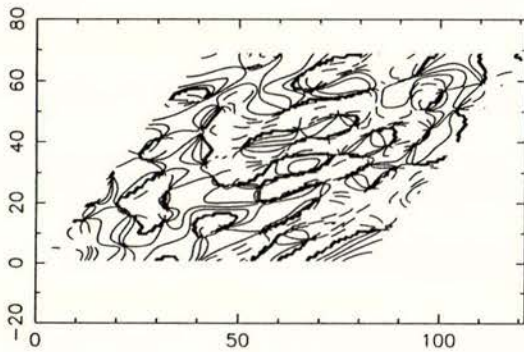
Level 3 for small region, model B



phase Ux

Y input with  $(k_x, k_y) = (0, 0)$ , freq = 4.50

phase Uy



phase Uz

Level 0 for small region, model B

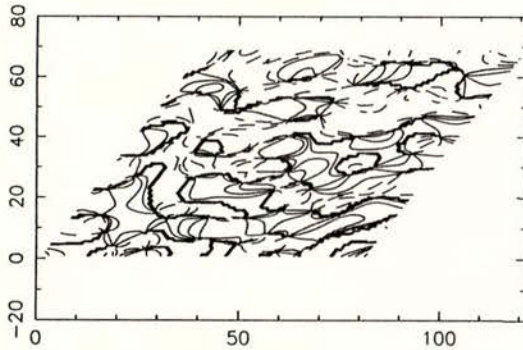
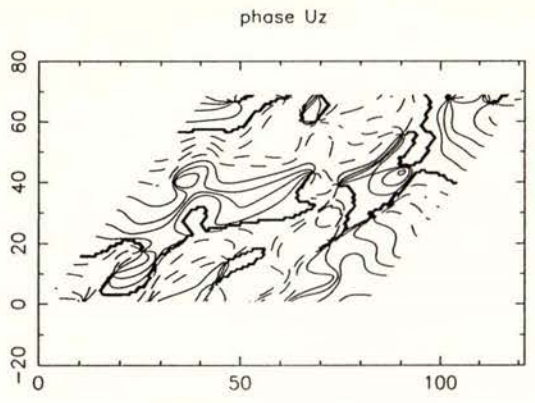
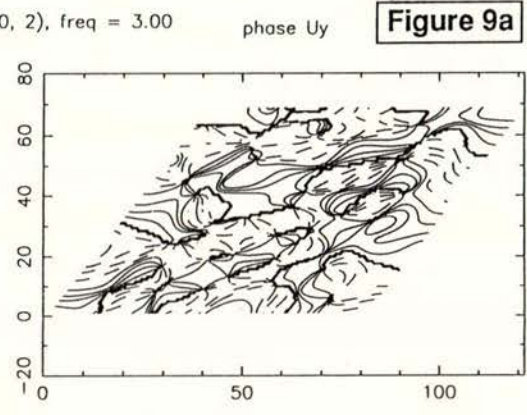
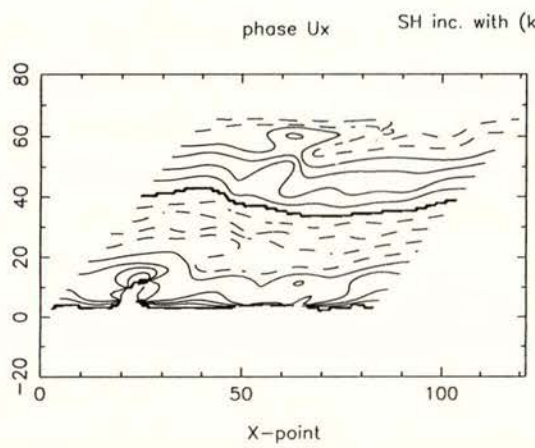
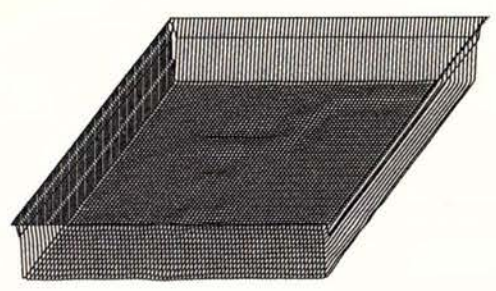


Figure 9a

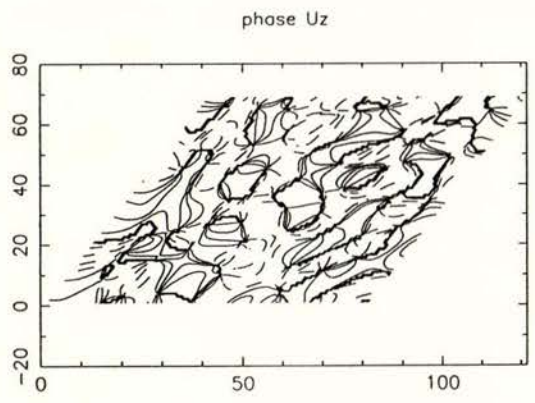
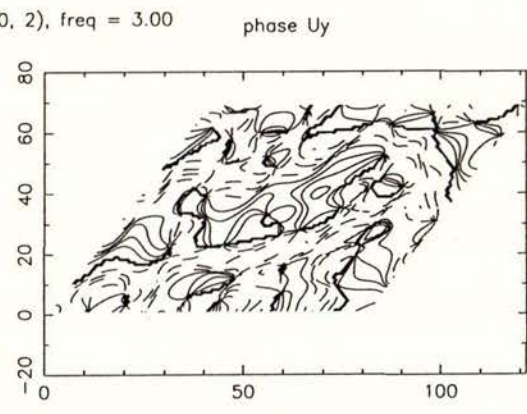
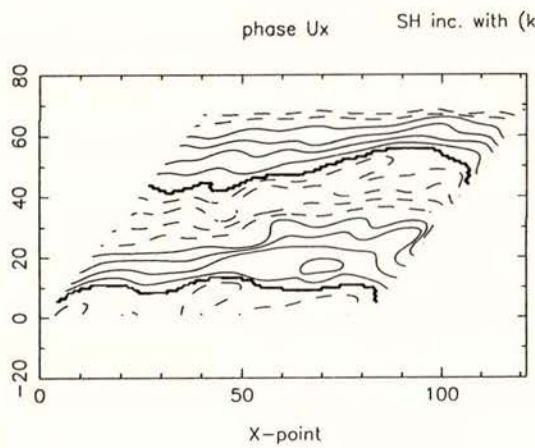
SH inc. with  $(k_x, k_y) = (0, 2)$ , freq = 3.00



Level 3 for small region, model A



SH inc. with  $(k_x, k_y) = (0, 2)$ , freq = 3.00



Level 0 for small region, model A

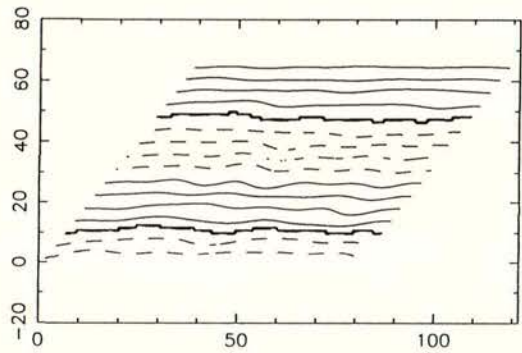
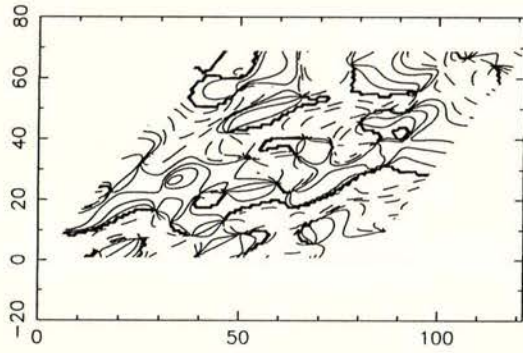


**Figure 9b**

phase Ux

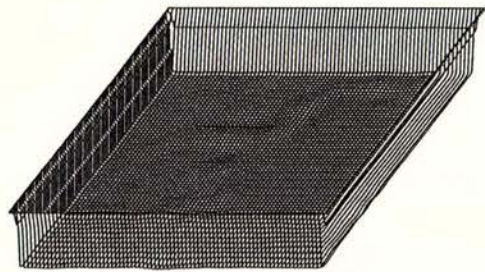
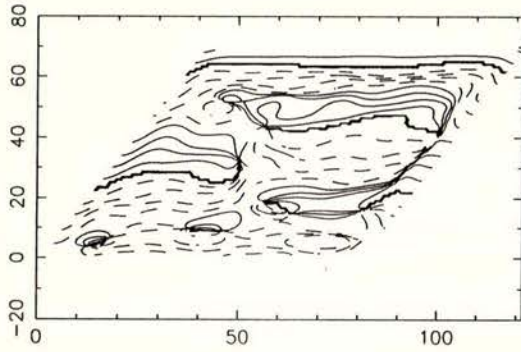
SV inc. with  $(k_x, k_y) = (0, 2)$ , freq = 3.00

phase Uy



phase Uz

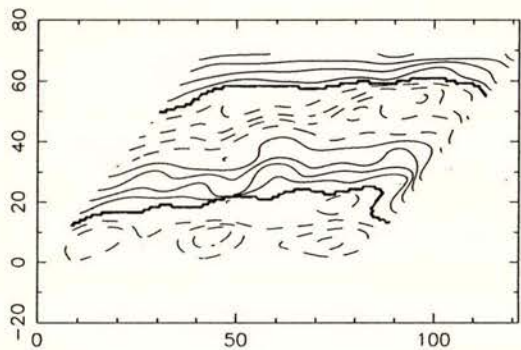
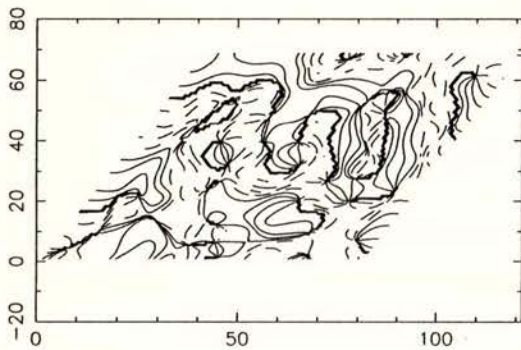
Level 3 for small region, model A



phase Ux

SV inc. with  $(k_x, k_y) = (0, 2)$ , freq = 3.00

phase Uy



phase Uz

Level 0 for small region, model A

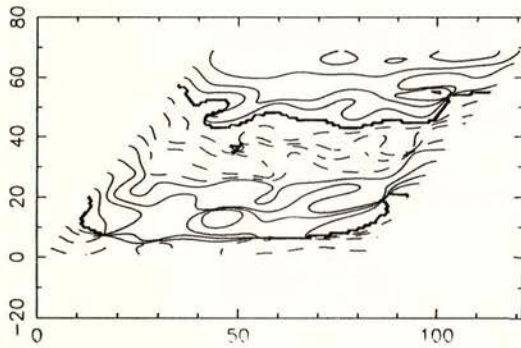
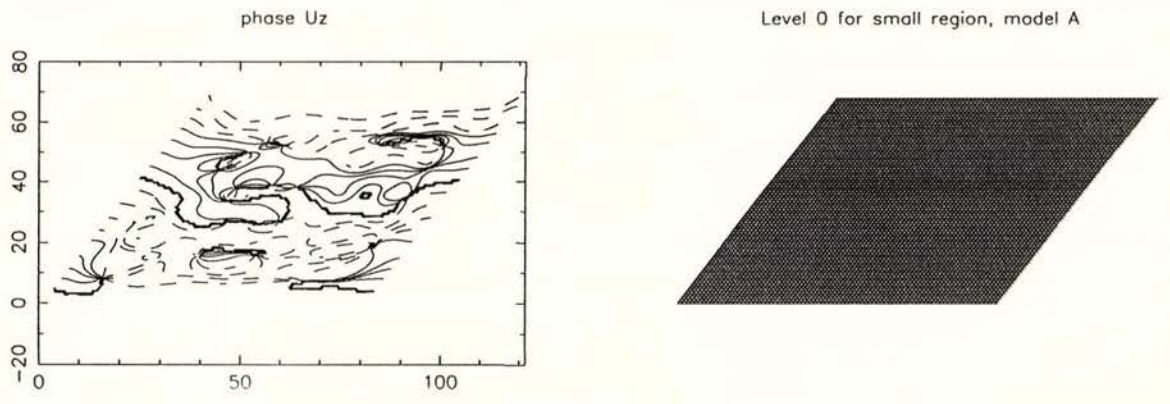
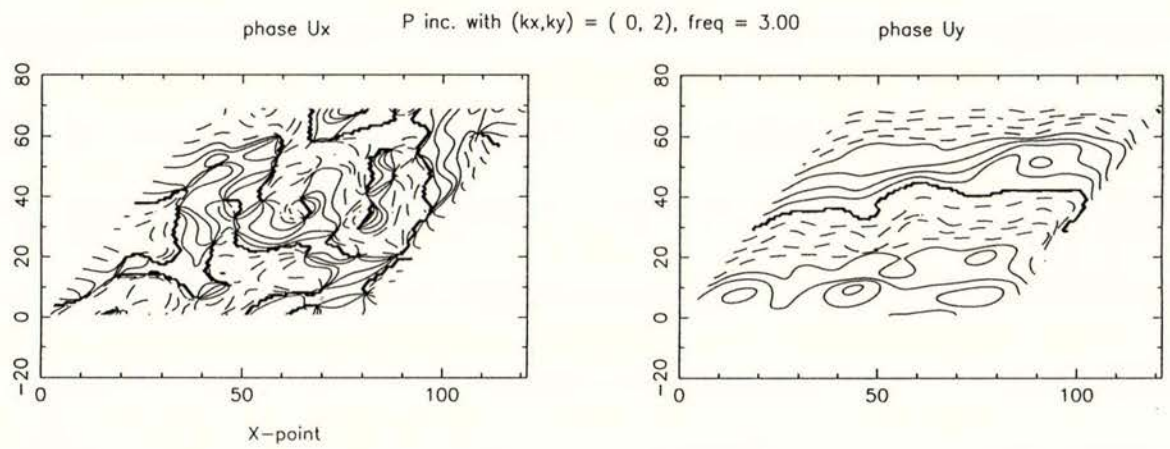
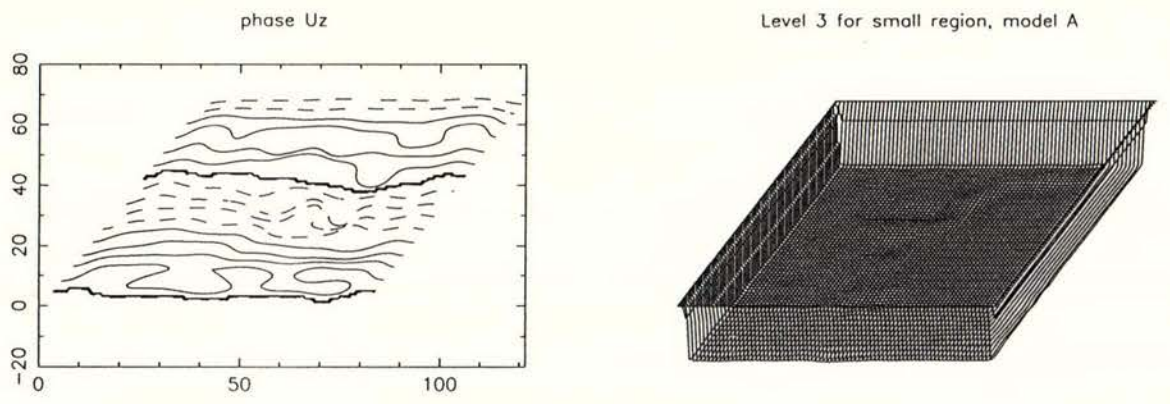
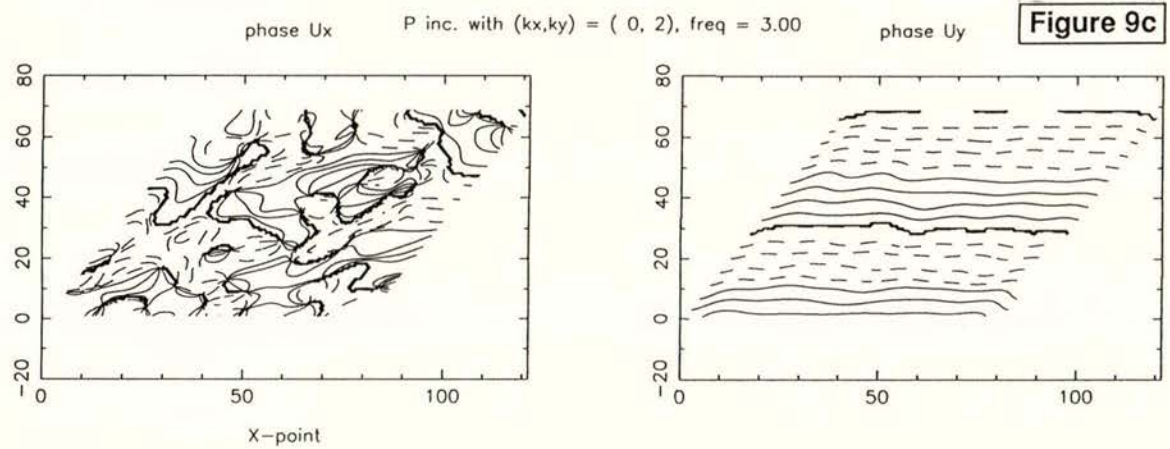


Figure 9c

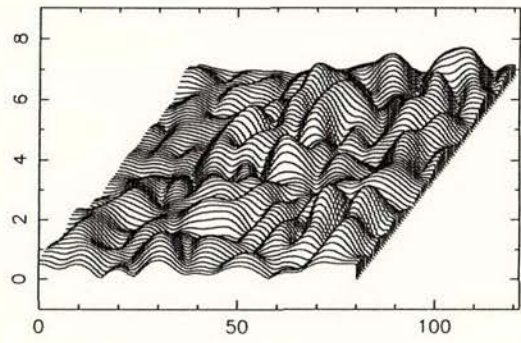
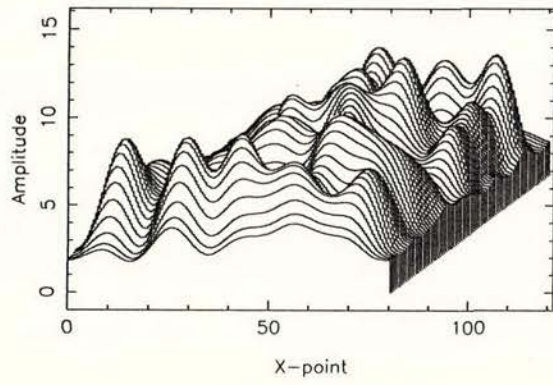


Ux

SH inc. with  $(k_x, k_y) = (0, 1)$ , freq = 3.00

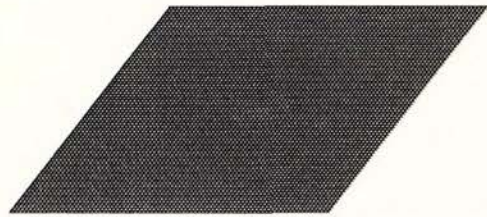
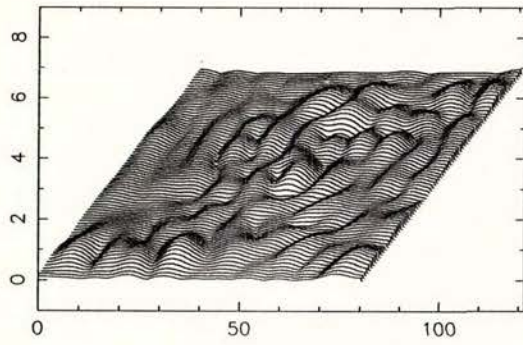
Uy

Figure 10a



Uz

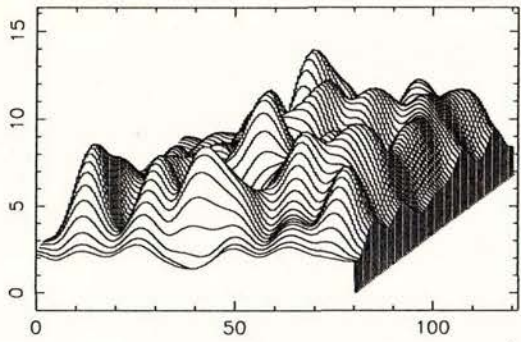
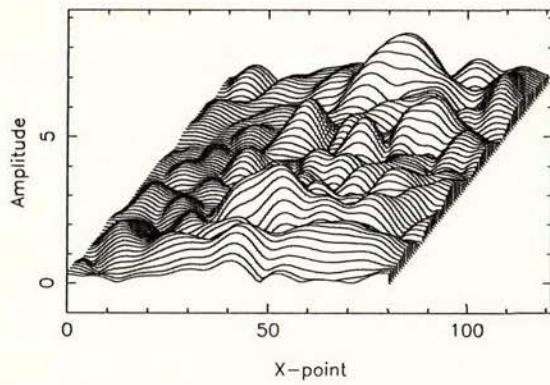
Level 0 for small region, model A



Ux

SH inc. with  $(k_x, k_y) = (1, 0)$ , freq = 3.00

Uy



Uz

Level 0 for small region, model A

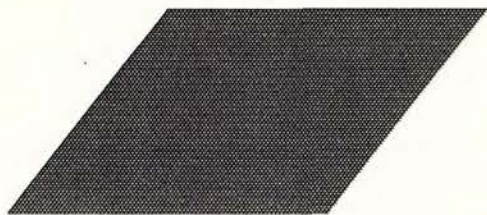
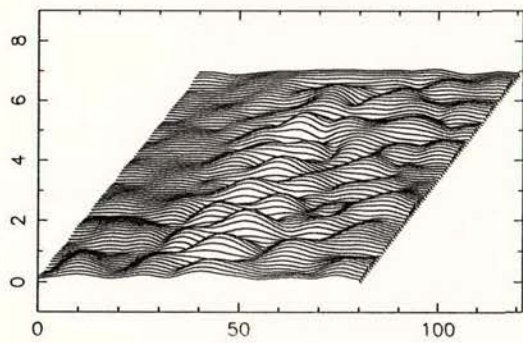
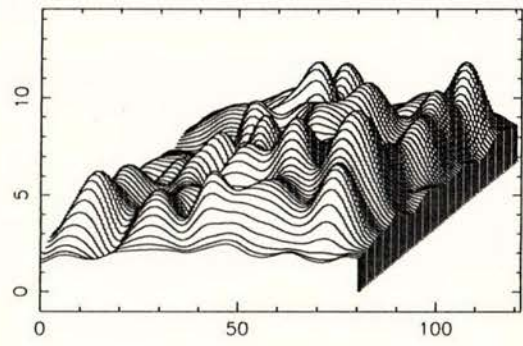
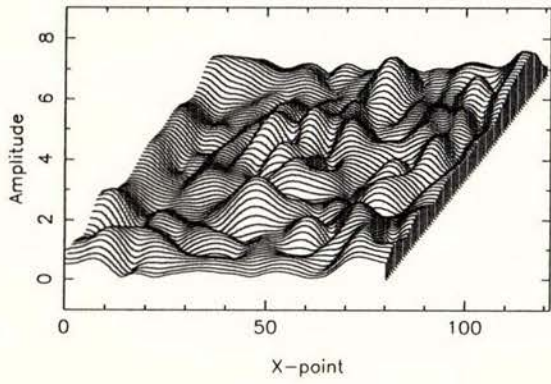
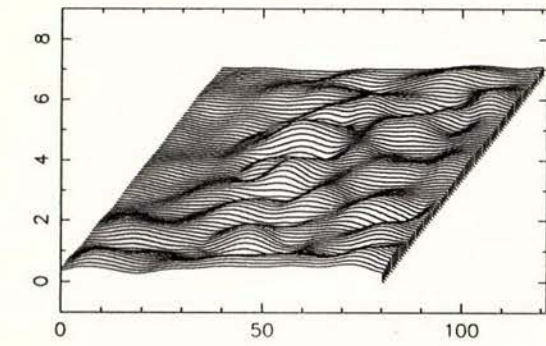


Figure 10b

SV inc. with  $(k_x, k_y) = (0, 1)$ , freq = 3.00



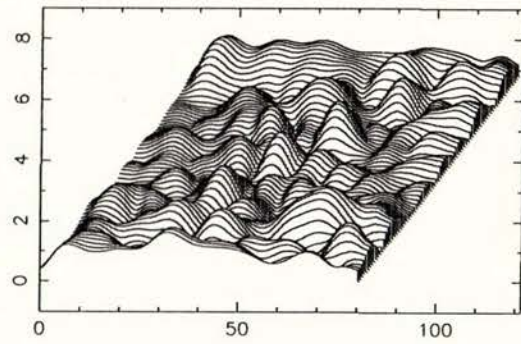
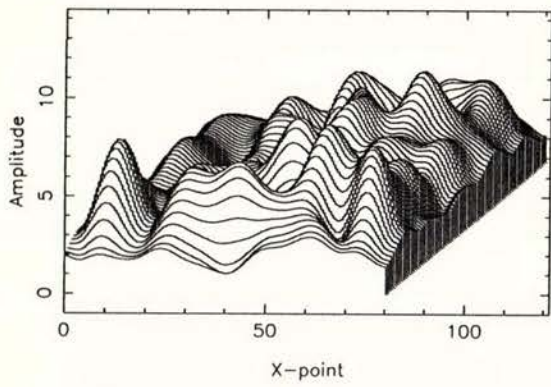
$U_z$



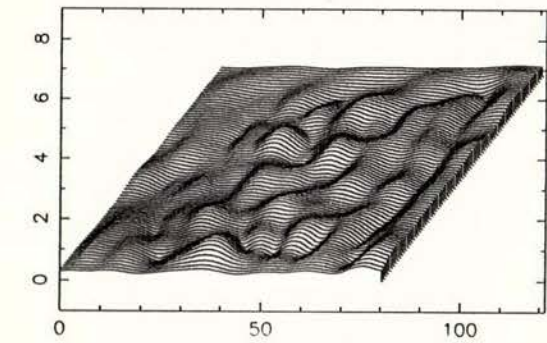
Level 0 for small region, model A



SV inc. with  $(k_x, k_y) = (1, 0)$ , freq = 3.00



$U_z$



Level 0 for small region, model A

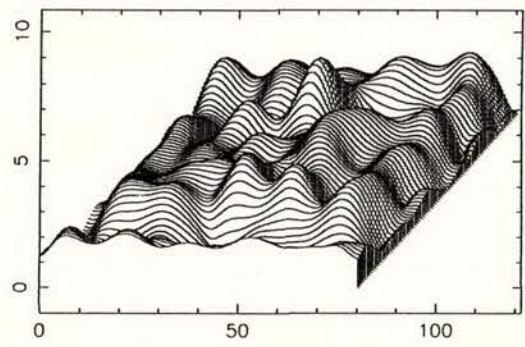
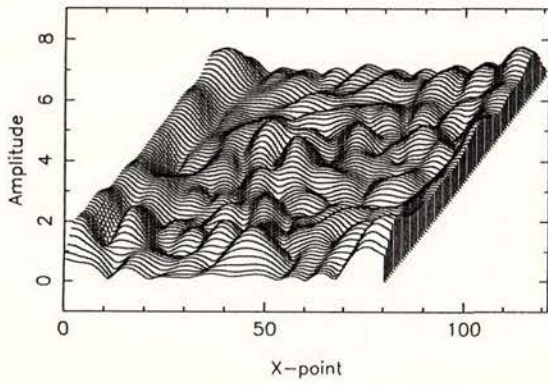


Figure 10c

$U_x$

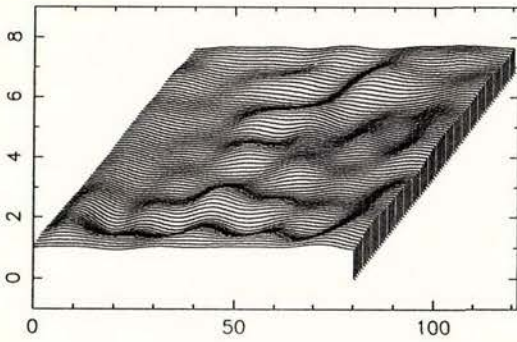
P inc. with  $(k_x, k_y) = (0, 1)$ , freq = 3.00

$U_y$



$U_z$

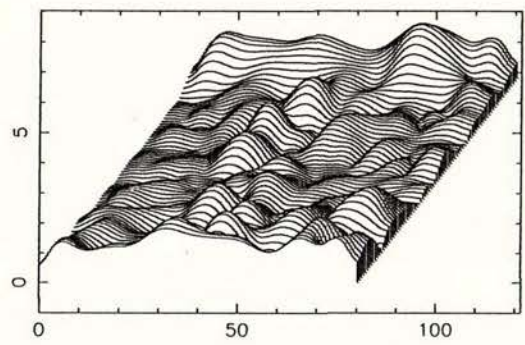
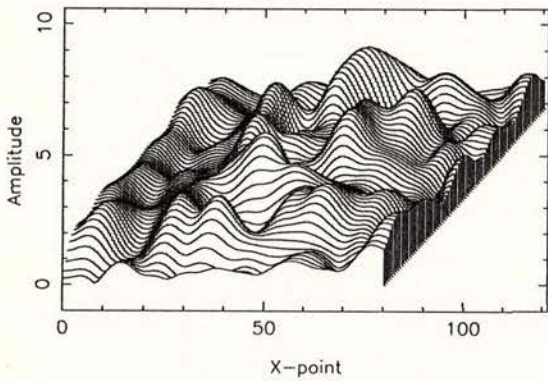
Level 0 for small region, model A



$U_x$

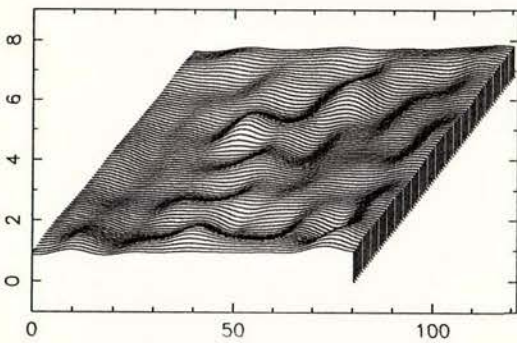
P inc. with  $(k_x, k_y) = (1, 0)$ , freq = 3.00

$U_y$



$U_z$

Level 0 for small region, model A

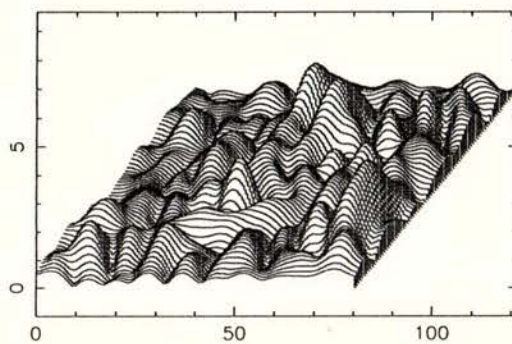
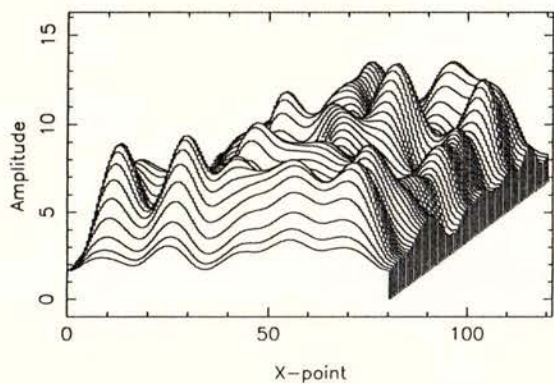


$U_x$

SH inc. with  $(k_x, k_y) = (0, 2)$ , freq = 3.00

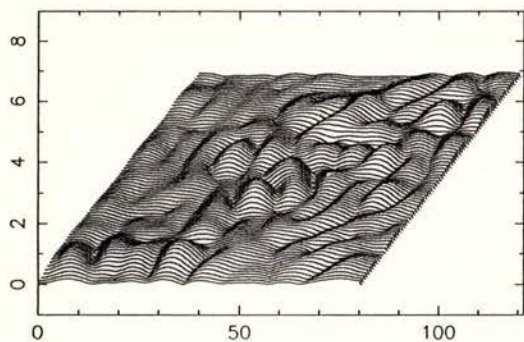
$U_y$

Figure 10d



$U_z$

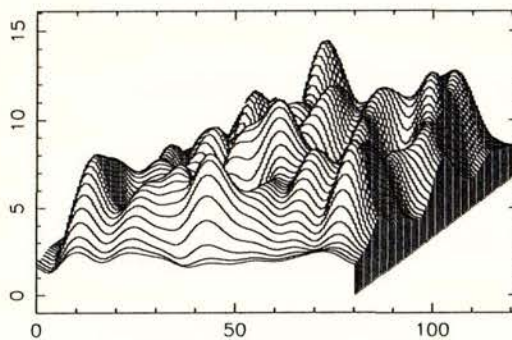
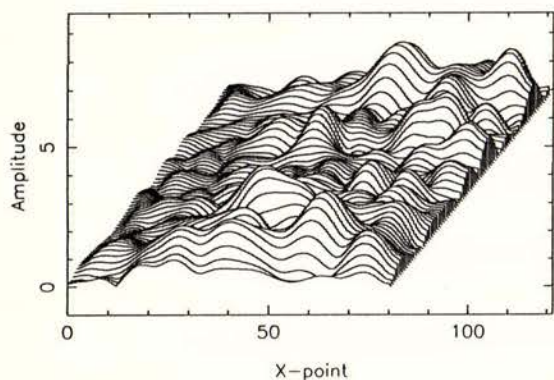
Level 0 for small region, model A



$U_x$

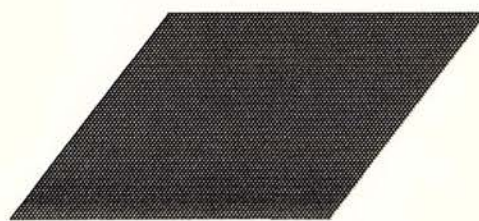
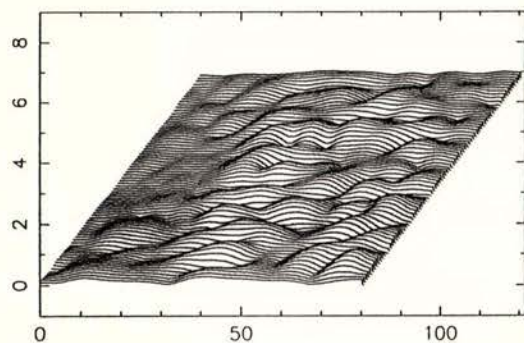
SH inc. with  $(k_x, k_y) = (2, 0)$ , freq = 3.00

$U_y$



$U_z$

Level 0 for small region, model A

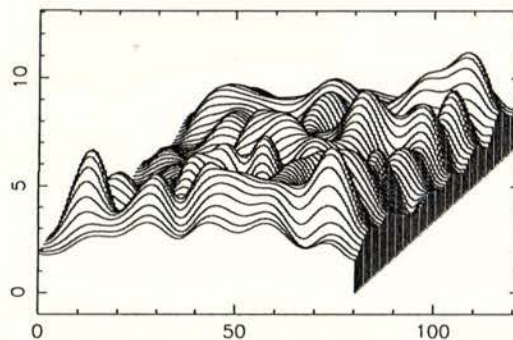
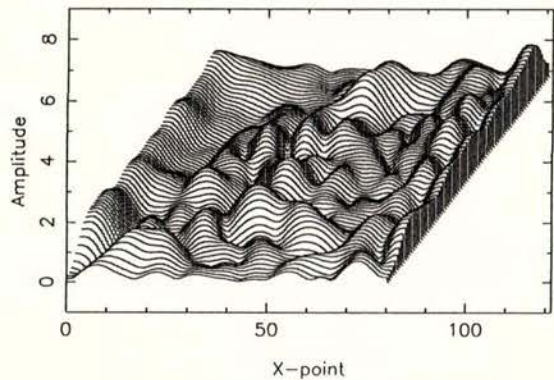


$U_x$

SV inc. with  $(k_x, k_y) = (0, 2)$ , freq = 3.00

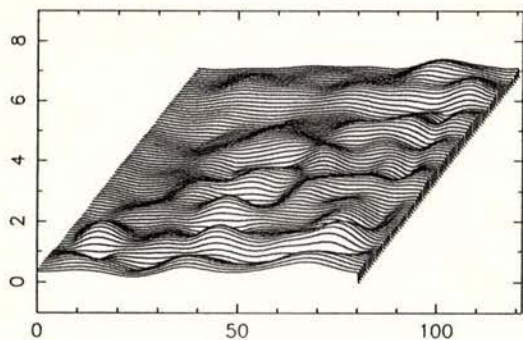
$U_y$

Figure 10e



$U_z$

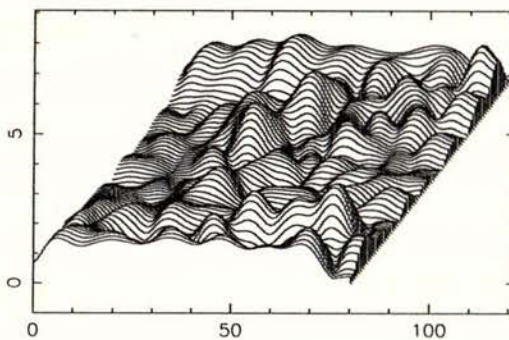
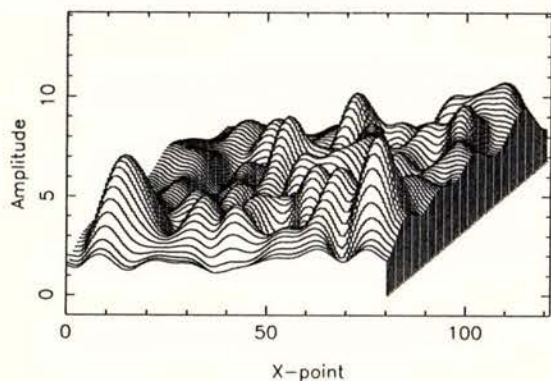
Level 0 for small region, model A



$U_x$

SV inc. with  $(k_x, k_y) = (2, 0)$ , freq = 3.00

$U_y$



$U_z$

Level 0 for small region, model A

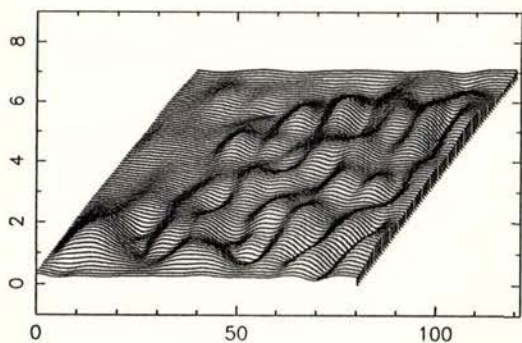
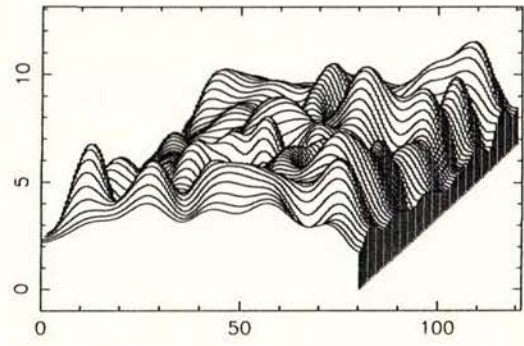
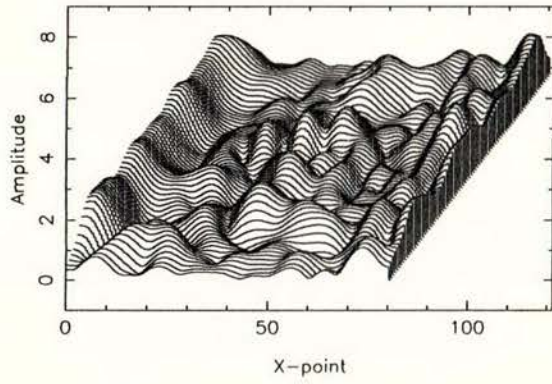


Figure 10f

$U_x$

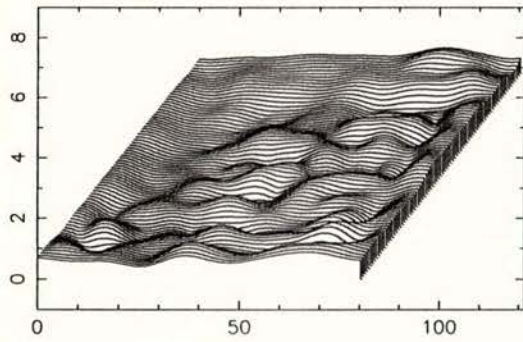
P inc. with  $(k_x, k_y) = (0, 2)$ , freq = 3.00

$U_y$



$U_z$

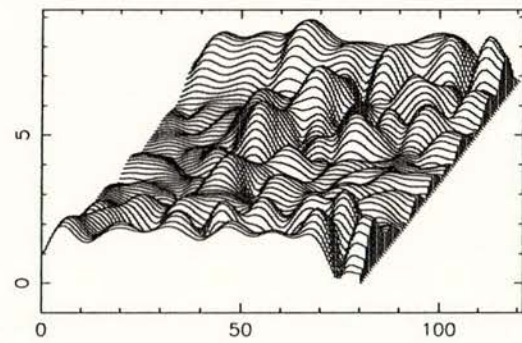
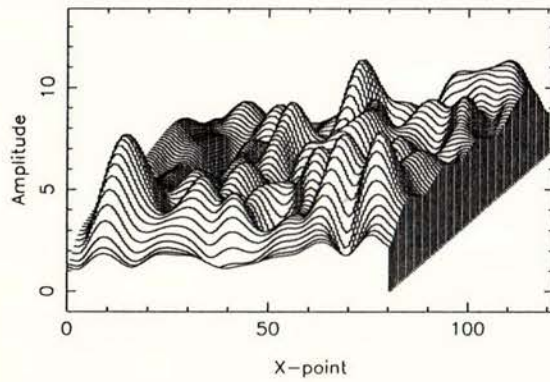
Level 0 for small region, model A



$U_x$

P inc. with  $(k_x, k_y) = (2, 0)$ , freq = 3.00

$U_y$



$U_z$

Level 0 for small region, model A

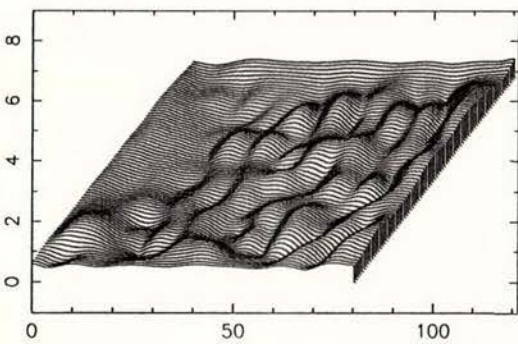
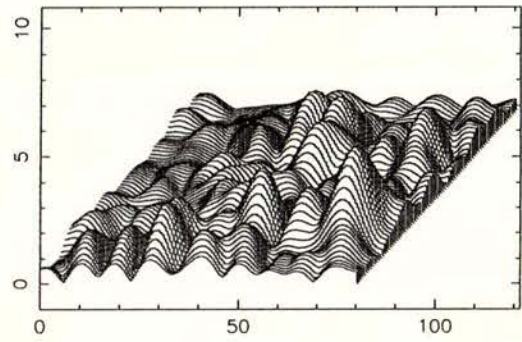
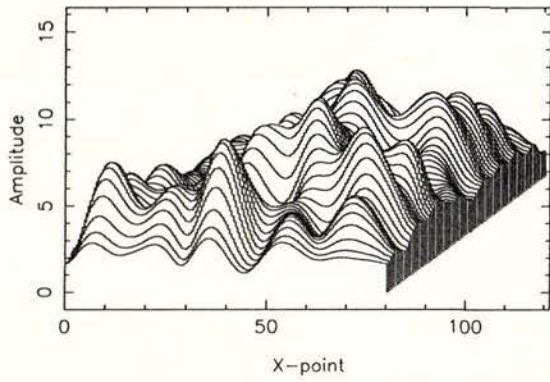


Figure 10g

$U_x$

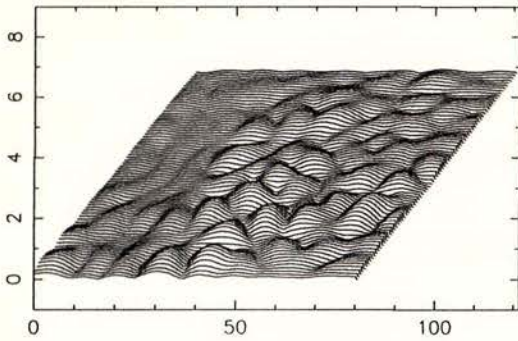
SH inc. with  $(k_x, k_y) = (0, 4)$ , freq = 3.00

$U_y$



$U_z$

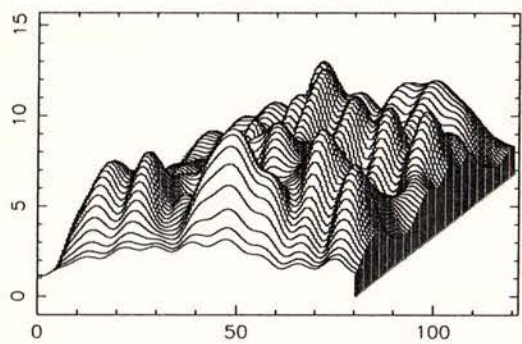
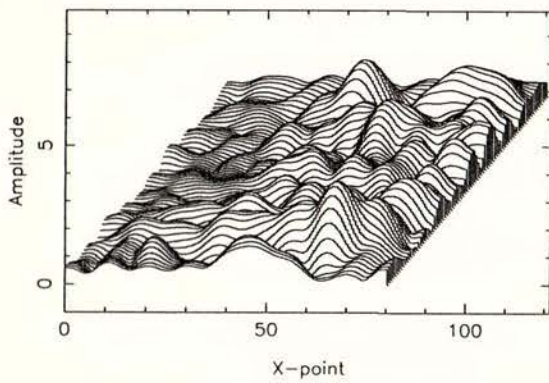
Level 0 for small region, model A



$U_x$

SH inc. with  $(k_x, k_y) = (4, 0)$ , freq = 3.00

$U_y$



$U_z$

Level 0 for small region, model A

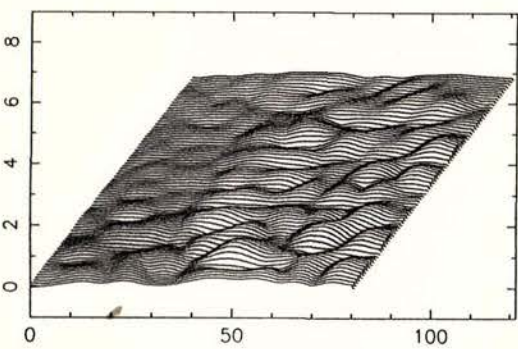
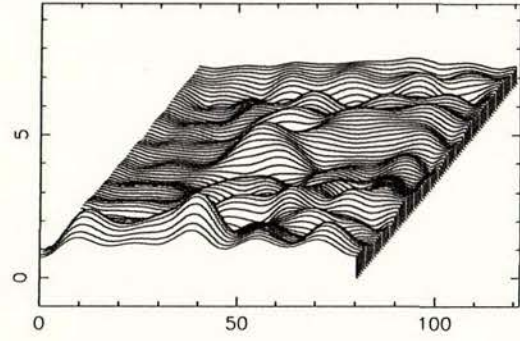
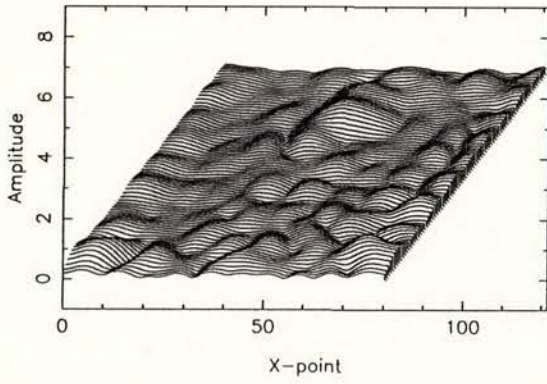


Figure 10h

$U_x$

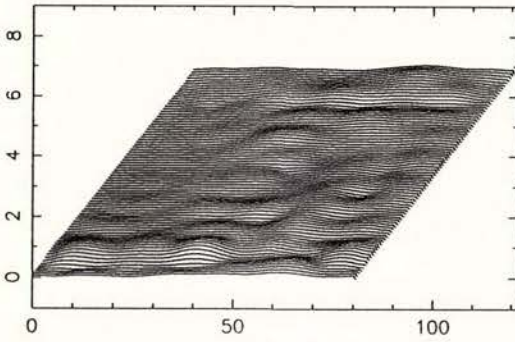
SV inc. with  $(k_x, k_y) = (0, 4)$ , freq = 3.00

$U_y$



$U_z$

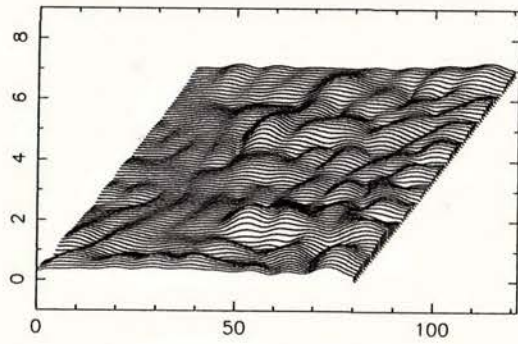
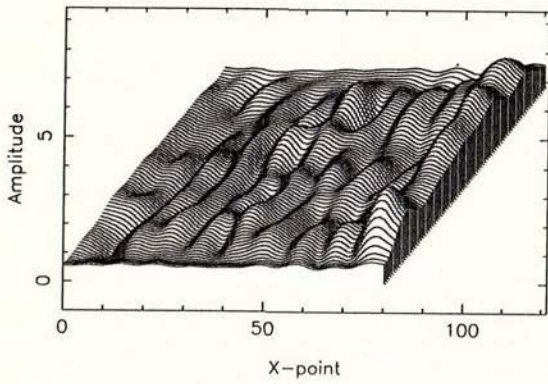
Level 0 for small region, model A



$U_x$

SV inc. with  $(k_x, k_y) = (4, 0)$ , freq = 3.00

$U_y$



$U_z$

Level 0 for small region, model A

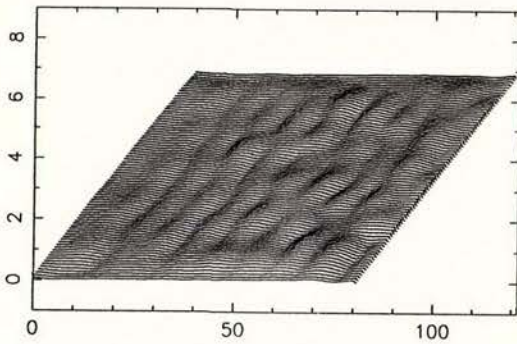
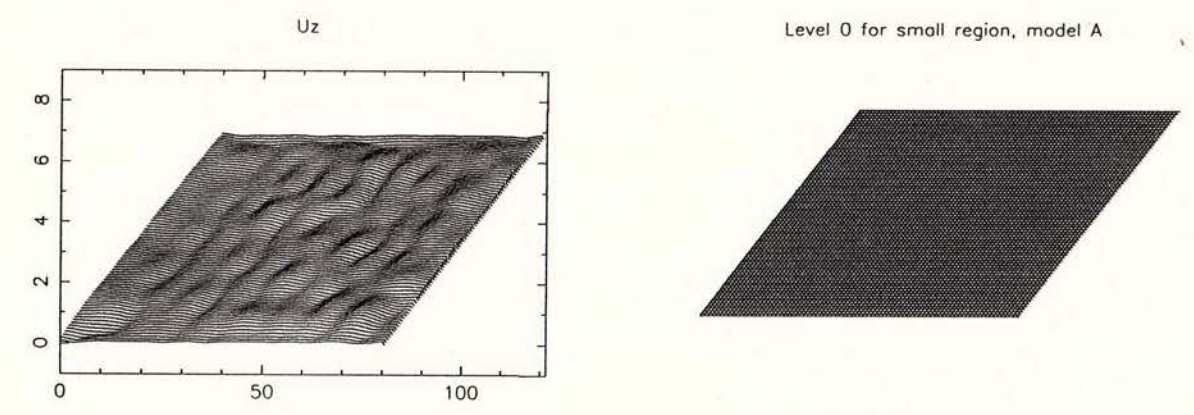
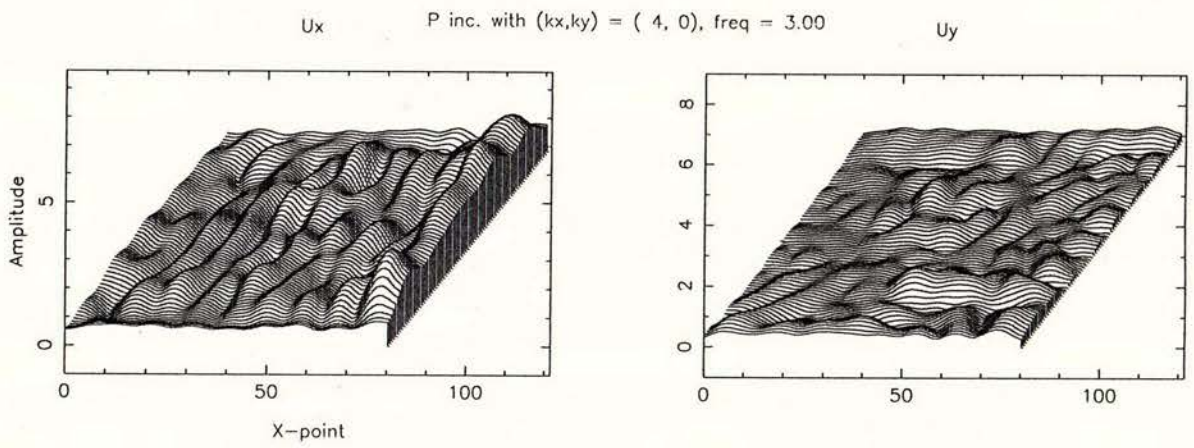
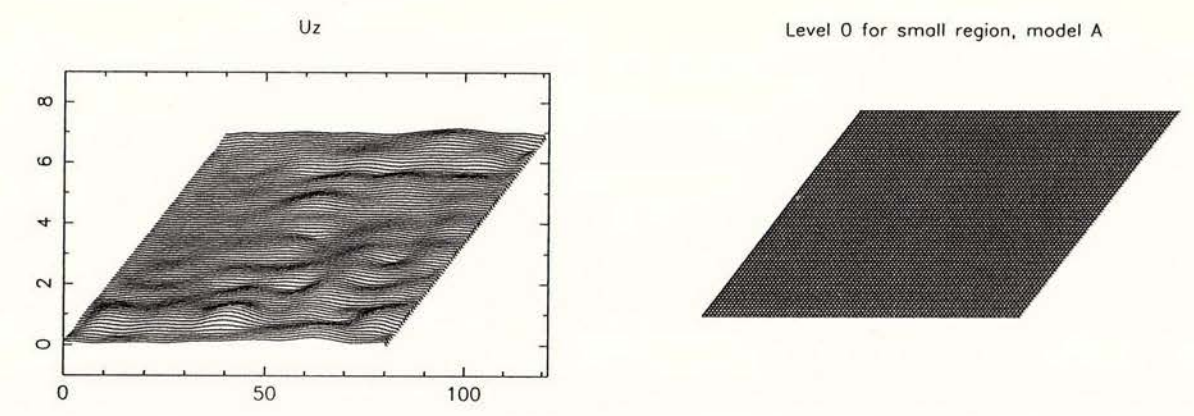
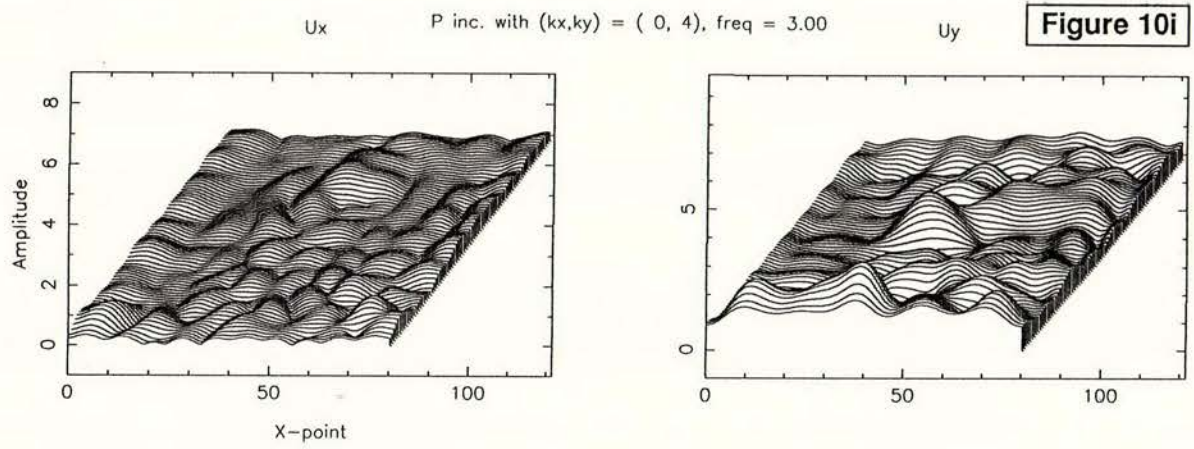


Figure 10i



INSTITUTE OF GEOLOGICAL & NUCLEAR SCIENCES LIMITED

Corporate Services  
Gracefield Road  
PO Box 30 368  
Lower Hutt  
New Zealand  
Phone +64-4-570 1444  
Fax +64-4-569 0600

30 Gracefield Road  
PO Box 31 312  
Lower Hutt  
New Zealand  
Phone +64-4-569 0637  
Fax +64-4-569 0657

State Insurance Building  
Andrews Avenue  
PO Box 30 368  
Lower Hutt  
New Zealand  
Phone +64-4-569 9059  
Fax +64-4-569 5016

32 Salamanca Road  
Kelburn  
PO Box 1320  
Wellington  
New Zealand  
Phone +64-4-473 8208  
Fax +64-4-471 0977

Wairakei Research Centre  
State Highway 1, Wairakei  
Private Bag 2000  
Taupo  
New Zealand  
Phone +64-7-374 8211  
Fax +64-7-374 8199

Crown Research Dunedin  
764 Cumberland Street  
Private Bag  
Dunedin  
New Zealand  
Phone +64-3-477 4050  
Fax +64-3-477 5232